THE CRUSTAL STRUCTURE AND SUBSIDENCE HISTORY of ASEISMIC RIDGES AND MID-PLATE ISLAND CHAINS

by

ROBERT SHERMAN DETRICK, JR.

B. S., Lehigh University
(1971)

M. S., University of California, San Diego
Scripps Institution of Oceanography
(1974)

SUBMITTED IN PARTIAL FULFILLMENT
OF THE REQUIREMENTS FOR THE
DEGREE OF

DOCTOR OF PHILOSOPHY

at the

MASSACHUSETTS INSTITUTE OF TECHNOLOGY ©
and the
WOODS HOLE OCEANOGRAPHIC INSTITUTION

September, 1978

Signature of Author _____

Joint Program in Oceanography, Massachusetts Institute of Technology-Woods Hole Oceanographic Institution, and the Department of Earth and Planetary Sciences, Massachusetts Institute of Technology, June, 1978

Certified by _____

Thesis Supervisor

Accepted by _____

Chairman, Joint Oceanography Committee in the Earth Sciences, Massachusetts Institute of Technology-Woods Hole Oceanographic Institution

WITHDRAWN
FROM
MIT LIBRARIES
MASSACHUSETTS INSTITUTE OF TECHNOLOGY
AUG 1 1978
LIBRARIES

TABLE OF CONTENTS

LIST OF FIGURES

Page No.

Page No.

APPENDIX A

LIST OF TABLES

BIOGRAPHICAL SKETCH

I was born in Pittsburgh, Pennsylvania, on November 19, 1949. I attended Lehigh University (Bethlehem, Pennsylvania) from 1967-1971 and was graduated in June, 1971, with a Bachelor of Science Degree in physics and geology, awarded with highest honors. My introduction to marine geology and geophysics came in 1970, when I was a summer fellow at Woods Hole Oceanographic Institution, working with Dr. Carl Bowin. In September, 1971, I enrolled at the Scripps Institution of Oceanography (La Jolla, California). While there I worked with the Scripps deep tow group, participating in surveys of the Galapagos Spreading Center (1972) and the Mid-Atlantic Ridge (FAMOUS area, 1973). After receiving my Master of Science Degree in June, 1974, I worked for one year as an exploration geophysicist with Standard Oil Company of California in San Francisco.

In the fall of 1975 I entered the MIT-WHOI Joint Program in Oceanography. Since then my work has concentrated on using gravity and seismic refraction techniques to investigate the crustal structure of anomalous sea floor features such as aseismic ridges and fracture zones.

I am presently a post-doctoral research investigator in the Department of Geology and Geophysics, Woods Hole Oceanographic Institution.

My publications include:

1. Detrick, R. S., and A. B. Watts, Isostasy in the World's Oceans; Part 3 Aseismic Ridges, submitted to J. Geophys. Res., 1978.
2. Detrick, R. S., and S. T. Crough, Island subsidence, hot spots and lithospheric thinning, J. Geophys. Res., 83, 1236-1244, 1978.

3. Detrick, R. S., J. G. Sclater and J. Thiede, The subsidence of aseismic ridges, Earth Planet. Sci. Lett., 34, 185-196, 1977.

4. Detrick, R. S., and W. S. Lynn, The origin of high-amplitude magnetic anomalies at the intersection of the Juan de Fuca Ridge and Blanco fracture zone, Earth Planet. Sci. Lett., 26, 105-113, 1975.

5. Detrick, R. S., D. L. Williams, J. D. Mudie and J. G. Sclater, The Galapagos spreading center: Bottom water temperatures and the significance of geothermal heating, Geophys. J. R. Astr. Soc., 38, 627-637, 1974.

6. Detrick, R. S., J. D. Mudie, B. P. Luyendyk and K. C. Macdonald, Near-bottom observations of an active transform fault (MAR 37^{o}N), Nature Phys. Sci., 246, 59-61, 1973.

7. Purdy, G. M., and R. S. Detrick, A seismic refraction experiment in the central Banda Sea, J. Geophys. Res., in press, 1978.

8. Sclater, J. G., and R. S. Detrick, Elevation of mid-ocean ridges and the basement ages of JOIDES Deep Sea Drilling Sites, Geol. Soc. Amer. Bull., 84, 1547-1554, 1973.

ACKNOWLEDGMENTS

Since this thesis is a collection of three co-authored papers, I first want to acknowledge the contributions my co-authors have made to this research. John Sclater suggested I use Deep Sea Drilling results to examine the subsidence history of aseismic ridges and provided the initial encouragement I needed to begin this project. Jörn Thiede contributed his insight into the subsidence history of the Rio Grande Rise. These results, included here in Chapter 3, have been published in Earth and Planetary Science Letters, 34, 185-196, 1977. The work reported in Chapter 4 grew out of a student seminar I presented in October, 1976. I had discussed available data on island subsidence and shown that islands formed on old sea floor were subsiding much faster than expected. Tom Crough suggested that lithospheric thinning might explain this excess atoll subsidence, and together we developed the model for the origin of mid-plate island swells presented in Chapter 4. This research has been published in Journal of Geophysical Research, 83, 1236-1244, 1978. Impressed by the potential of transfer function techniques of analyzing gravity data, I was interested in using these techniques to investigate the crustal structure of aseismic ridges. Tony Watts generously allowed me to use Lamont gravity data and computer programs in the work presented in Chapter 2. This manuscript has been submitted to the Journal of Geophysical Research for publication.

Of the many scientists, staff and students at Woods Hole and MIT who have helped make my graduate experience rewarding, I would particularly like to thank Mike Purdy, my thesis advisor and friend, whose support and guidance have been invaluable; Hans Schouten and Chuck Denham for

teaching me principles of time series analysis; and Jake Pierson for guiding me through the combined bureaucracies of MIT and WHOI. I am also particularly grateful to John Sclater, LeRoy Dorman and Pete Molnar, for without their encouragement it is unlikely that I would have returned to graduate school.

The one individual to whom I am most indebted is my wife, Sandy. Without her patience, support and constant encouragement this thesis would never have been completed. I am also grateful to her for typing the final draft of the thesis.

THE CRUSTAL STRUCTURE AND SUBSIDENCE HISTORY of ASEISMIC RIDGES AND MID-PLATE ISLAND CHAINS

by

Robert Sherman Detrick, Jr.

Submitted to the Woods Hole Oceanographic Institution-Massachusetts Institute of Technology Joint Program in Oceanography on May 5, 1978 in partial fulfillment of the requirements for the degree of Doctor of Philosophy.

ABSTRACT

This thesis consists of three papers examining problems related to the crustal structure, isostasy and subsidence history of aseismic ridges and mid-plate island chains. Analysis of gravity and bathymetry data across the Ninetyeast and eastern Walvis Ridges indicates these features are locally compensated by an overthickening of the oceanic crust. Maximum crustal thicknesses are 15-30 km. The western Walvis Ridge is also compensated by crustal thickening; however, the isostasy of this part of the ridge is best explained by a plate model of compensation with elastic plate thicknesses of 5-8 km. These results are consistent with the formation of the Ninetyeast and Walvis Ridges near spreading centers on young lithosphere with flexural rigidities at least an order of magnitude less than those typically determined from flexural studies in older parts of the ocean basins. As the lithosphere cools and thickens, its rigidity increases, explaining the differences in isostasy between aseismic ridges and mid-plate island chains. The long-term subsidence of aseismic ridges and island/seamount chains can also be explained entirely by lithospheric cooling. Aseismic ridges form near ridge crests and subside at nearly the same rate as normal oceanic crust. Mid-plate island chains subside at slower rates because they are built on older crust. However, some island chains have subsided faster than expected based on the age of the surrounding sea floor, probably because of lithospheric thinning over mid-plate hot spots, like Hawaii. This lithospheric thinning model has major implications both for lithospheric and mantle convection studies as well as the origin of continental rift systems.

Thesis Supervisor: G. M. Purdy
Title: Assistant Scientist

CHAPTER 1

INTRODUCTION AND OVERVIEW

The cooling and thickening of oceanic lithosphere as it ages can explain much of the regional bathymetry of the ocean basins. However, this pattern of increasing depth with age is interrupted by seamount chains, aseismic ridges and various plateau-like features that stand several kilometers shallower than the surrounding sea floor (Figure 1). A few of these features, such as Seychelles, Orphan Knoll and Rockall Plateau, are clearly continental fragments isolated by rifting and sea floor spreading; however, most of these highland areas appear to be oceanic and volcanic in origin. While various models have been proposed to explain the origin of island/seamount chains and aseismic ridges, there is increasing evidence that many of these features have formed by the passage of the lithosphere over a hot spot or mantle plume (Wilson, 1963; Morgan, 1972).

The hot spot model postulates that there are deep volcanic sources in the mantle which create rising plumes of asthenospheric material. These plumes may be fixed relative to the deep mantle (Morgan, 1972), or they may move relative to one another at rates on the order of that observed for lithospheric plates (Molnar and Atwater, 1973). Material associated with these rising plumes penetrates the lithosphere, resulting in the formation of a volcanic center that remains nearly stationary relative to the moving lithosphere. An aseismic ridge is built if the volcanism is continuous and an island or seamount chain if the volcanism is discontinuous. Generally aseismic ridges form from hot spots located on or near spreading centers, while seamount chains form from hot spots located off-ridge (Wilson, 1973).

FIGURE 1

Physiographic map of the World's Oceans by B. C. Heezen and M. Tharp showing location of aseismic ridges and mid-plate island chains discussed in this thesis.

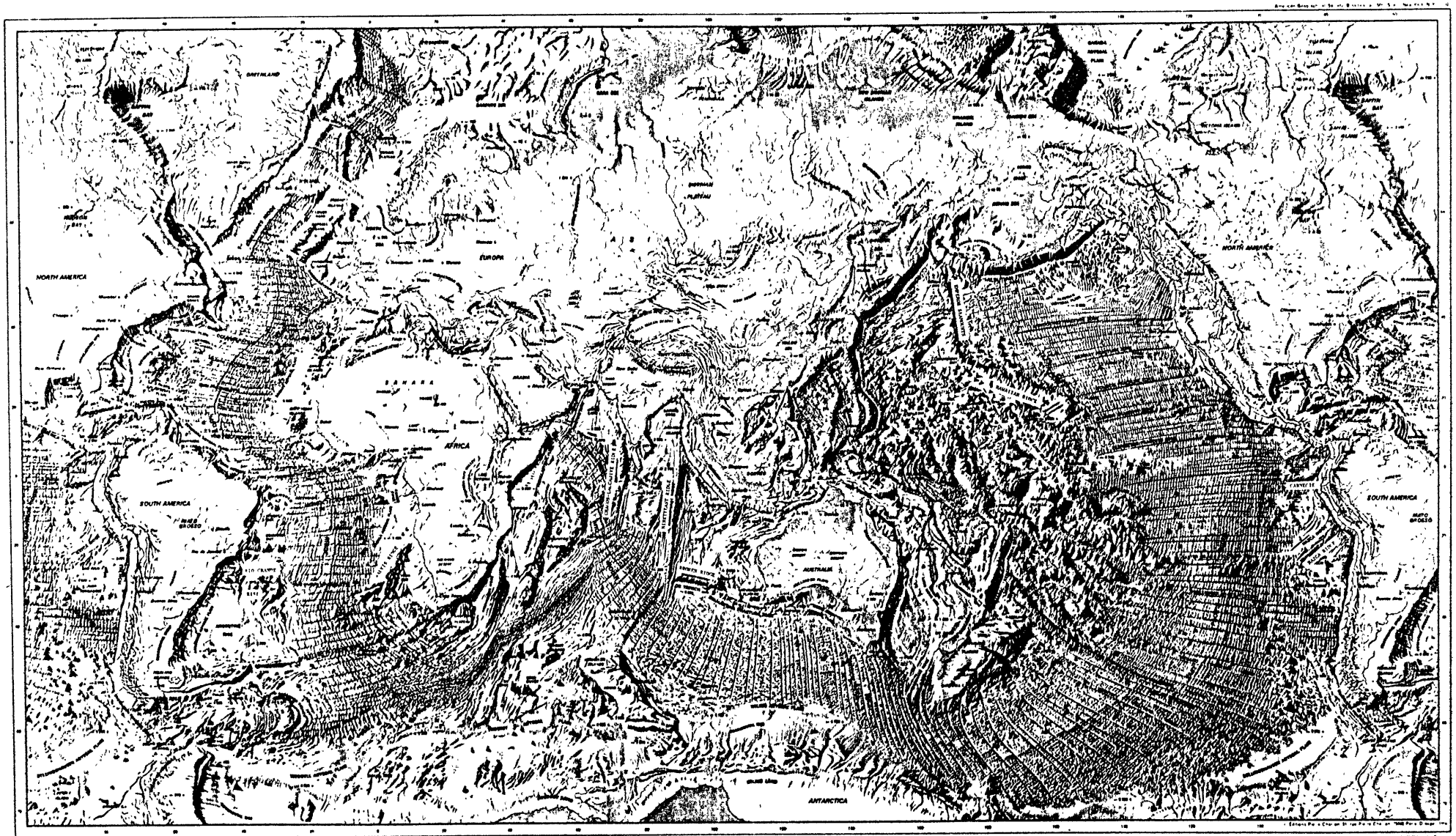

THE FLOOR OF THE OCEANS

Based on Bathymetric studies by
Bruce C. Heezen and Marie Tharp
of the Lamont Doherty Geological Observatory
Columbia University Palisades, New York, 10964

SUPPORTED BY THE UNITED STATES NAVY
OFFICE OF NAVAL RESEARCH

This thesis is a collection of three papers examining problems related to the crustal structure, isostasy and subsidence history of aseismic ridges and mid-plate island chains. The basic objectives of this research are (a) to gain insight into the mechanical properties of the lithosphere by studying the manner in which lithosphere of different ages responds to these volcanic loads; (b) to examine the effect of hot spots on the thermal structure of the lithosphere by studying the subsidence history of aseismic ridges and mid-plate island chains.

We find that the isostasy of aseismic ridges require plate rigidities near spreading centers to be at least an order of magnitude less than that typically determined for old (>80 m.y.) oceanic lithosphere. The differences in isostasy between aseismic ridges and mid-plate island chains can, thus, be largely explained by the increasing rigidity of the lithosphere as it cools and thickens. The long-term subsidence of aseismic ridges and island/seamount chains can also be explained entirely by lithospheric cooling; there is no evidence for significant viscoelastic behavior of oceanic lithosphere. Aseismic ridges generally form near ridge crests; consequently, they subside at nearly the same rate as normal oceanic crust. Mid-plate island chains subside at slower rates because they are built on older crust. However, some mid-plate island chains subside faster than expected based on the age of the surrounding sea floor, probably because of lithospheric thinning over mid-plate hot spots.

* * *

Plate tectonics is based on a relatively simple mechanical model for the outer layers of the Earth in which a strong, rigid layer (lithosphere) overlies a weak layer (asthenosphere). The existence of the asthenosphere can be inferred from the gravitational compensation of surface loads. This compensation must be achieved by the lateral flow of material in a weak asthenospheric layer. A rigid lithosphere is required in order to support large surface mass inequalities, like mountain ranges, for many millions of years.

Studies of the response of the lithosphere to different surface loads have provided much information on the structure, thickness and rheology of the lithosphere. In the oceans these studies have been made for seamounts (Watts et al., 1975), seamount chains (Walcott, 1970a; Watts and Cochran, 1974) and at deep sea trenches (Hanks, 1971; Watts and Talwani, 1974; Parsons and Molnar, 1976). In these situations the oceanic lithosphere appears to respond to long-term ($>10^6$ yrs) surface loads as would a thin elastic plate overlying a weak fluid layer. The equilibrium vertical displacement, w, of the lithosphere under a load P is

$$D\nabla^4 w + \Delta\rho g w = P \qquad \text{(Walcott, 1970b)}$$

where D is the flexural rigidity of the lithosphere and $\Delta\rho$ is the difference in density between the displaced fluid (asthenosphere) and the material above the plate infilling the deflection (water, sediments, basalt, etc.). The flexural rigidity of an elastic plate is a measure of its resistance to bending and is principally determined by, T, the plate thickness (Walcott, 1970b):

$$D = \frac{ET^3}{12(1-\sigma^2)}$$

where E is Young's modulus and σ is Poisson's ratio. From these studies, the flexural rigidity of oceanic lithosphere has been estimated to fall in the range 5×10^{29} to 10^{31} dyn-cm. These rigidities correspond to effective elastic plate thicknesses of 18 to 48 km. These thicknesses are much less than the seismically determined thickness of the lithosphere. They represent, in essence, that part of the lithosphere that responds elastically to long-term ($>10^6$ yrs) surface loads.

Most of these flexural determinations have, however, been limited to older parts (>80 my) of the oceanic lithosphere. There is increasing evidence that the elastic properties of the lithosphere are temperature dependent. For example, McKenzie and Bowin (1976) have treated the irregularities of normal sea floor topography as a load created at a spreading center and have estimated a best fitting effective elastic plate thickness of ~10 km. This is considerably less than that typically determined for loads on old oceanic crust. Watts (in press) has argued that at temperatures above $450^{\circ} \pm 150^{\circ}$ C stresses in the lithosphere are relieved by plastic flow. Thus the hot, young lithosphere near mid-ocean ridges should be much weaker than the thicker and colder lithosphere in older parts of the ocean basins.

This should have a profound effect on the isostasy of aseismic ridges, which are generally believed to form at or near spreading centers. By studying the isostasy of aseismic ridges we can obtain information on the mechanical properties of young oceanic lithosphere. The isostasy of aseismic ridges is, however, still poorly known. Refraction data from aseismic ridges have been used to argue both for (Bott et al., 1971; Goslin and Sibuet, 1975) and against (Francis and Raitt, 1967) crustal thickening, and even though there is general agreement that aseismic

ridges are compensated at depth, several different isostatic models (Airy, Pratt or flexure) have been used to describe the manner in which these ridges are supported (compare Bott et al., 1971, with Bowin, 1973, and Kogan, 1976).

In Chapter 2 we have investigated the crustal structure of two prominent aseismic ridges, the Ninetyeast and Walvis Ridges, in order to place better constraints on their deep crustal structure and isostasy. In this study we have used linear transfer function techniques of analyzing gravity and bathymetry data similar to those previously used by McKenzie and Bowin (1976). This relatively new method of analyzing marine gravity data treats the free-air gravity and bathymetry data as time series. Using cross-spectral techniques a transfer function (or admittance) between gravity and bathymetry is computed, and this function is used to examine the state of isostasy of features along the profiles (see Appendix A). The advantage of these techniques is that they use observational data and are not based on any particular model of isostasy. The transfer functions can, however, be interpreted in terms of different isostatic models (McKenzie and Bowin, 1976).

From this analysis of gravity and bathymetry across the Ninetyeast and Walvis Ridges we draw the following conclusions:

1) The Ninetyeast Ridge and the eastern Walvis Ridge are locally compensated by an overthickening of the oceanic crust. Maximum crustal thicknesses beneath these ridges are estimated to be 15-30 km. The western Walvis Ridge is also compensated by crustal thickening; however, this part of the ridge is regionally supported by a lithosphere with an effective elastic

plate thickness of 5-8 km. This compares with elastic plate thicknesses of 20-30 km typically determined around Hawaii (Walcott, 1970; Watts and Cochran, 1974).

2) These results are consistent with the formation of the Ninetyeast and Walvis Ridges near spreading centers on lithosphere that is thin and weak with little or no elastic strength. The differences in isostasy and morphology between the eastern and western Walvis Ridge are attributed to an off-axis shift (relative to the Mid-Atlantic Ridge) of the "hot-spot" forming the Walvis Ridge beginning ~80 mybp.

3) Comparison of the wavelength and amplitude of gravity anomalies across aseismic ridges and mid-plate island chains indicate that the rigidity of the lithosphere increases by about an order of magnitude from ~10^{28} to 10^{29} dyn-cm near ridge crests to ~10^{29} to 10^{30} dyn-cm for lithosphere 90-100 my old. This increased rigidity is attributed entirely to the cooling and thickening of the lithosphere as it becomes older.

* * *

The long-term subsidence of oceanic islands has been known since the time of Darwin. Recent Deep Sea Drilling results from a number of different aseismic ridges indicate that these features have also experienced a long history of subsidence (Pimm et al., 1974; Vincent et al., 1974; Thiede, 1977). The simplest explanation for the widespread occurrence of atolls and guyots and the subsidence of aseismic ridges is that these features ride passively atop the underlying lithosphere and subside as

this lithosphere cools and thickens. In Chapter 3 the geological evidence for aseismic ridge subsidence is reviewed in the context of this simple model. From this study we have concluded:

1) At least five major aseismic ridges--the Ninetyeast Ridge, the Rio Grande Rise, the Walvis Ridge, the Chagos-Laccadive Ridge and the southeast Mascarene Plateau--have formed at or close to sea level and have since subsided at rates comparable to that of normal oceanic crust. Other aseismic ridges such as the Iceland-Faeroe Ridge and Broken Ridge have probably undergone a similar but more complicated subsidence history.

2) This long-term subsidence of aseismic ridges can be explained entirely by the cooling and thickening of the lithospheric plate on which these ridges are built. Since most aseismic ridges appear to have formed on very young lithosphere near spreading centers, their rates of subsidence are comparable to that of normal oceanic crust.

* * *

The long-term subsidence of island and seamount chains formed on older crust away from spreading centers should also be attributable to the cooling and thickening of the underlying lithosphere. That is, after an initial, relatively short period of rapid isostatic adjustments, these islands should subside at the same rate as the surrounding sea floor. The subsidence of western Pacific atolls and guyots has been well documented (Menard and Ladd, 1963); however, geological evidence from drilling on several of these atolls indicates their long-term

subsidence is much greater than this model would predict. In Chapter 4 these data are presented and several possible explanations for this excess subsidence are discussed. We conclude:

1) This excess subsidence cannot be explained by isostatic adjustments either to the weight of the volcano or the weight of the coral reef cap. It also cannot be explained by visco-elastic flexure of the underlying lithosphere.

2) This excess subsidence is apparently related to island formation atop areas of anomalously shallow sea floor, such as the Hawaiian swell, associated with mid-plate hot spots. As this sea floor returns to its normal depth, the islands subside an extra amount equal to the original height of the swell.

3) The Hawaiian swell is caused by lithospheric thinning over the Hawaiian hot spot. Since the lithosphere is denser than the asthenosphere, this thinning results in broad regional isostatic uplift. As the lithosphere moves away from the hot spot, it cools and thickens, and the swell disappears. The subsidence of the Hawaiian swell and a number of western Pacific atolls is in quantitative agreement with this model. The model also satisfies gravity data over the Hawaiian swell which appear to require compensation in the lower half of the lithosphere.

* * *

These three studies demonstrate that the thermal and mechanical properties of the lithosphere largely determine the state of isostasy and subsidence history of both aseismic ridges and mid-plate island chains. Additional studies of how lithosphere of various ages responds to these and other volcanic loads can provide new insight into the thermal and mechanical evolution of the lithosphere. Perhaps the most exciting result of this work is the evidence found for lithospheric thinning over the Hawaiian hot spot. This model, if correct, has major implications both for lithospheric and mantle convection studies as well as the origin of continental rift systems. It has also pointed out the need for additional geophysical data on the origin of hot-spot related swells both in the oceans (Hawaii, Cook-Austral, Iceland) and on the continents (East African rifts, Rhine graben, Lake Baikal). Surface wave studies and the analysis of long wavelength free-air gravity and geoidal height anomalies probably offer the best hope of resolving the deep lithospheric structure associated with these features.

REFERENCES

Bott, M. H. P., C. W. A. Browitt, and A. P. Stacey, The deep structure of the Iceland-Faeroe Ridge, Mar. Geophys. Res., 1, 328-351, 1971.

Bowin, C., Origin of the Ninety East Ridge from studies near the Equator, J. Geophys. Res., 78, 6029-6043, 1973.

Francis, T. J. G., and R. W. Raitt, Seismic refraction measurements in the southern Indian Ocean, J. Geophys. Res., 72, 3015-3041, 1967.

Goslin, J., and J. C. Sibuet, Geophysical study of the easternmost Walvis Ridge, South Atlantic: Deep structure, Geol. Soc. Am. Bull., 86, 1713-1724, 1975.

Hanks, T. C., The Kuril trench Hokkaido rise system: Large shallow earthquakes and simple models of deformation, Geophys. J. Roy. astr. Soc., 23, 173-189, 1971.

Kogan, M. G., The gravity field of oceanic block ridges, Izvestiya, Physics of the Solid Earth, 12, 710-717, 1976.

McKenzie, D. P., and C. Bowin, The relationship between bathymetry and gravity in the Atlantic Ocean, J. Geophys. Res., 81, 1903-1915, 1976.

Menard, H. W., and H. S. Ladd, Oceanic islands, seamounts, guyots and atolls, in The Sea, vol. 3, edited by A. E. Maxwell, pp. 365-387, Interscience, New York, 1963.

Molnar, P., and T. Atwater, Relative motion of hot spots in the mantle, Nature, 246, 288-291, 1973.

Morgan, W. J., Plate motions and deep mantle convection, in Studies in Earth and Space Sciences (Hess volume), edited by R. Shagam et al., Geol. Soc. Amer. Mem. 132, 7-22, 1972.

Parsons, B., and P. Molnar, The origin of outer topographic rises associated with trenches, Geophys. J. Roy. astr. Soc., 45, 707-712, 1976.

Pimm, A. C., B. McGowran and S. Gartner, Early sinking history of the Ninetyeast Ridge, Northeastern Indian Ocean, Geol. Soc. Am. Bull., 85, 1219-1224, 1974.

Thiede, J., Subsidence of aseismic ridges: Evidence from sediments on Rio Grande Rise (Southwest Atlantic Ocean), Am. Assoc. Petrol. Geol. Bull., 61, 929-940, 1977.

Vincent, E., J. M. Gibson and L. Bran, Paleocene and early Eocene microfacies, benthonic foraminifera, and paleobathymetry of Deep Sea Drilling Project Sites 236 and 237, western Indian Ocean, in Fisher, R. L., Bunce, E. T., et al., Initial Reports of the Deep Sea Drilling Project, 24, 1974.

Walcott, R. I., Flexure of the lithosphere at Hawaii, Tectonophysics, 9, 435-446, 1970a.

Walcott, R. I., Flexural rigidity, thickness and viscosity of the lithosphere, J. Geophys. Res., 75, 3941-3954, 1970b.

Watts, A. B., An analysis of isostasy in the world's oceans: Part 1--Hawaiian-Emperor seamount chain, submitted to J. Geophys. Res.

Watts, A. B., and J. R. Cochran, Gravity anomalies and flexure of the lithosphere along the Hawaiian-Emperor seamount chain, Geophys. J. R. astr. Soc., 38, 119-141, 1974.

Watts, A. B., and M. Talwani, Gravity anomalies seaward of deep-sea trenches and their tectonic implications, Geophys. J. R. astr. Soc., 36, 57-90, 1974.

Watts, A. B., J. R. Cochran and G. Selzer, Gravity anomalies and flexure of the lithosphere: A three-dimensional study of the Great Meteor Seamount, Northeast Atlantic, J. Geophys. Res., 80, 1391-1398, 1975.

Wilson, J. T., Evidence from islands on the spreading of ocean floors, Nature, 197, 536-538, 1963.

Wilson, J. T., Mantle plumes and plate motions, Tectonophysics, 19, 149-164, 1973.

CHAPTER 2

AN ANALYSIS OF ISOSTASY AT ASEISMIC RIDGES

AN ANALYSIS OF ISOSTASY IN THE WORLD'S OCEANS: PART 3--ASEISMIC RIDGES*

Robert S. Detrick
Woods Hole Oceanographic Institution
Woods Hole, MA 02543
Massachusetts Institute of Technology
Cambridge, MA 02139

A. B. Watts
Lamont-Doherty Geological Observatory
and Department of Geological Sciences
of Columbia University
Palisades, New York 10964

*Submitted to Journal of Geophysical Research.

ABSTRACT

Cross-spectral estimation techniques have been used to analyze the relationship between gravity and bathymetry on 26 profiles across the Walvis and Ninetyeast Ridges. The resulting filters or transfer functions have been used to study the state of isostasy at these ridges. Transfer functions for the eastern Walvis Ridge and the Ninetyeast Ridge profiles can be best explained by an Airy-type thickening of the crust beneath these ridges. The crustal thicknesses required are in the range 15 to 25 km, in good agreement with available seismic refraction data. The transfer function for the western Walvis Ridge can be best explained by a flexure model in which the oceanic lithosphere is treated as a thin elastic plate overlying a weak fluid. The elastic plate thicknesses required are 5 to 8 km. These plate thicknesses are substantially less than those typically determined from flexural studies of loads on older crust, but are similar to estimates determined for sea floor topography at mid-ocean ridges. These observations are consistent with the formation of aseismic ridges near spreading centers on lithosphere that is young, thin and relatively weak. The differences in isostasy between the eastern and western Walvis Ridge are attributed to an off-axis shift relative to the South Atlantic spreading center of the "hot spot" forming the Walvis Ridge about 80 m.y.B.P. These observations suggest that the isostatic parameters determined for these aseismic ridges were "frozen in" at the time of their formation at or near a spreading center and have not significantly changed through time.

INTRODUCTION

Scattered throughout the ocean basins are various ridge and plateau-like features that stand 2-3 km shallower than the surrounding sea floor. Some of these features such as Jan Mayen Ridge, Seychelles and Rockall Plateau are clearly continental in structure and probably were isolated by the processes of rifting and sea floor spreading. More difficult to explain are features such as the Ninetyeast Ridge, the Walvis Ridge or the Rio Grande Rise, which are composed mainly of basaltic (volcanic) rocks. These ridges, which are noticeably free of earthquake activity, have been called aseismic ridges (Laughton et al., 1970). While various models have been proposed for the origin of aseismic ridges, there is increasing evidence that many aseismic ridges have formed from "hot spots" centered on or near a mid-ocean ridge (Wilson, 1963; Morgan, 1971).

Deep Sea Drilling results from aseismic ridges have confirmed their volcanic nature and have demonstrated that basement ages along many aseismic ridges vary systematically along their length and are approximately the same as the surrounding sea floor (von der Borch, C. C., Sclater, J. G., et al., 1974; Davies, T. A., Luyendyk, B. P., 1974; Perch-Nielson, K., Supko, P. R., et al., 1975; Bolli, H. M., Ryan, W. B. F., et al., 1975). Sediments recovered from aseismic ridges indicate they have experienced a long history of subsidence. The oldest sediments indicate shallow water, even subaerial conditions, followed by progressively deeper water and more open marine depositional environments (Pimm et al., 1974; Vincent et al., 1974; Thiede, 1977). The rates of subsidence are similar to that of normal oceanic crust (Detrick et al., 1977).

FIGURE 1

Summary of published seismic refraction data from aseismic ridges. Also shown for reference is a typical oceanic crustal section and an interpretation of the crustal structure beneath Iceland. Velocities are in km/sec; parentheses indicate unreversed velocities; asterisks indicate assumed velocities.

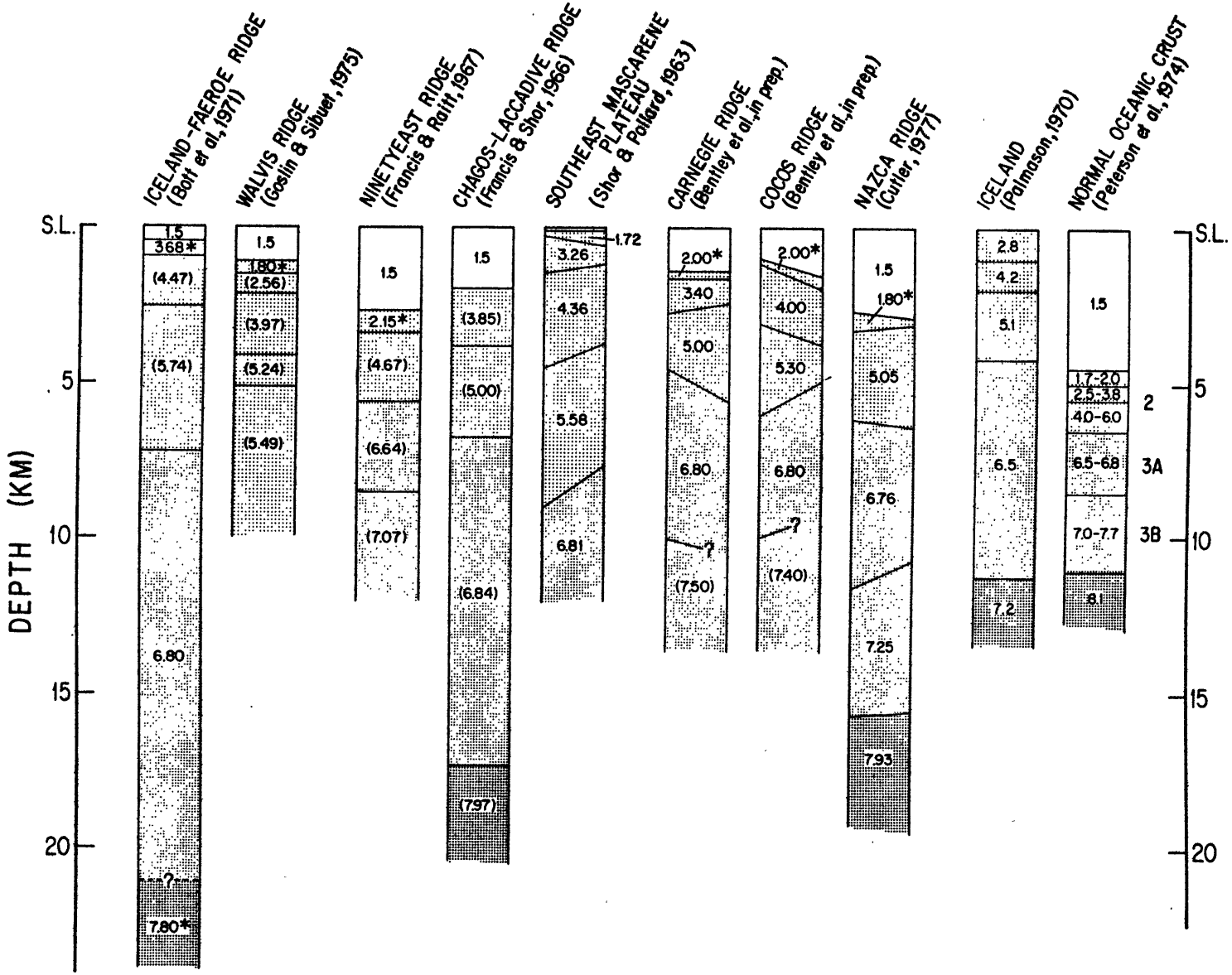
ICELAND-FAEROE RIDGE (Bott et al, 1971)
WALVIS RIDGE (Goslin & Sibuet, 1975)
NINETYEAST RIDGE (Francis & Raitt, 1967)
CHAGOS-LACCADIVE RIDGE (Francis & Shor, 1966)
SOUTHEAST MASCARENE PLATEAU (Shor & Pollard, 1963)
CARNEGIE RIDGE (Bentley et al, in prep.)
COCOS RIDGE (Bentley et al, in prep.)
NAZCA RIDGE (Cutler, 1977)
ICELAND (Palmason, 1970)
NORMAL OCEANIC CRUST (Peterson et al, 1974)
DEPTH (KM)
S.L.
5
10
15
20
1.5
3.68*
(4.47)
(5.74)
6.80
?
7.80*
1.80*
(2.56)
(3.97)
(5.24)
(5.49)
2.15*
(4.67)
(6.64)
(7.07)
(3.85)
(5.00)
(6.84)
(7.97)
3.26
1.72
4.36
5.58
6.81
2.00*
3.40
5.00
6.80
(7.50)
4.00
5.30
(7.40)
1.80*
5.05
6.76
7.25
7.93
2.8
4.2
5.1
6.5
7.2
1.7-2.0
2.5-3.8
4.0-6.0
6.5-6.8
7.0-7.7
8.1
2
3A
3B

The deep crustal structure of aseismic ridges, however, remains poorly known despite a number of seismic refraction experiments (Figure 1). Mantle-type velocities have only been identified beneath three aseismic ridges, the Chagos-Laccadive Ridge, the Iceland-Faeroe Ridge and the Nazca Ridge. Only one of these velocities (Nazca Ridge) was a reversed determination. Deep refraction data are unavailable from many aseismic ridges including the Walvis Ridge, the Rio Grande Rise and the Cocos and Carnegie Ridges. Even where refraction data are available the results show considerable variability, especially in shallow crustal structure (Figure 1). Francis and Shor (1966) reported "Moho" beneath the Chagos-Laccadive Ridge at depths of about 17 km. Similar mantle depths have been reported beneath the Iceland-Faeroe Ridge (16-18 km) by Bott et al. (1971) and the Nazca Ridge (16 km) by Cutler (1977). Since the depth to "Moho" in normal oceanic crust is 9-11 km, these studies indicate crustal thickening of ~8-10 km beneath aseismic ridges. However, Francis and Raitt (1967) argued against crustal thickening beneath the Ninetyeast Ridge. They interpreted their refraction data as indicating about the same crustal thickness beneath the ridge as in the adjacent Wharton Basin and suggested the Ninetyeast Ridge was a horst-type structure underlain by low-velocity (7.1 km/sec) mantle material.

Because of the lack of reliable deep refraction data from many aseismic ridges, most information on their deep crustal structure has been inferred from gravity studies. Free-air gravity anomalies over aseismic ridges are generally small in amplitude indicating that the ridges are in approximate isostatic equilibrium. Bott et al. (1971) found, for example, that the small free-air gravity high (~20 mgal) over the Iceland-Faeroe

Ridge could be best explained by an Airy-type thickening of the crust. The amount of thickening deduced was about 8 km, in general agreement with seismic refraction results. Goslin and Sibuet (1975) and Kogan (in preparation) have interpreted gravity data over the Walvis Ridge also in terms of a thickening of the crust. The main difference in these studies is the model of isostasy which is preferred. Goslin and Sibuet (1975) found their gravity data could be best explained by an Airy-type model of local compensation, while Kogan (in preparation) preferred a regional compensation model for the ridge. The amount of crustal thickening deduced was about 10-15 km for the Airy model and about 7-10 km for the regional (flexural) case. However, Bowin (1973) suggested a different compensation mechanism for the Ninetyeast Ridge. He proposed a Pratt-type model of compensation in which the ridge is supported by an emplacement of gabbro and serpentinized peridotite beneath normal crustal layers rather than by a thickening of the crust. In his preferred model (Bowin, 1973; Figure 7), the thickness of the layers of normal crust beneath the ridge is about the same (or slightly less) than in the adjacent ocean basin and intermediate density material (gabbro and serpentinized peridotite) extends to depths of about 25 km.

These previous seismic refraction and gravity studies suggest a number of outstanding problems. They include: (1) the overall structure of aseismic ridges and whether or not the crust is thicker beneath the ridges than in the adjacent ocean basins, (2) the state of isostasy of the ridges and whether or not an Airy, Pratt or flexure model best describes the manner in which the ridges are supported and (3) the origin of the ridges and whether or not they formed near mid-ocean ridge crests.

A useful approach to these problems can be made by using linear transfer function techniques of analyzing gravity and bathymetry data, similar to those previously used by Lewis and Dorman (1970), Dorman and Lewis (1970) and McKenzie and Bowin (1976). These techniques examine the relationship of gravity and bathymetry as a function of wavelength. The resulting transfer function (or admittance) contains information on the mechanism of isostasy. The advantage of these techniques is that they use observational data and are not based on any particular model of isostasy. The transfer function can, however, be interpreted in terms of different isostatic models and may in some cases be used to distinguish between them.

The purpose of this paper is to apply linear transfer function techniques to the study of isostasy at aseismic ridges. One limitation of many previous studies is that the transfer functions have been calculated over rather broad regions comprising different tectonic provinces. Therefore we have used a modification of the techniques previously described by Dorman and Lewis (1970), Lewis and Dorman (1970) and McKenzie and Bowin (1976) designed to study isostasy over a single two-dimensional geological feature. This method, which has been presented by Watts (in preparation), differs from these earlier techniques in that cross-spectral rather than Wiener filtering techniques are used to compute the transfer function and in that many profiles of gravity and bathymetry over the same geological feature are used to obtain smooth spectral estimates. The three main objectives of this work are (1) to determine the transfer function which describes the relationship between gravity and bathymetry over aseismic ridges, (2) to interpret this transfer function in terms of

various isostatic models and (3) to use the preferred model of isostasy to provide new constraints on the origin of aseismic ridges.

DATA SOURCES AND ACCURACY

In this study we have used 26 gravity and bathymetry profiles across two prominent aseismic ridges, the Walvis Ridge in the eastern South Atlantic and the Ninetyeast Ridge in the Indian Ocean. These ridges were chosen primarily because of the large amount of available gravity data. Most of the data used in this study have not been previously published.

The ship's tracks along which these data were collected are shown in Figures 2 and 4. The data sources and information on instruments and navigation are presented in Table 1. The overall accuracy of the gravity measurements depends on the type of instrument and navigation used. Generally the accuracy is estimated to be 2 to 5 mgal for the Gss2 sea gravimeter and the vibrating-string gravimeter when used with satellite navigation. Somewhat larger errors are expected for those data collected using celestial navigation. The gravity anomalies were reduced to the International Reference Ellipsoid (flattening = 1/297.0); however, the choice of a reference ellipsoid is not important since the mean and trend were removed before the data were Fourier transformed.

DATA DESCRIPTION

Ninetyeast Ridge

The Ninetyeast Ridge (Figure 2) is a remarkably linear, 5000 km long aseismic ridge striking approximately NNE along the 90th meridian from

TABLE 1

SUMMARY OF NAVIGATION AND INSTRUMENTATION

PROFILE	SHIP	YEAR	CRUISE & LEG	GRAVIMETER	STABLE PLATFORM	NAVIGATION	CROSS-COUPLING
Ninetyeast Ridge							
1	Argo	1963	LU14	LaCoste-Romberg	Gimbal mounted	Celestial	-
2,7	Robert D. Conrad	1971	1402	Graf-Askania Gss2	Anschütz	Satellite	Yes
3,4,6,8	Chain	1971	100-6	VSA	Sperry Gyrotable	Satellite	-
5	Vema	1976	3308	Graf-Askania Gss2	Aeroflex	Satellite	Yes
9	Vema	1971	2901	Graf-Askania Gss2	Aeroflex	Satellite	Yes
10	Vema	1976	3305	Graf-Askania Gss2	Aeroflex	Satellite	Yes
11	Atlantis	1976	93-11	VSA	Sperry Gyrotable	Satellite	-
12	Argo	1960	MN05	LaCoste-Romberg	Gimbal Mounted	Celestial	-
13	Vema	1963	1909	Graf-Askania Gss2	Alidade	Celestial	No
14	Vema	1962	1811	Graf-Askania Gss2	Alidade	Celestial	No
Walvis Ridge							
1,5	Vema	1963	1912	Graf-Askania Gss2	Alidade	Celestial	No
2	Vema	1964	2011	Graf-Askania Gss2	Alidade	Celestial	No
3	Atlantis	1972	67-5	VSA	Sperry Gyrotable	Satellite	-
4	Atlantis	1972	67-2	VSA	Sperry Gyrotable	Satellite	-
6,10,12	Robert D. Conrad	1970	1313	Graf-Askania Gss2	Anschütz	Satellite	No
7,9	Vema	1970	2712	Graf-Askania Gss2	Alidade	Satellite	Yes
8	Robert D. Conrad	1963	0801	Graf-Askania Gss2	Anschütz	Celestial	No
11	Vema	1962	1809	Graf-Askania Gss2	Alidade	Celestial	No

FIGURE 2

Location of free-air gravity anomaly and bathymetry profiles across the Ninetyeast Ridge used in this study. The thin lines indicate the actual ship track while thick lines represent the projected profiles. Magnetic anomalies (dots) and fracture zones (long dashes) after Sclater and Fisher (1974), Sclater and others (1976) and Pierce (1977). The bathymetry is based on a map by Sclater and Fisher (1974).

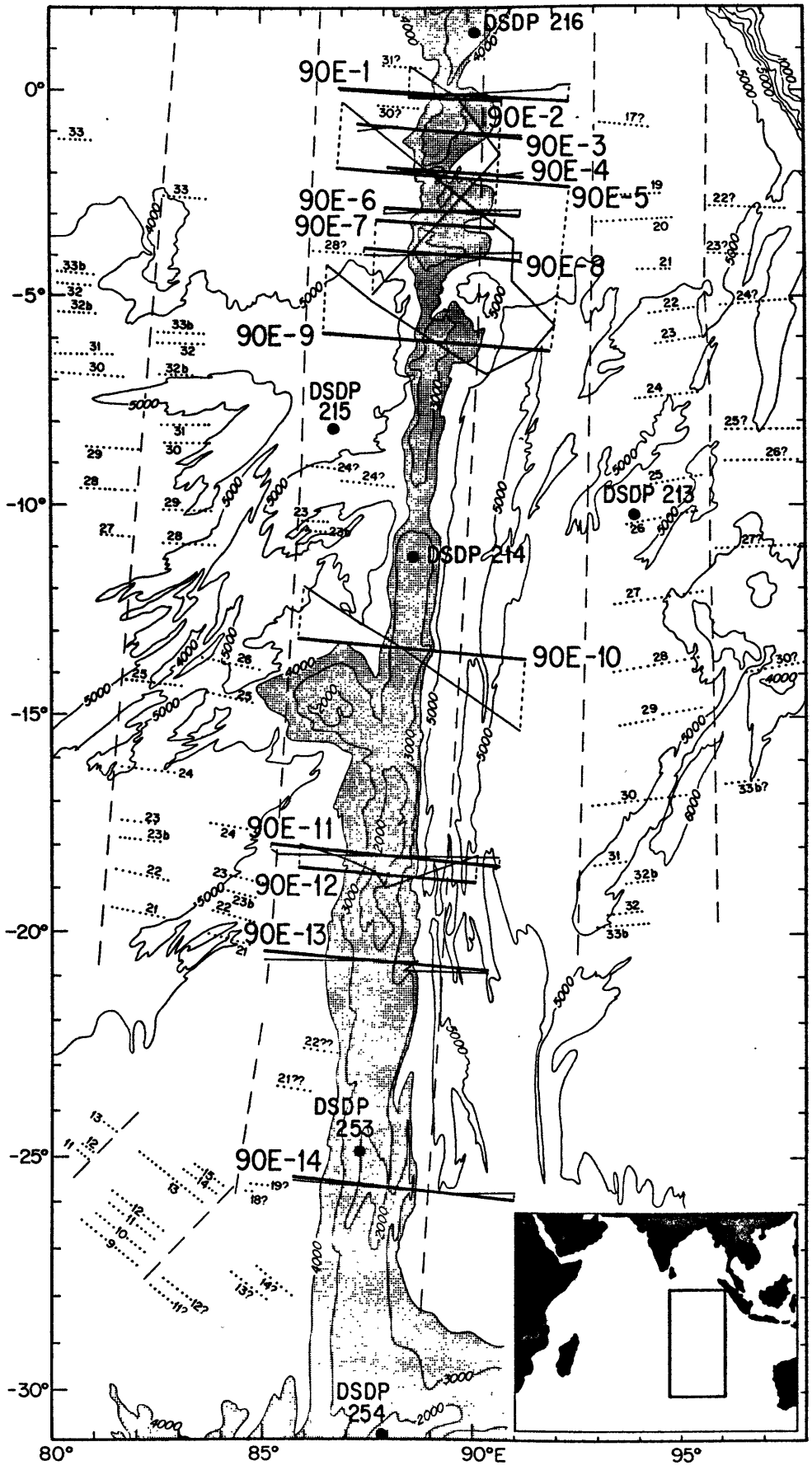
DSDP 216
90E-1
90E-2
90E-3
90E-4
90E-5
90E-6
90E-7
90E-8
90E-9
DSDP 215
DSDP 213
DSDP 214
90E-10
90E-11
90E-12
90E-13
DSDP 253
90E-14
DSDP 254
0°
-5°
-10°
-15°
-20°
-25°
-30°
80°
85°
90°E
95°

about 31°S until it is buried by the sediments of the Bengal Fan near 9°N. Sclater and Fisher (1974) found that the crust east of the ridge becomes older to the south while the crust west of the ridge becomes older to the north. The ages of the oldest sediments recovered at DSDP sites on the ridge increase from Oligocene (22.5 to 37.5 m.y.) at Site 254 (Davies, T. A., Luyendyk, B. P., et al., 1974) to Campanian (71 to 82 m.y.) at Site 217 (von der Borch, C. C., Sclater, J. G., et al., 1974) indicating that the Ninetyeast Ridge also progressively increases in age to the north. These ages are similar to oceanic crust to the west, suggesting the Ninetyeast Ridge has always been part of the Indian plate (Sclater and Fisher, 1974).

The 14 gravity and bathymetry profiles across the Ninetyeast Ridge used in this study are shown in Figure 3. These profiles illustrate the asymmetric, blocky nature of the Ninetyeast Ridge. It is typically 200-300 km wide and averages about 2 km shallower than the surrounding sea floor. Sediment cover on the ridge is patchy with locally thick accumulations of sediment; however, steeper slopes are almost sediment free. A positive free-air gravity anomaly is associated with the ridge. It is small in amplitude, generally not exceeding 75 mgal peak to peak, indicating that the ridge is compensated at depth (Bowin, 1973).

Large, steep scarps are common on many profiles suggesting that block faulting has contributed to the formation of ridge topography. Several of these scarps have relief in excess of 2000 m. While the steepest, largest scarps often occur on the eastern flank of the ridge (Profiles 90E-2, 90E-4, 90E-11, 90E-13, 90E-14, Figure 3), it is almost equally common for the largest scarps to occur on the western ridge flank (Profiles 90E-1, 90E-3, 90E-8, 90E-10 and 90E-12, Figure 3). On some profiles there

FIGURE 3

Projected free-air gravity anomaly and bathymetry profiles across the Ninetyeast Ridge. Location of profiles shown in Figure 2. Acoustic basement indicated by shading where seismic reflection data are available.

NINETYEAST RIDGE

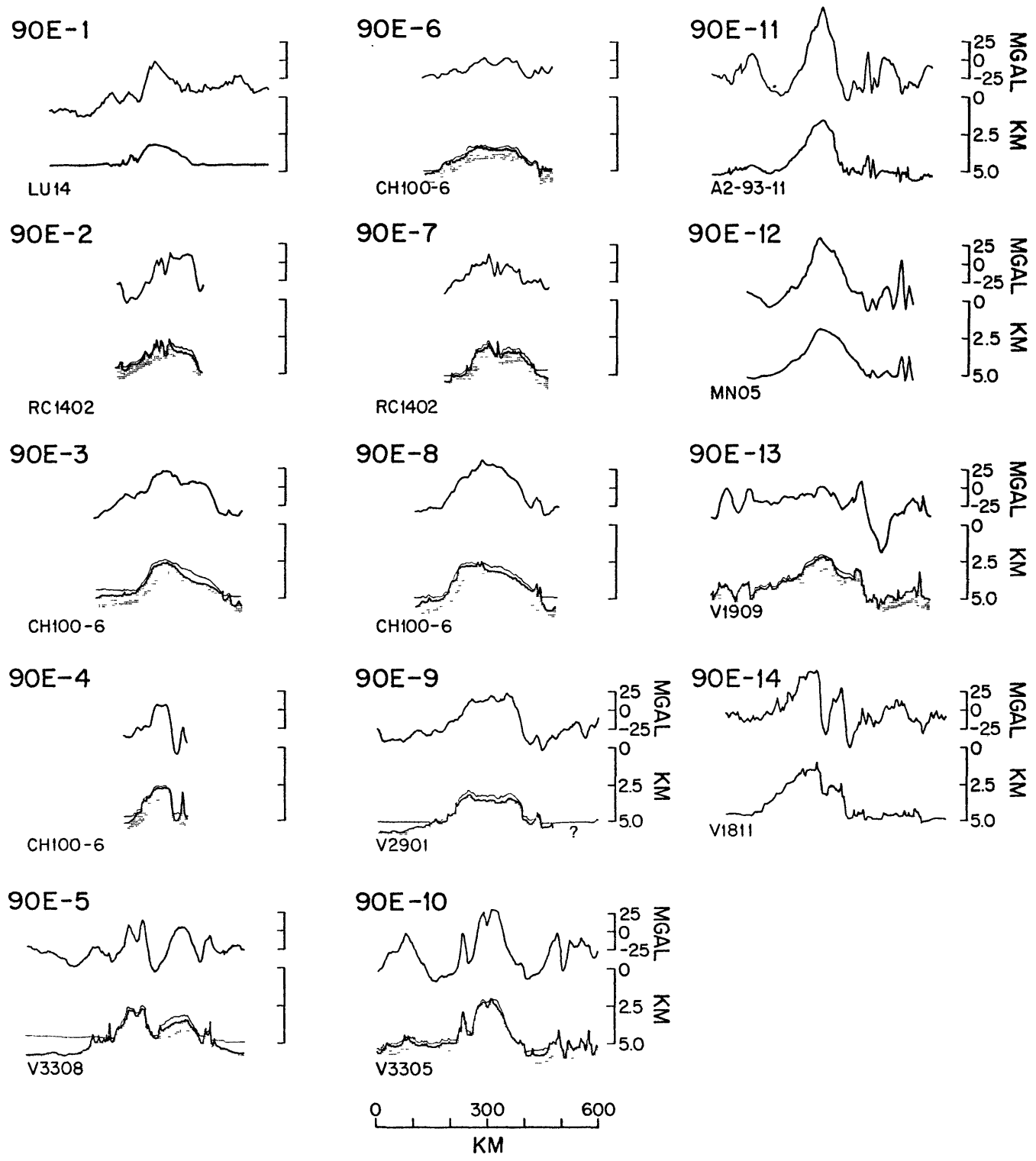

is little or no indication for large scale faulting (Profiles 90E-5, 90E-6, Figure 3), an observation which led Bowin (1973) to suggest that block faulting was only a secondary process in forming the ridge topography.

Walvis Ridge

The Walvis Ridge extends WSW some 2800 km from the South West African continental margin to the Mid-Atlantic Ridge near Tristan da Cunha and Gough Islands (Figure 4). The eastern part of the Walvis Ridge (east of 3^{o}E) has a continuous block-like structure with several distinct segments trending at nearly right angles. Further west the ridge develops into two branches, one trending N-S and the other trending NE-SW, both composed of individual seamounts, guyots or short elongate ridges. The N-S trending branch disappears near 34^{o}S; however, the other branch continues WSW to the eastern flank of the Mid-Atlantic Ridge.

The location of the 12 gravity and bathymetry profiles from the Walvis Ridge used in this study are shown in Figure 4. Profiles 1-5 cross a 400 km long, continuous N-S trending segment of the eastern Walvis Ridge located near 6^{o}E. These profiles, shown in Figure 5, indicate this part of the Walvis Ridge has an asymmetric blocky cross-section remarkably similar to the Ninetyeast Ridge. It is typically 200-300 km wide with a steep eastern flank and a gentler, sediment-covered western flank. Evidence for large scale block faulting is common on many profiles. Like the Ninetyeast Ridge, this part of the Walvis Ridge is associated with only a small positive free-air gravity anomaly, generally not exceeding 75 mgal in amplitude. This gravity high is flanked by smaller amplitude gravity lows (~25 mgal) which return to near zero values within 50 to 100 km of the ridge axis.

FIGURE 4

Location of free-air gravity anomaly and bathymetry profiles across the Walvis Ridge used in this study. The thin lines indicate the actual ship track while thick lines represent projected profiles. Magnetic anomalies (dots) and fracture zones (long dashes) after Ladd (1974) and Rabinowitz and LaBreque (in press). The bathymetry is based on a map by Uchupi and Hays (1978).

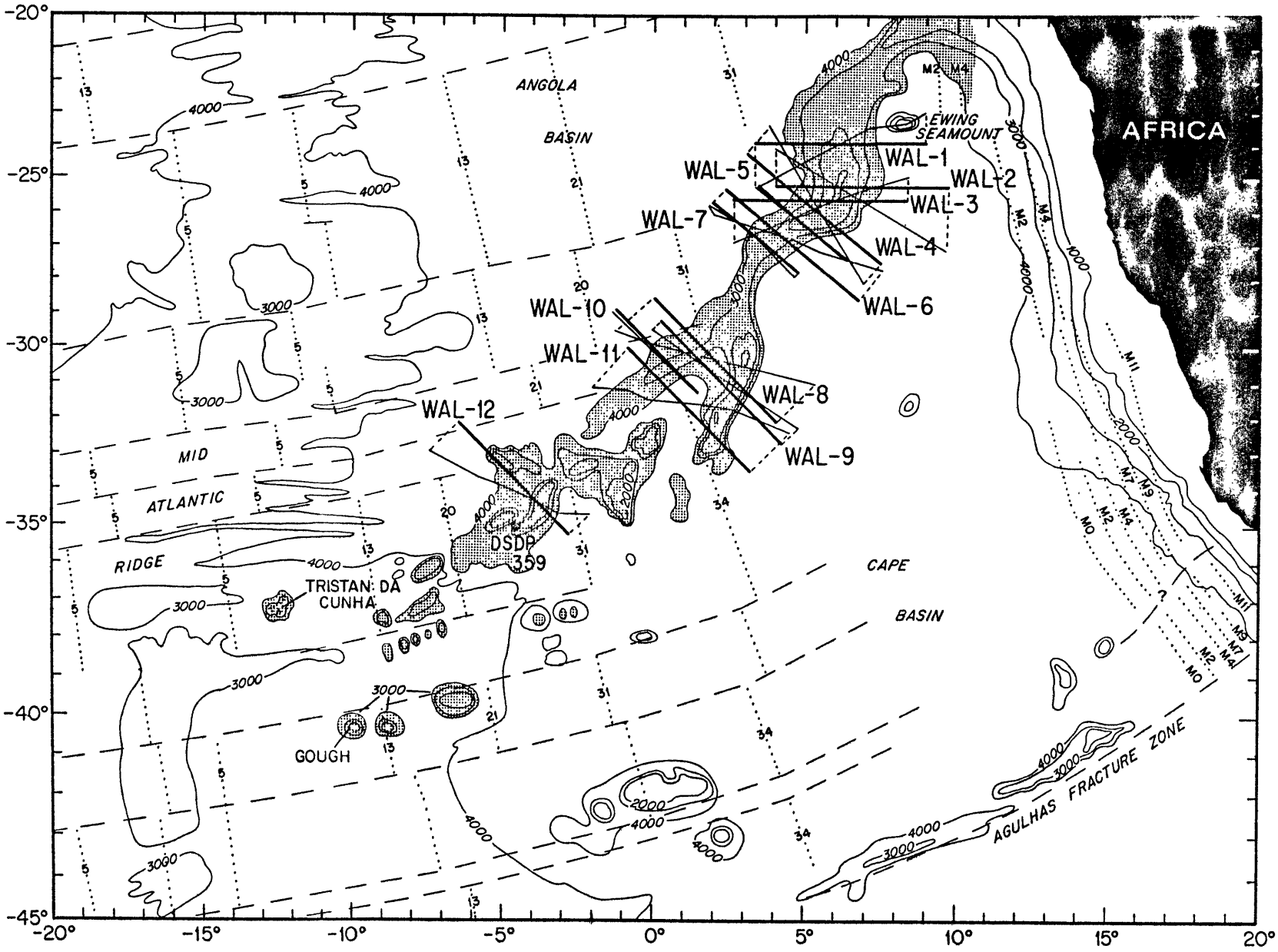
AFRICA
ANGOLA
BASIN
MID
ATLANTIC
RIDGE
CAPE
BASIN
EWING
SEAMOUNT
WAL-1
WAL-2
WAL-3
WAL-4
WAL-5
WAL-6
WAL-7
WAL-8
WAL-9
WAL-10
WAL-11
WAL-12
DSDP
359
TRISTAN DA
CUNHA
GOUGH
AGULHAS FRACTURE ZONE
-20°
-25°
-30°
-35°
-40°
-45°
-20°
-15°
-10°
-5°
0°
5°
10°
15°
20°

FIGURE 5

Projected free-air gravity anomaly and bathymetry profiles across the Walvis Ridge. Location of profiles shown in Figure 4. Acoustic basement indicated by shading where seismic reflection data available.

WALVIS RIDGE

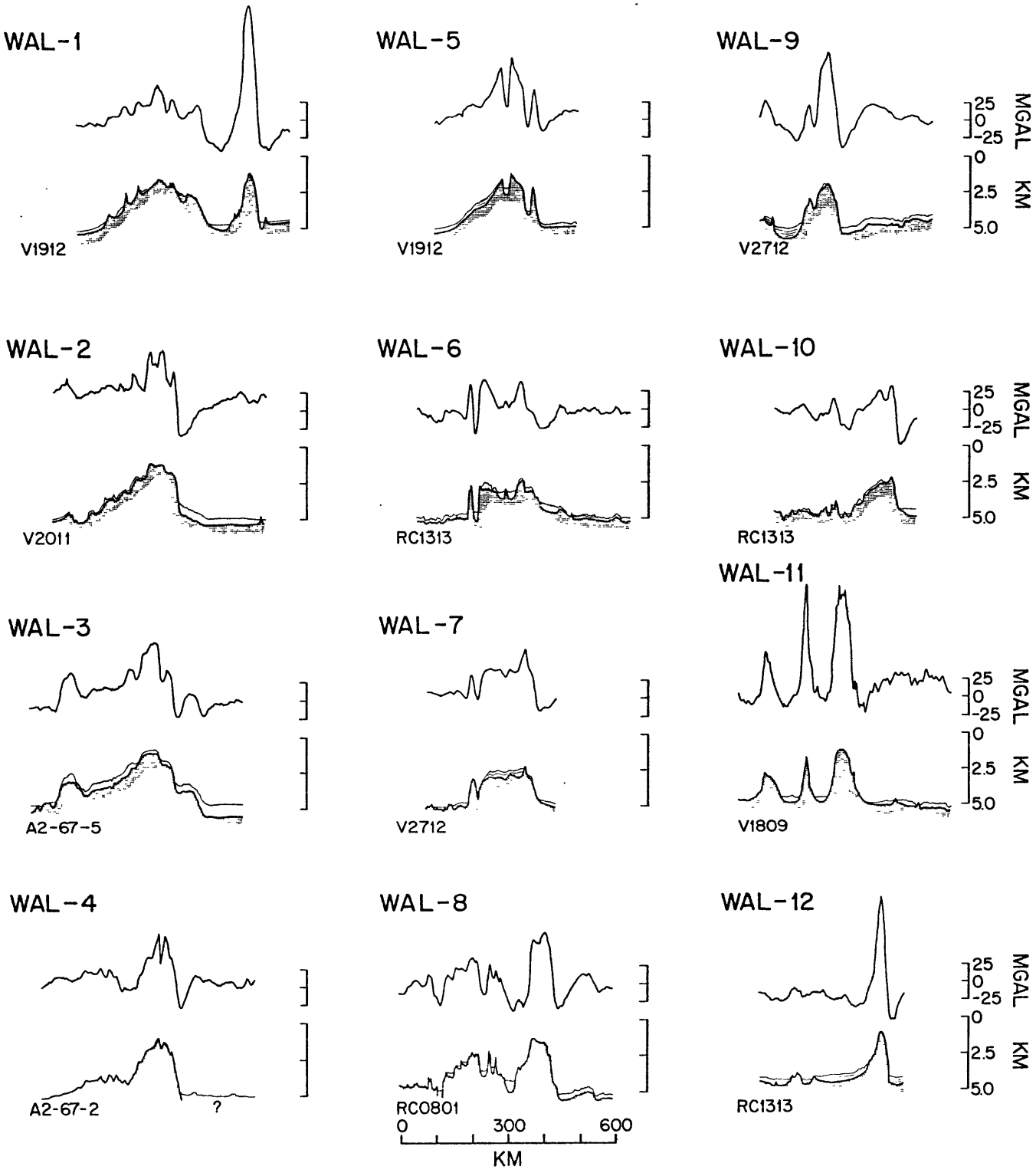

Profiles WAL-6 and WAL-7 (Figure 5) cross the central Walvis Ridge near 27°S. The ridge in this area is similar in morphology to the ridge farther east, although it is slightly deeper and more symmetric in cross-section. West of 3°E the Walvis Ridge develops into two seamount and guyot chains. The easterly branch is the more prominent with rounded or elongate peaks often rising to depths of less than 1000 m while the western branch is composed mostly of isolated seamounts and guyots (Connary, 1972; Dingle and Simpson, 1976). Profiles WAL-8 to WAL-12 all cross the western Walvis Ridge; however, most of the profiles are located between 30° and 34°S near where the ridge bifurcates. One striking feature of these crossings is the much higher amplitude free-air gravity anomalies associated with the ridge in this area. These anomalies are generally 100-150 mgal peak to peak or about twice the typical amplitude of anomalies over the eastern Walvis Ridge.

DATA ANALYSIS

The basic computational procedure involved in applying transfer function techniques to these data has been discussed by McKenzie and Bowin (1976) and Watts (in preparation) and will only be briefly summarized here.

We wish to obtain a filter which when applied to an observed bathymetry profile converts it to a series which resembles the observed gravity. The wavenumber (or frequency) domain representation of this filter is the complex admittance $Z(k_n)$ defined simply as

$$Z(k_n) = \frac{G(k_n)}{B(k_n)} \qquad (1)$$

where $G(k_n)$ and $B(k_n)$ are the discrete Fourier transforms of the gravity and bathymetry and k_n is the wavenumber ($k_n = 2\pi/\lambda$). In the presence of noise a better estimate of the admittance is given (McKenzie and Bowin, 1976) by

$$Z(k_n) = \frac{G(k_n) \cdot B(k_n)^*}{B(k_n) \cdot B(k_n)^*} \qquad (2)$$

where * indicates the complex conjugate. In this case the admittance is the cross spectrum of gravity and bathymetry divided by the power spectrum of the bathymetry. In order to reduce the noise in this estimate of the admittance some form of spectral smoothing is required. In this study the smoothing has been accomplished by using many profiles over the same geological feature. Each profile represents an independent estimate of the cross spectrum and power spectrum of gravity and bathymetry. These spectra are summed and the resulting averaged spectra used to obtain a single admittance function for the feature. This admittance is based completely on the observed relationship between gravity and bathymetry and is not tied to any particular isostatic model. However, it can easily be compared with isostatic models based on different compensation mechanisms (McKenzie and Bowin, 1976).

The Ninetyeast Ridge and the Walvis Ridge were treated as separate data sets. Each gravity and bathymetry profile was projected normal to the local trend of the ridge and interpolated at a 2.3 km interval. The profiles extended 300 km on either side of the ridge axis; shorter profiles were extended out to this length in order to be included in the study. Both mean and trend were removed and a cosine bell taper applied to the first and last 5% of each profile before the time series were Fourier

transformed. These profiles were then used to calculate the complex admittance $Z(k_n)$ for each ridge using the spectral smoothing techniques outlined above.

The calculated admittance functions (amplitude and phase) are plotted against wavenumber in Figure 6 for the Ninetyeast Ridge and Figure 7 for the Walvis Ridge. Also plotted is the coherence $\gamma^2(k_n)$. The coherence is a measure of that portion of the observed gravity that can be directly attributed to the bathymetry. An estimate of the coherence is given (Munk and Cartwright, 1966) by

$$\gamma^2 = (N(cc^*/E_G E_B)-1)/(N-1) \qquad (3)$$

where $c = c(k_n)$ is the complex cross spectrum of gravity and bathymetry, E_G and E_B are the power spectra of gravity and bathymetry respectively and N is the total number of profiles. The coherence is high ($\gamma^2>0.5$) for wavelengths longer than about 20 km reflecting the fact that a significant portion of the energy in the observed gravity can be attributed to the bathymetry.

The admittance phase, $\phi(k_n)$, is close to zero for $\lambda>20$ km implying that the admittance at these wavelengths is real. The relative smoothness of the $\log_{10}$ admittance curve for $\lambda>20$ km is evidence that the same signal was present in each profile and that the smoothing procedure satisfactorily reduces noise. The $\log_{10}$ admittance curve peaks at wavelengths of about 100 km and decreases linearly to wavelengths of 10-20 km. This reflects the increasing attenuation of the gravity signal from short wavelength topography. The decrease in the amplitude of the admittance at long wavelengths reflects the effects of isostatic compensation.

FIGURE 6

The coherence, $\log_{10}$ admittance amplitude, admittance phase, and filter generated from the gravity and bathymetry profiles shown in Figures 2 and 3 from the Ninetyeast Ridge.

NINETYEAST RIDGE

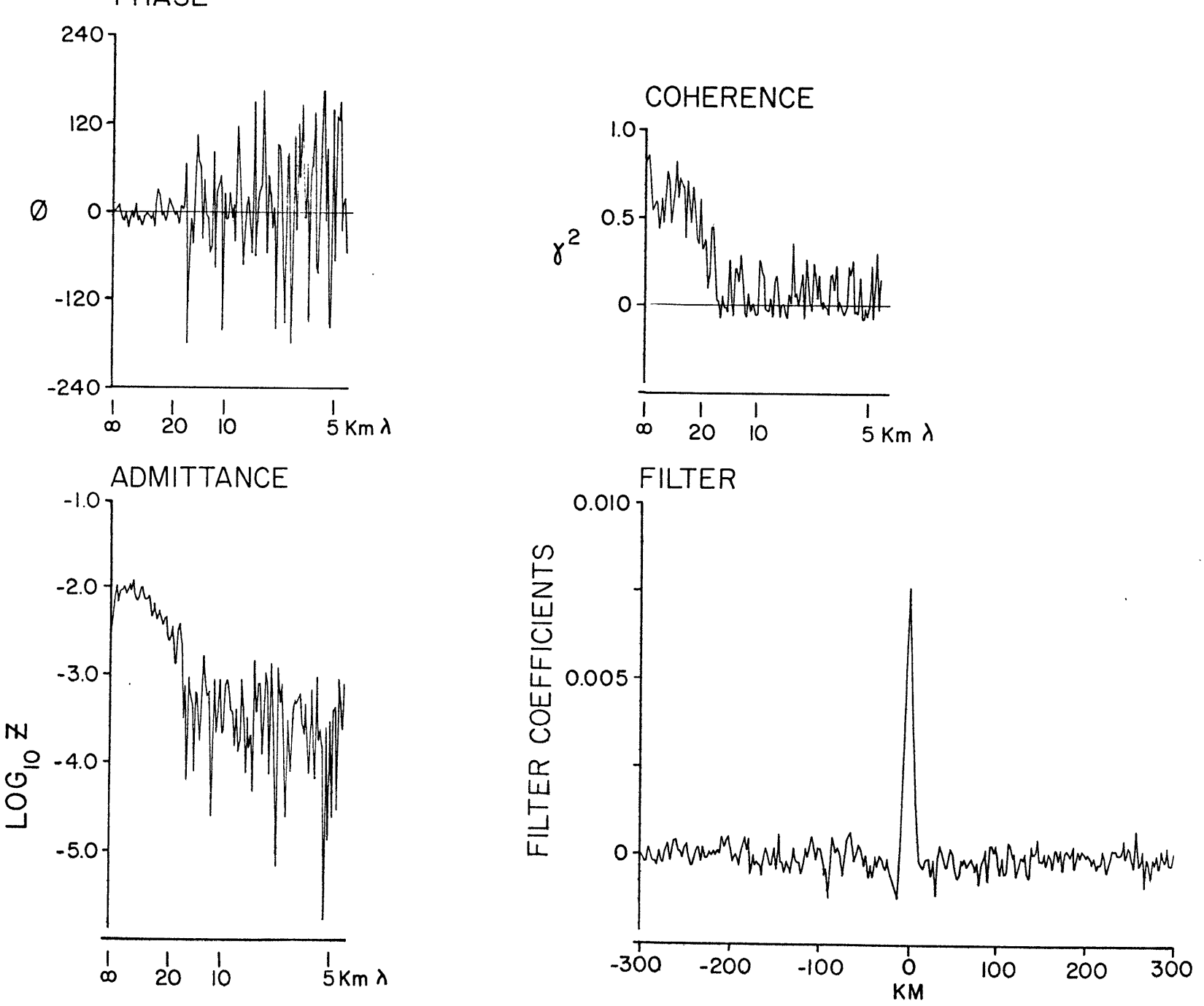

FIGURE 7

The coherence, $\log_{10}$ admittance amplitude, admittance phase, and filter generated from the gravity and bathymetry profiles shown in Figure 4 and 5 from the Walvis Ridge.

WALVIS RIDGE

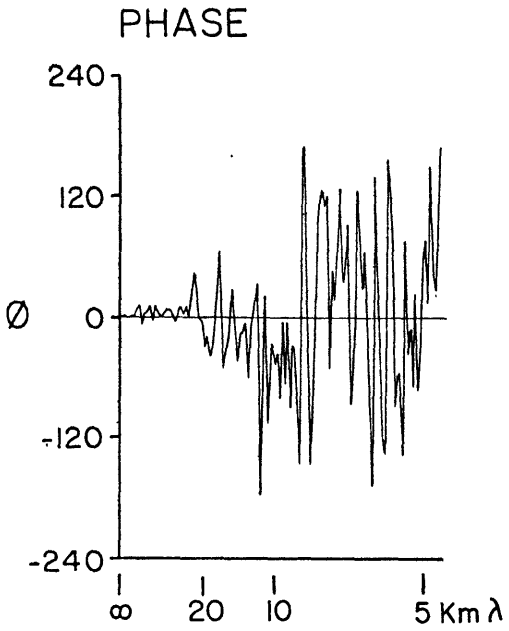

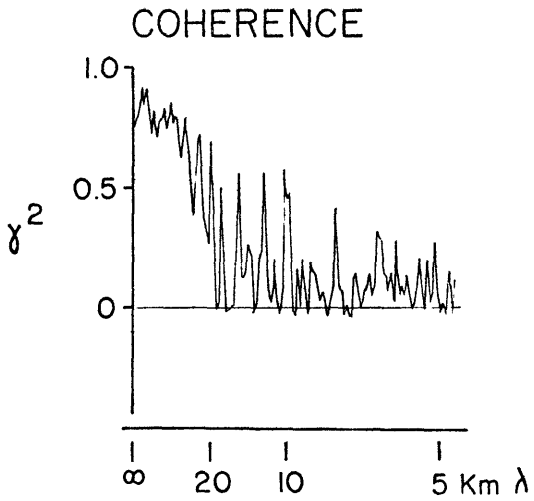

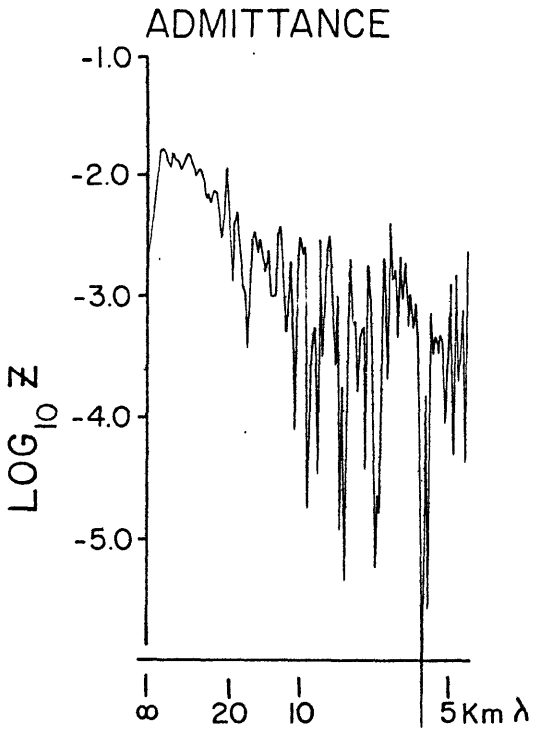

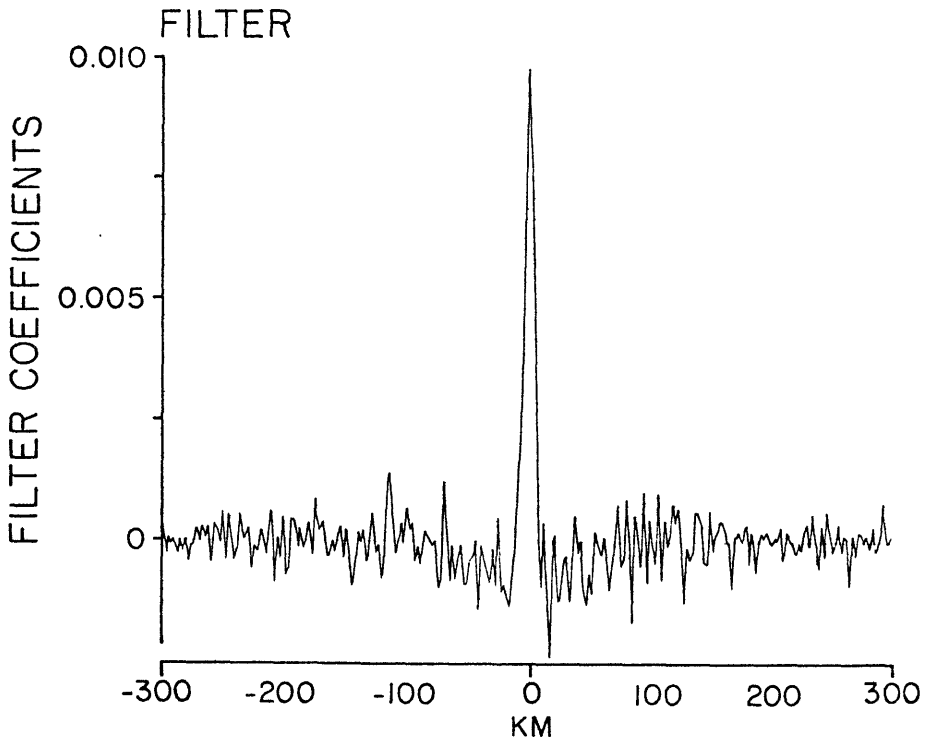

Also shown in Figures 6 and 7 are the filters obtained by inverse Fourier transforming the complex admittance. These filters can be considered as impulse response functions representing the gravity effect of a line load. The negative side lobes, most obvious for the Walvis Ridge filter (Figure 7), reflect the effects of isostatic compensation. The extent to which these filters can reproduce the observed gravity anomalies is shown in Figure 8 and 9. The "filtered topography" profiles in these figures were obtained by convolving the filter with the observed bathymetry. The "predicted" and observed gravity anomalies generally compare well. The mean variance between predicted and observed anomalies is ±8.9 mgal for the fourteen Ninetyeast Ridge profiles and ±9.6 mgal for the twelve Walvis Ridge profiles.

The largest discrepancies between predicted and observed anomalies are associated with locally thick sediment accumulations masking the true basement relief on the ridge or in the adjacent ocean basins (for example, 90E-9 and WAL-5). The Ninetyeast Ridge filter is also unable to explain completely the large amplitude free-air gravity anomalies associated with rugged topography east of ridge between 12^{o}S and 26^{o}S (90E-10 through 90E-14). This topography is probably the trace of the old Ninetyeast transform fault (Bowin, 1973) and unusual crustal mass distributions associated with this fracture zone may be responsible for the large gravity anomalies. The Walvis Ridge filter does a generally good job of predicting the shape and amplitude of gravity anomalies across the ridge; however, it cannot explain the large amplitude anomaly associated with the seamount at the eastern end of profile WAL-1. This feature, known as Ewing seamount, is located about 150 km east of the main Walvis Ridge (Figure 4) and its origin is probably unrelated to the ridge.

FIGURE 8

"Observed" bathymetry, filtered bathymetry, "observed" gravity and difference gravity for the fourteen profiles from the Ninetyeast Ridge. The "observed" gravity and bathymetry profiles are the observed profiles in Figure 3 with their mean and trend removed. The mean removed is indicated to the right of each gravity and bathymetry profile. Profiles shorter than 600 km have been extended to this length. The filtered bathymetry was produced by convolving the filter in Figure 6 with each "observed" bathymetry profile. The difference gravity profile is the difference between "observed" gravity and filtered bathymetry and represents that part of the gravity field which the filter cannot explain. Number to right of difference gravity is RMS residual between "observed" gravity and filtered bathymetry.

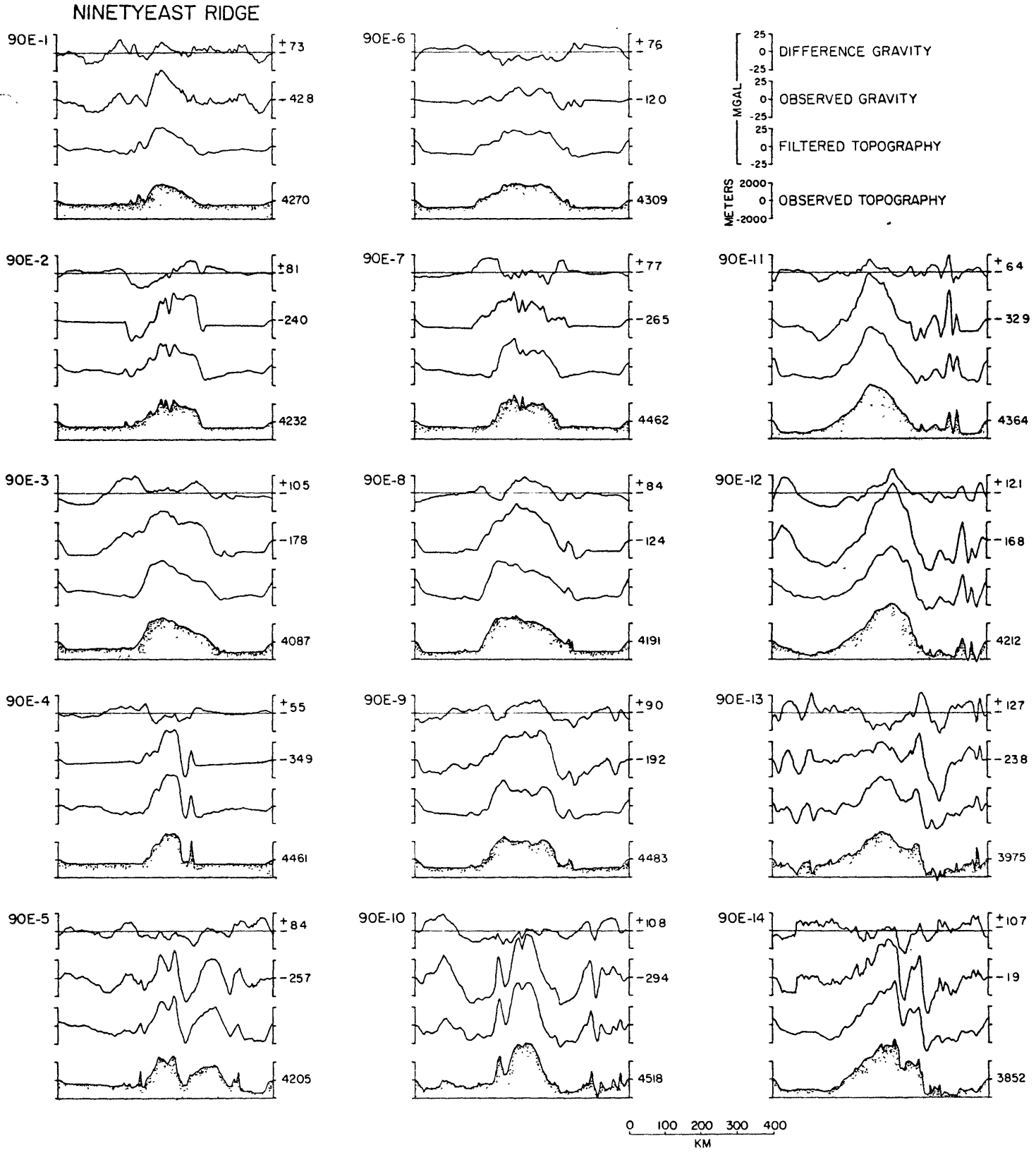
NINETYEAST RIDGE
90E-1
±73
-428
4270
90E-2
±81
-240
4232
90E-3
±105
-178
4087
90E-4
±55
-349
4461
90E-5
±84
-257
4205
90E-6
±76
-120
4309
90E-7
±77
-265
4462
90E-8
±84
-124
4191
90E-9
±90
-192
4483
90E-10
±108
-294
4518
90E-11
±64
-329
4364
90E-12
±121
-168
4212
90E-13
±127
-238
3975
90E-14
±107
-19
3852
MGAL
25
0
-25
DIFFERENCE GRAVITY
OBSERVED GRAVITY
FILTERED TOPOGRAPHY
METERS
2000
0
-2000
OBSERVED TOPOGRAPHY
0 100 200 300 400
KM

FIGURE 9

"Observed" bathymetry, filtered bathymetry, "observed" gravity and difference gravity for the twelve profiles from the Walvis Ridge. Caption is as described in Figure 8 except that filter convolved with "observed" bathymetry was, in this case, the filter shown in Figure 7.

WALVIS RIDGE

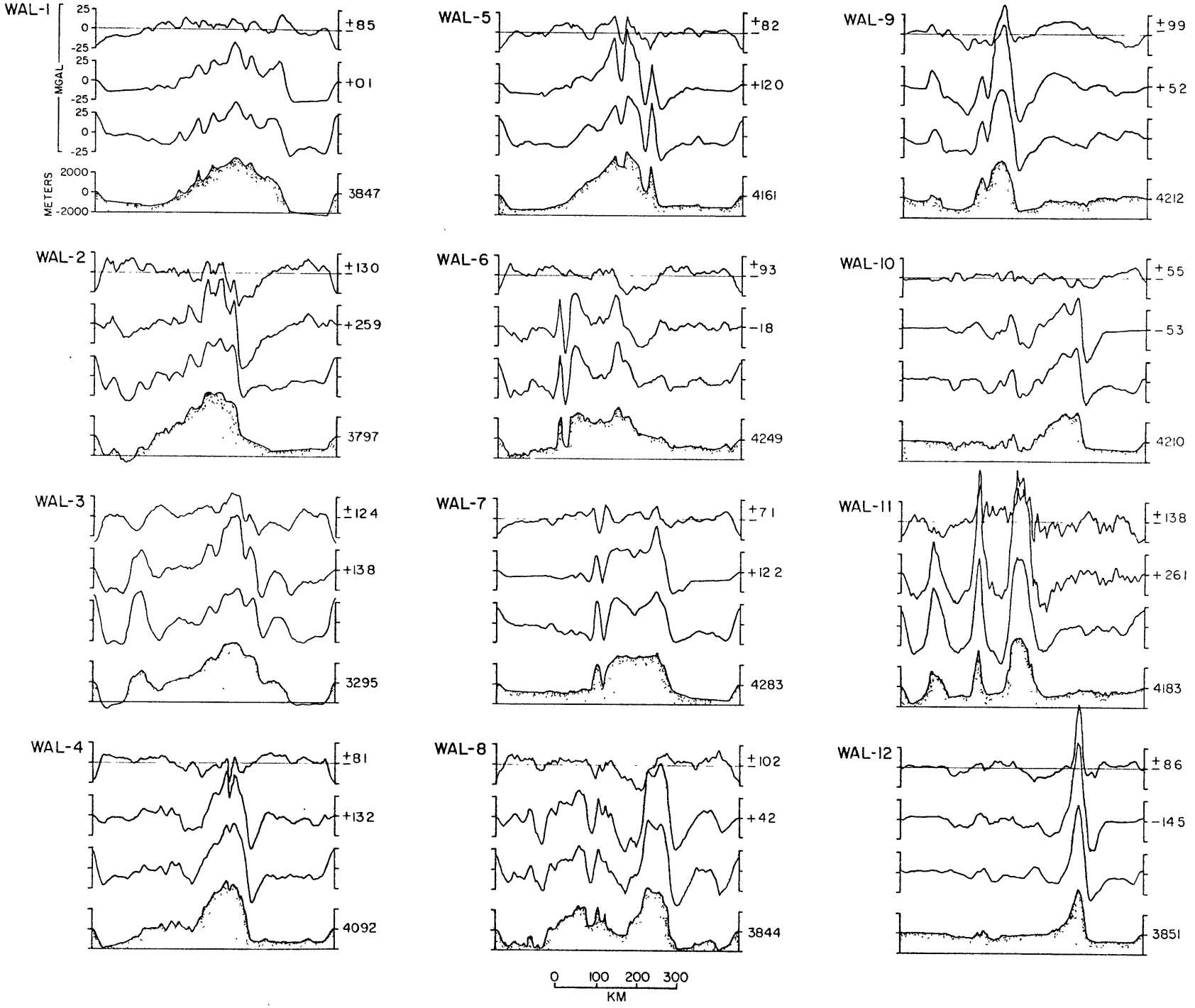

The observed admittance values (Figure 6, 7) only contain information on the overall state of isostasy along each ridge. Any changes in isostasy between different parts of the ridges will be smoothed out by the spectral averaging process. Major morphological differences exist between the eastern and western Walvis Ridge. Free-air gravity anomalies over the western Walvis Ridge are also about twice as large as those over the eastern part of the ridge. The Walvis Ridge filter, being averaged over all twelve profiles, is unable to predict completely the large amplitude of these gravity anomalies (profiles 9-12 in Figure 7). In order to evaluate whether or not significant differences exist in the state of isostasy of these two parts of Walvis Ridge, we have divided the ridge into two separate data sets: the eastern Walvis Ridge (profiles 1-7 in Figures 4 and 5) and the western Walvis Ridge (profiles 8-12). Separate admittance functions were computed from these two sets of profiles and they are used in the subsequent analysis (see Figure 11).

ISOSTATIC MODELS

The decrease in amplitude of the admittance (Figures 6, 7) at long wavelengths (λ>100 km) reflects the fact that both the Ninetyeast and Walvis Ridges are in approximate isostatic equilibrium. The mechanism of isostasy can be investigated by comparing the observed admittance values with theoretical curves calculated for various isostatic models.

Several refraction and gravity studies from aseismic ridges suggest an Airy-type model of crustal thickening. The admittance for an Airy model of compensation is given by the sum of the Fourier transforms of two sinusoidal density layers, one representing the sea floor topography and

one representing the base of the compensating mass (McKenzie and Bowin, 1976). The resulting admittance is

$$Z(k_n) = 2\pi G(\rho_2 - 1.03)e^{-k_n d}(1-e^{-k_n t}) \qquad (4)$$

where ρ_2 is the density of the crustal layer, d is the mean water depth and t is the average Airy crustal thickness.

While this and other local compensation schemes have often been suggested for aseismic ridges, Kogan (in preparation) preferred a regional isostasy model for the western Walvis Ridge like those used to explain gravity anomalies across the Hawaiian-Emperor seamount chain (Gunn, 1943; Walcott, 1970; Watts and Cochran, 1974). McKenzie and Bowin (1976) also found that a plate model of compensation best fit the observed admittance values calculated for a 6000 km long profile which crossed the eastern part of the Walvis Ridge (WAL-3 is part of this profile). In these flexural or plate models the sea floor topography is treated as a load to which the lithosphere responds as would a thin elastic sheet overlying a weak fluid layer. An important parameter in these models is the flexural rigidity which is a measure of the stiffness of the lithosphere. The flexural rigidity determines both the amplitude and wavelength of flexure due to a surface load. In the ocean these rigidities have been estimated to range from about 10^{28} dyn-cm for mid-ocean ridge topography (McKenzie and Bowin, 1976; Cochran and Watts, in preparation) to 10^{30} or 10^{31} dyn-cm for loads on old (>80 m.y.) lithosphere (Walcott, 1970; Watts and Cochran, 1974). Since the flexural rigidity is determined mainly by the plate thickness, these ranges imply effective elastic plate thicknesses of 5-40 km for the oceanic lithosphere.

TABLE 2

SUMMARY OF PARAMETERS ASSUMED IN MODEL COMPUTATIONS

t_2 (layer 2 thickness) = 2 km

t_c (mean thickness of oceanic crust) = 5 km

ρ_2 (density of topography) = 2.7 gm cm^{-3} Walvis Ridge

= 2.5 gm cm^{-3} Ninetyeast Ridge

ρ_3 (density of layer 3) = 2.9 g cm^{-3}

ρ_m (density of mantle) = 3.4 g cm^{-3}

d (mean water depth) = 4.0 km

E (Young's Modulus) = 10^{12} dyn cm^{-2}

The admittance for a plate model of compensation has been derived by McKenzie and Bowin (1976). In this study we have used a slightly different expression in which another density contrast is introduced within the crust corresponding to the Layer 2/Layer 3 transition. The resulting admittance (Watts, in preparation) is then

$$Z(k_n) = 2\pi G(\rho_2-1.03)e^{-k_n d}\{1-(e^{-k_n t_2}(\rho_3-\rho_2)+e^{-k_n t_c}(\rho_m-\rho_3)) /((\rho_m-\rho_2)+4(\rho_m-1.03)Mk'^2AB^{-1})\} \quad (5)$$

where t_2 is the thickness of Layer 2; t_c the mean thickness of the crust; ρ_3 the density of Layer 3, ρ_m the density of the upper mantle; $M = E/3gh(\rho_m-1.03)$ where E is Young's Modulus and the plate thickness is 2h; $k' = kh$; $A = \{(\sinh 2k')/2k'\}^2-1$ and $B =\{(\mathrm{Sinh}\ 4k')/4k'\}^2+1$.

Calculated admittance curves for both the Airy and the plate models of compensation for various crustal and elastic plate thicknesses are shown in Figures 10 and 11. The model parameters used are given in Table 2. The main difference between these two compensation models occurs at long wavelengths (λ>100 km); for shorter wavelengths both models asymptotically approach a line representing uncompensated topography.

The Airy model is a good fit to the observed admittance values from the Ninetyeast Ridge. The data fall between T_c = 10km and T_c = 30km with a best fitting crustal thickness of about 15-20 km. The Airy model is also a satisfactory fit for the eastern Walvis Ridge (open triangles in Figure 11). The best fitting crustal thicknesses are in the range 10-20 km, which is not significantly different from the Ninetyeast Ridge results. In both cases the plate model is a poor fit, particularly at long wavelengths.

These Airy crustal thicknesses reflect the thickness of the crust beneath the aseismic ridge and are not an "average" of the crustal thickness

FIGURE 10

Observed admittance values (solid dots) for Ninetyeast Ridge plotted against wavenumber. Vertical bars are standard error estimates computed from the coherence assuming a normal probability distribution for the ratio of true/sample admittance (Munk and Cartwright, 1966). The solid lines indicate theoretical admittance curves based on Airy and plate models of isostasy. The theoretical models are based on the parameters summarized in Table 2 and the assumed values of crustal thickness T_c or elastic plate thickness T_e shown.

NINETYEAST RIDGE

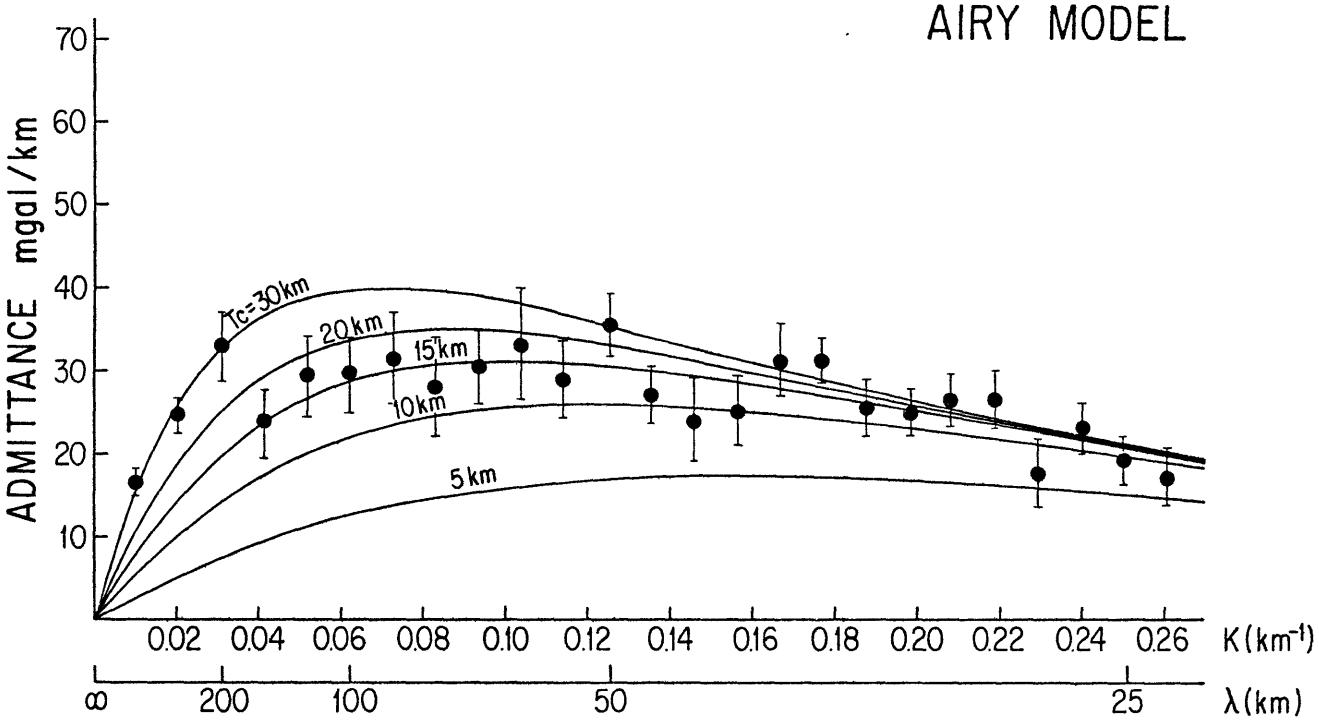

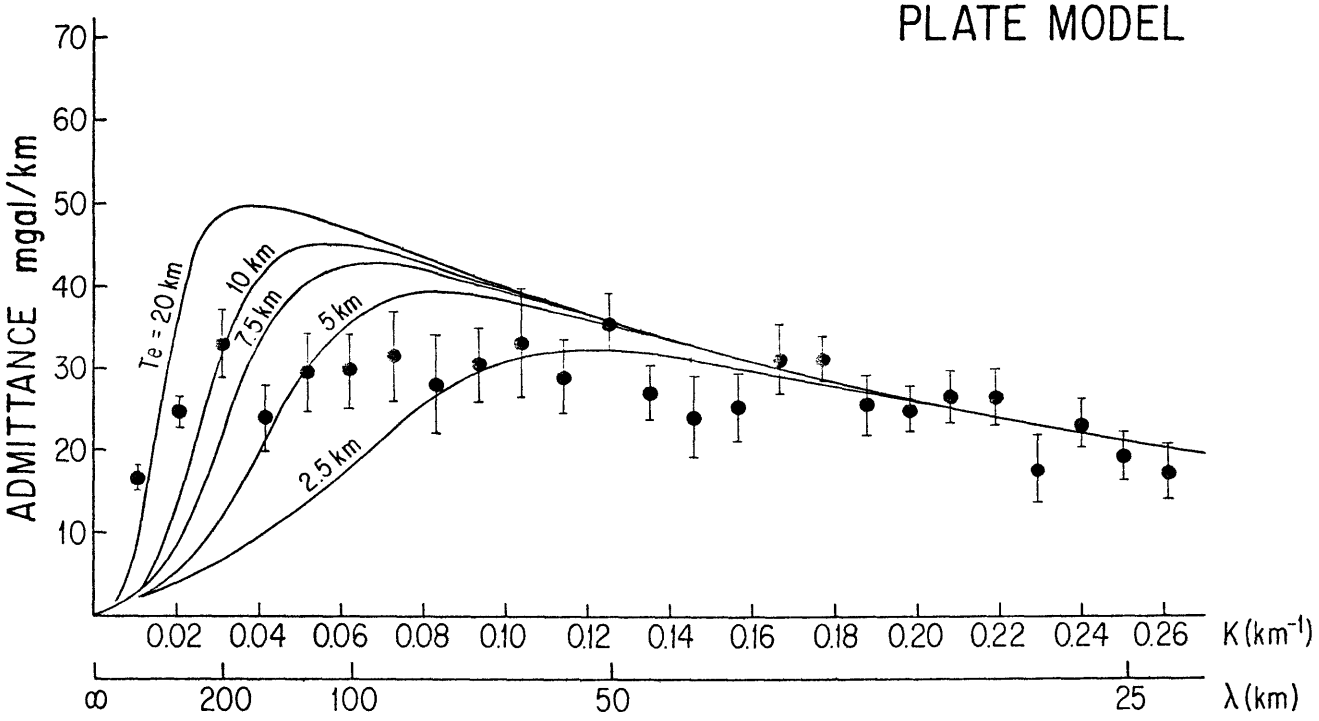

FIGURE 11

Open triangles are admittance values computed for profiles WAL-1 through WAL-7 from the eastern Walvis Ridge and solid triangles are admittance values computed for profiles WAL-8 through WAL-12 from western Walvis Ridge. Otherwise caption is same as in Figure 10.

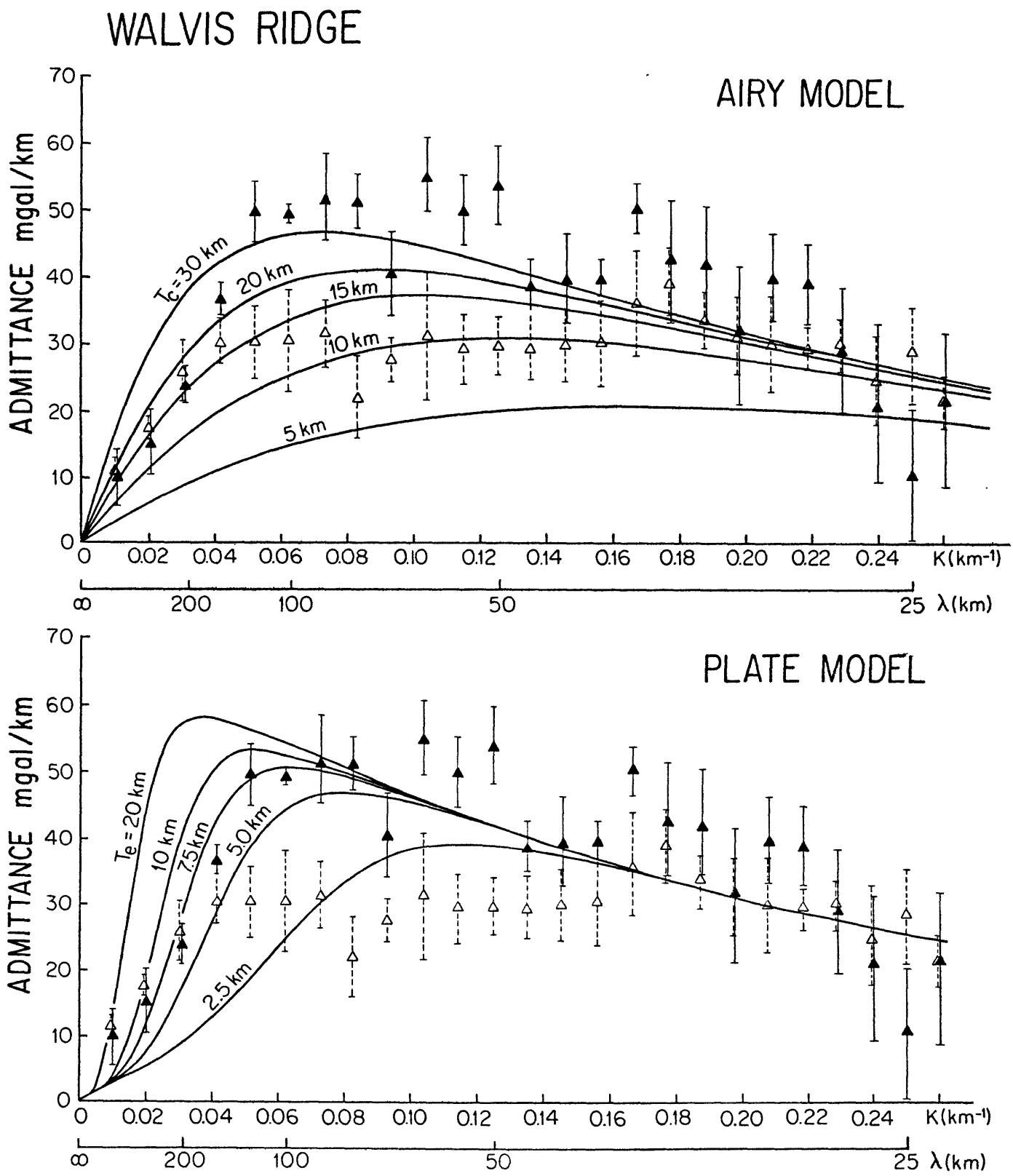
WALVIS RIDGE
AIRY MODEL
ADMITTANCE mgal/km
70
60
50
40
30
20
10
0
Tc=30 km
20 km
15 km
10 km
5 km
0
0.02
0.04
0.06
0.08
0.10
0.12
0.14
0.16
0.18
0.20
0.22
0.24
K(km-1)
∞
200
100
50
25 λ(km)
PLATE MODEL
ADMITTANCE mgal/km
Te = 20 km
10 km
7.5km
5.0km
2.5 km
0
0.02
0.04
0.06
0.08
0.10
0.12
0.14
0.16
0.18
0.20
0.22
0.24
K(km-1)
∞
200
100
50
25 λ(km)

along the entire profile. This is because most of the power in the observed gravity and bathymetry is associated with the ridge and its compensating root. The best fitting Airy crustal thickness, T_c, is actually a measure of the difference in mean depth of the principal mass excess, the ridge, and the principal mass deficit, the compensating mass (Figure 12). This thickness is less than the true crustal thickness, T, beneath the ridge which is

$$T = \frac{\Delta Z_1}{2} \{1 + (\rho_2 - 1.03)/(\rho_m - \rho_c)\} + T_c \qquad (6)$$

where ΔZ_1 is the average height of the ridge above the surrounding sea floor. Our results thus indicate actual crustal thicknesses beneath the Ninetyeast and eastern Walvis Ridges of 15-25 km. These thicknesses are significantly greater than that expected for normal oceanic crust, but are within the range of crustal thickening inferred from available seismic refraction studies of aseismic ridges (Figure 1). Here we have assumed that mantle densities beneath aseismic ridges are the same as in the adjacent ocean basins. If mantle densities are lower beneath aseismic ridges, this will partly compensate the ridge, and the actual amount of crustal thickening will be slightly less than that inferred using these methods.

While an Airy compensation model appears to be a realistic isostatic model for the Ninetyeast Ridge and the eastern part of the Walvis Ridge, it does not fit the observed admittance values from the western Walvis Ridge (solid triangles in Figure 11). At long wavelengths, where the effects of different isostatic models are most pronounced, the observed admittance increases much faster than would be expected from any Airy-type model of local compensation. In order to fit the peak admittance values crustal thicknesses in excess of 30 km are required. Although no deep seismic refraction data are available for the western Walvis Ridge, this amount of crustal thickening seems unrealistically large. In

FIGURE 12

Comparison of the gravity effect for a simple Airy crustal model of an aseismic ridge using line integral method (dashed line) and Fourier method (solid line). The gravity effect has been computed for three Airy crustal thicknesses $T_c = 5$, $T_c = 10$ and $T_c = 15$ km. The best fitting Airy crustal thickness ($T_c = 10$ km) reflects a crustal thickness of T = 15 km beneath the ridge. See text for discussion.

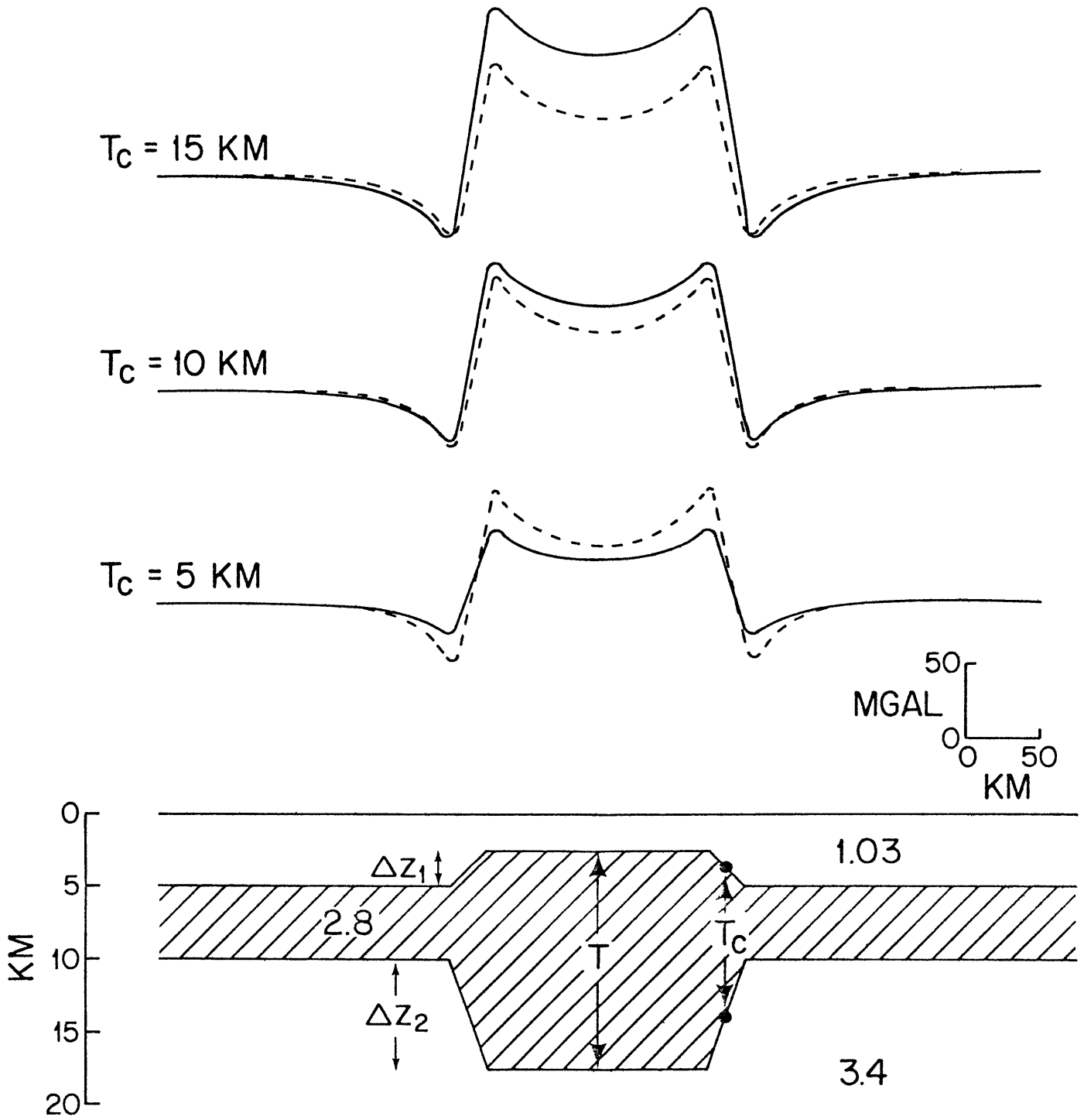
T_c = 15 KM
T_c = 10 KM
T_c = 5 KM
50
MGAL
0
0
50
KM
0
5
10
15
20
KM
Δz_1
2.8
Δz_2
T
T_c
1.03
3.4

contrast, the computed curves for the plate model fit the long wavelength admittance values from the western Walvis Ridge rather well. The best fitting effective elastic plate thickness is 5 to 8 km.

This inferred difference in isostatic mechanism between the eastern and western Walvis Ridge can also be illustrated by comparing the observed gravity anomalies from individual profiles with the anomalies expected for these two different isostatic models. This is done in Figure 13 for one profile from the eastern Walvis Ridge (WAL-7) and one profile from the western Walvis Ridge (WAL-9). The predicted gravity anomalies were computed in each case by convolving the bathymetry with a theoretical filter assuming different values of crustal (Airy) or elastic plate thickness. The best fitting value is that which minimizes the RMS residual between the "observed" and computed gravity anomalies. For these profiles the RMS residuals are minimized for Airy crustal thicknesses of ~20 km or elastic plate thicknesses of ~7.5-10 km. However, the Airy model has consistently smaller RMS residuals for the eastern Walvis Ridge profile while the plate model produces consistently smaller residuals for the western Walvis Ridge profile (Figure 13). One problem with this approach is that amplitude rather than wavelength is emphasized in the sums of squares computation (Walcott, 1976); however, it does illustrate that the differences observed in admittance values between the eastern and western Walvis Ridge are reflected in the observed gravity anomalies.

DISCUSSION

These differences in isostasy are summarized in Figure 14 where the isostatic response function $\phi(k_n)$ is plotted against wavelength for the Ninetyeast and Walvis Ridges. The function $\phi(k_n)$ is a useful parameter,

FIGURE 13

"Observed" gravity and bathymetry profiles WAL-7 (eastern Walvis Ridge) and WAL-9 (western Walvis Ridge) compared to theoretical profiles generated for various Airy and elastic plate thicknesses. Number to right of theoretical profiles is RMS difference between "observed" and calculated gravity anomalies. Note that the smallest RMS errors are obtained with an Airy model for the eastern Walvis Ridge and a plate model for the western Walvis Ridge.

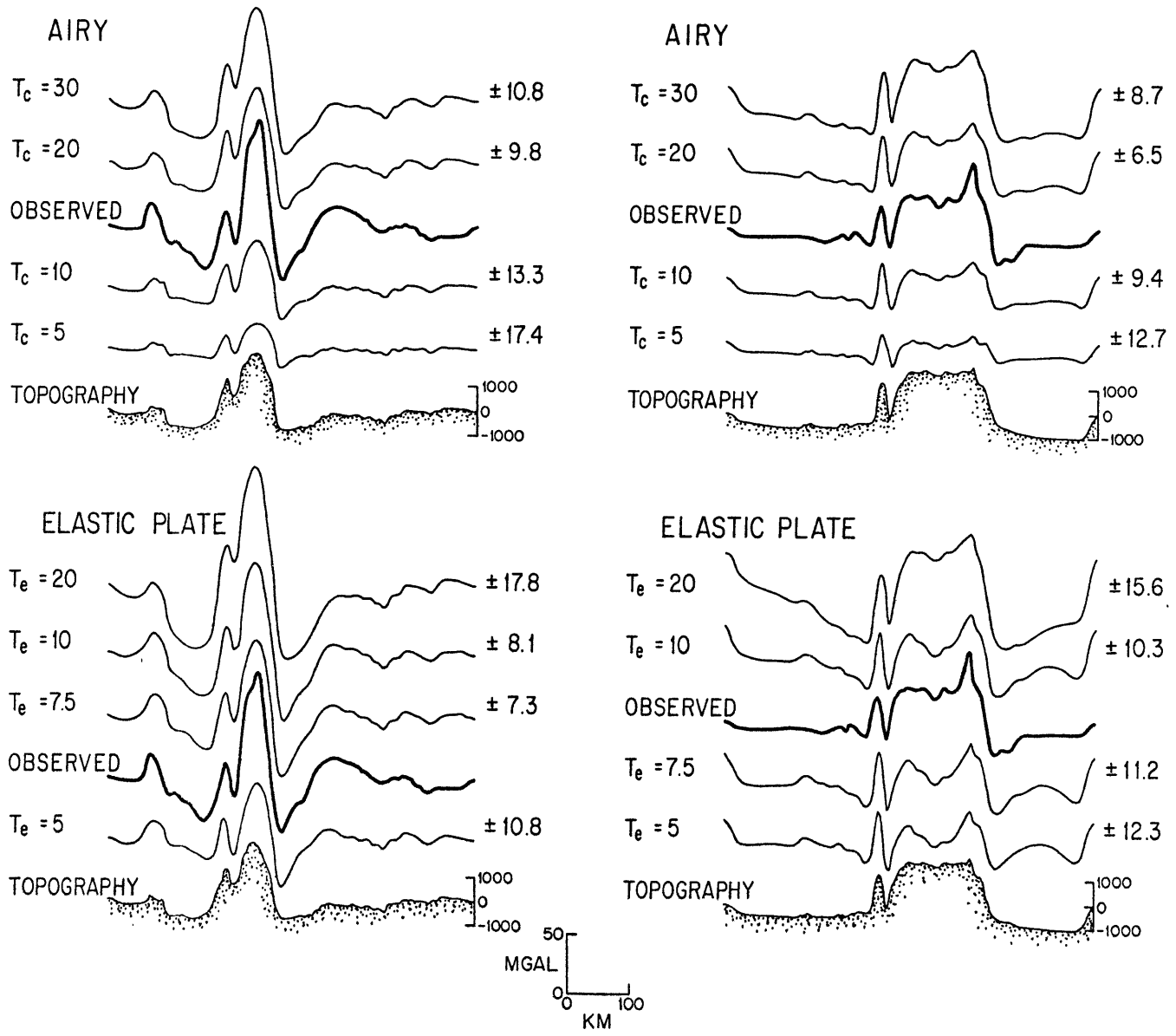
WALVIS RIDGE (WEST)
AIRY
Tc =30
±10.8
Tc =20
±9.8
OBSERVED
Tc =10
±13.3
Tc =5
±17.4
TOPOGRAPHY
1000
0
-1000
ELASTIC PLATE
Te =20
±17.8
Te =10
±8.1
Te =7.5
±7.3
OBSERVED
Te =5
±10.8
TOPOGRAPHY
1000
0
-1000
50
MGAL
0
0
100
KM
WALVIS RIDGE (EAST)
AIRY
Tc =30
±8.7
Tc =20
±6.5
OBSERVED
Tc =10
±9.4
Tc =5
±12.7
TOPOGRAPHY
1000
0
-1000
ELASTIC PLATE
Te =20
±15.6
Te =10
±10.3
OBSERVED
Te =7.5
±11.2
Te =5
±12.3
TOPOGRAPHY
1000
0
-1000

since it is largely independent of the water depth and crustal density, but is dependent on plate (or Airy crustal) thickness. The function $\phi(k_n)$ is obtained from

$$\phi(k_n) = 1 - \frac{Z(k_n)}{2\pi G(\rho_2 - 1.03)e^{-k_n d}} \qquad (7)$$

where $Z(k_n)$ is the observed admittance. The values of ρ_2 and d were estimated from the short wavelength admittance for each aseismic ridge (Table 2, Figures 6 and 7). Figure 14 illustrates that gravity and bathymetry data across the eastern Walvis and Ninetyeast Ridge require an Airy model of local compensation with crustal thicknesses beneath these ridges of 15-25 km. In contrast the western Walvis Ridge data are best explained by a plate model of regional compensation with effective elastic plate thicknesses of 5 to 8 km. The amount of crustal thickening inferred is about 7-10 km for the plate model and 10-20 km for the Airy model.

These results are in substantial agreement with previous gravity studies of the Walvis Ridge. Goslin and Sibuet (1975) produced a series of two-dimensional structural models for the easternmost Walvis Ridge. They used two similar local compensating schemes: (1) the thickness of layer 2 was kept constant and an overthickened layer 3 (ρ = 2.96 gm cm^{-3}) formed the compensating mass and (2) the ratio of the thickness of layer 2 and layer 3 were kept constant and both layers thickened beneath the ridge. With these models they found the base of the compensating mass must reach depths of 25-30 km. While Goslin and Sibuet's work was confined to the easternmost Walvis Ridge, Kogan (in preparation) modeled five gravity profiles across the western Walvis Ridge between 3^{o}E and

FIGURE 14

Plot of isostatic response function, ϕ, as a function of $\log_{10}$ wavelength for (a) Airy model and (b) plate model. The isostatic response function (Walcott, 1976) is a useful parameter for comparing different regions since it corrects the observed admittance for different mean water depths and removes most of the effects of different crustal densities. The shaded bands represent the expected flexural response function for various effective elastic plate thicknesses and a range of crustal densities of 2.6-2.8 g cm^{-3}.

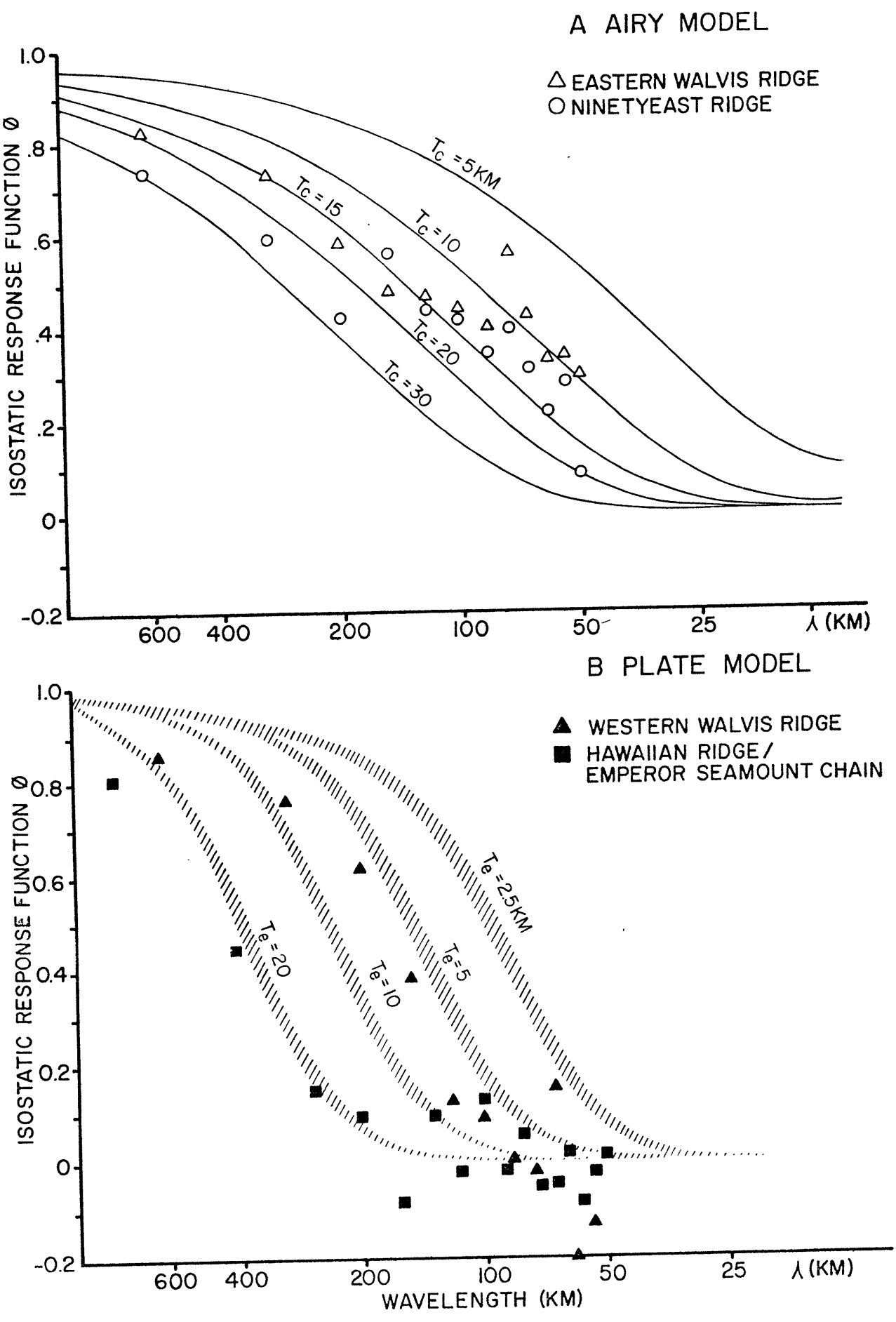
A AIRY MODEL
△ EASTERN WALVIS RIDGE
○ NINETYEAST RIDGE
ISOSTATIC RESPONSE FUNCTION Ø
1.0
.8
.6
.4
.2
0
-0.2
Tc =5KM
Tc =10
Tc =15
Tc =20
Tc =30
600
400
200
100
50
25
λ (KM)
B PLATE MODEL
▲ WESTERN WALVIS RIDGE
■ HAWAIIAN RIDGE/
EMPEROR SEAMOUNT CHAIN
ISOSTATIC RESPONSE FUNCTION Ø
1.0
0.8
0.6
0.4
0.2
0
-0.2
Te =2.5KM
Te =5
Te =10
Te =20
600
400
200
100
50
25
λ (KM)
WAVELENGTH (KM)

Tristan da Cunha using a simple plate model of compensation and different values for the flexural rigidity of the lithosphere. He found flexural rigidities in the range 2×10^{28} to 8×10^{28} dyn-cm best explained the observed profiles. This corresponds to effective elastic plate thicknesses of 6-10 km, within the range of values determined in this study.

While Bowin (1973) argued for similar depths of compensation beneath the Ninetyeast Ridge as are suggested by this study, he preferred a model in which the ridge was supported by a thick root of anomalous material rather than by thickening of normal crustal layers. This model was based in part on Francis and Raitt's (1967) interpretation of an unreversed 7.1 km/sec refraction as "Moho." Seismic refraction and gravity data from most other aseismic ridges (Figure 1) indicate substantial crustal thickening. Mantle velocities where observed are only slightly lower than normal (~7.9 km/sec). It is thus likely that the 7.1 km/sec velocity observed by Francis and Raitt is in fact a refraction from the lower crust corresponding to 3B; however, without good deep refraction data from the Ninetyeast ridge we cannot exclude a Pratt-type mechanism of lateral density changes beneath the ridge as suggested by Bowin (1973). The density differences between these models are small and probably not resolvable by these techniques.

TECTONIC IMPLICATIONS

The Airy isostatic model inferred for the Ninetyeast Ridge and the eastern Walvis Ridge indicates these features formed on lithosphere

with little or no long-term elastic bending strength. The isostasy of the western Walvis Ridge also requires a relatively weak plate with effective elastic plate thicknesses of only 5-8 km. These estimates are significantly less than values typically determined from flexural studies of loads on old (>80 my) oceanic crust. For example, studies of the Hawaiian-Emperor seamount chain (Watts and Cochran, 1974; Watts, in preparation) indicate best fitting elastic plate thicknesses of 20-30 km (Figure 14). Plate thicknesses of 5-10 km have, however, been determined for topography at mid-ocean ridges (McKenzie and Bowin, 1976; Cochran and Watts, in preparation).

These differences in isostasy are illustrated in Figure 15, which compares observed gravity anomalies over the Ninetyeast and Walvis Ridge with calculated anomalies based on South Atlantic (Cochran and Watts, in preparation) and Hawaiian-Emperor seamount chain filters (Watts, in preparation). The computed profiles were obtained by convolving each filter with the observed bathymetry. The South Atlantic filter represents the gravity effect of sea-floor topography which was probably formed at the Mid-Atlantic ridge crest while the Hawaiian-Emperor filter represents the gravity effect of topography formed on relatively old (>80 my) lithosphere. Figure 15 shows there is a much closer agreement between observed and computed anomalies based on the South Atlantic filter than those based on the Hawaiian-Emperor seamount chain filter. This result supports the hypothesis that aseismic ridges originate near ridge crests.

FIGURE 15

"Observed" gravity from Walvis Ridge profiles WAL-8 and Ninety-east Ridge profile 90E-10 compared with the predicted gravity anomalies obtained by convolving filters derived from the Hawaiian-Emperor chain (Watts, in preparation) and the South Atlantic (Cochran and Watts, in preparation) with the "observed" bathymetry. The gravity anomaly calculated with the South Atlantic filter fits the "observed" gravity quite well reflecting the fact that these aseismic ridges have formed at or near an oceanic spreading center.

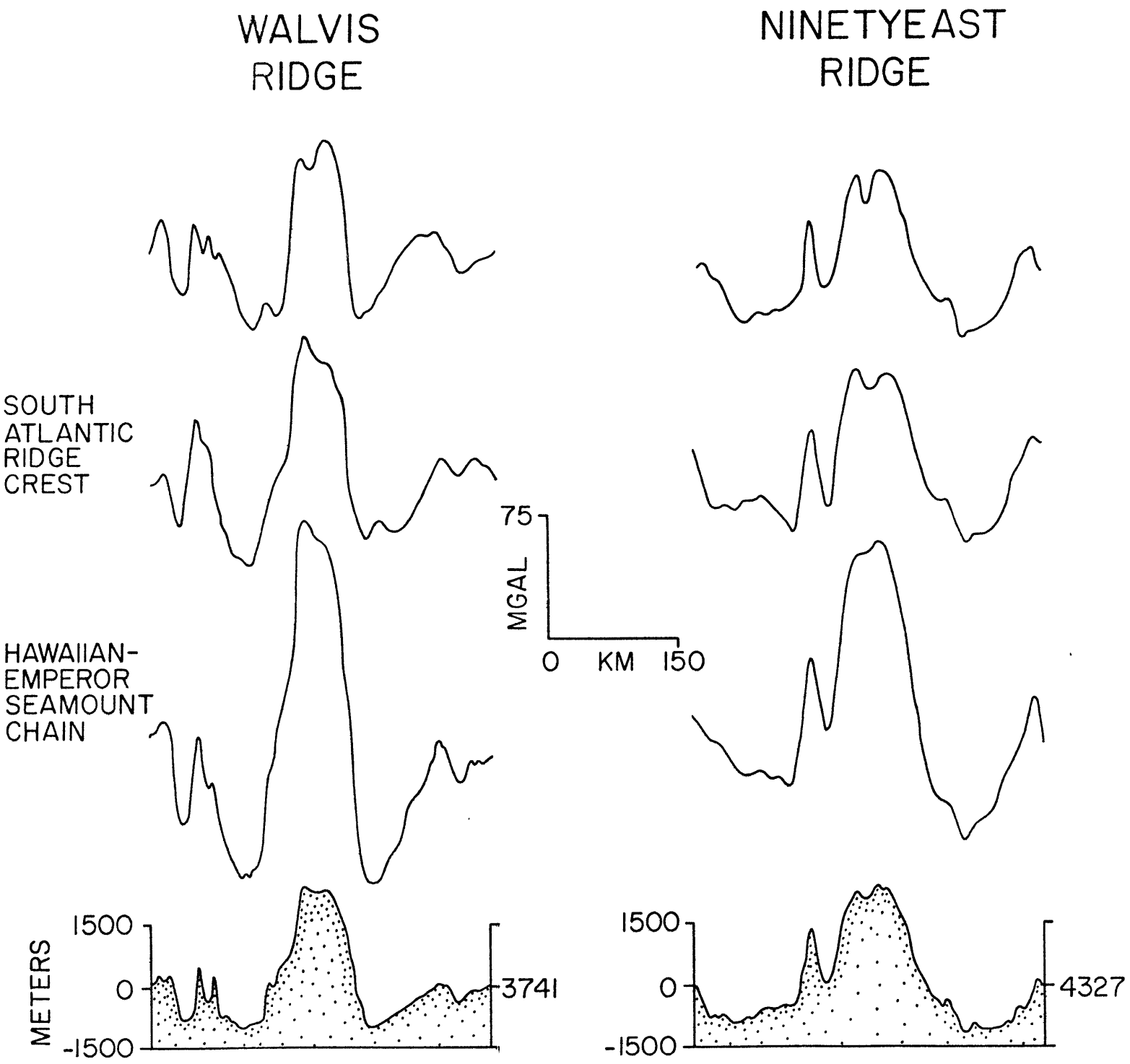
WALVIS RIDGE
NINETYEAST RIDGE
SOUTH ATLANTIC RIDGE CREST
HAWAIIAN-EMPEROR SEAMOUNT CHAIN
75
MGAL
0 KM 150
METERS
1500
0
-1500
3741
1500
0
-1500
4327

In an Airy isostatic model, like that inferred for the eastern Walvis and Ninetyeast Ridges, compensation is achieved by adjustment of vertical fault-bounded blocks. Faulted structures have been recognized on many aseismic ridges, although their origin is poorly understood. Early investigators favoring a tectonic origin for aseismic ridges argued that old oceanic crust had been uplifted along these large scarps giving the ridges basically a horst-type structure (Ewing et al., 1966; Francis and Raitt, 1967; Connary, 1972). However, gravity and seismic refraction data are inconsistent with this model, and it is now generally accepted that aseismic ridges are volcanic features. Francheteau and Le Pichon (1972) and Sclater and Fisher (1974) pointed out that parts of the Walvis and Ninetyeast Ridges trend along flow lines, and they suggested that these scarps may be associated with fracture zone topography. However, those parts of the Walvis Ridge that trend at nearly right angles to these flow lines also are characterized by a similar block-fault morphology. Fracture zones typically have steep scarps bordering a deep central trough and are usually flanked on one side by a high ridge ~25-50 km wide. Aseismic ridges, on the other hand, are usually much wider (200-300 km); their steep scarps are discontinuous and often limited to one side of the ridge. There is generally no evidence for deep fracture zone troughs bordering the ridges. Bowin (1973) and Hekinian (1974) have, therefore, argued that block faulting is only a secondary process in forming the topography of these aseismic ridges. However, they proposed no satisfactory mechanism for explaining the origin of these large scarps.

We believe the presence of Airy-type compensation and block-faults on the eastern Walvis Ridge and Ninetyeast Ridge are a consequence of

their formation at a ridge crest. The lithosphere at a ridge crest is relatively weak and would not be able to sustain the large loads associated with the volcanism forming aseismic ridges for long periods of geological time. Since the lithosphere is unable to distribute these loading stresses laterally by bending, isostatic adjustments occur by the vertical movement of large crustal blocks. These isostatic adjustments, which would occur concurrently with the volcanism forming the ridge, probably explain the large scarps and block-fault morphology of many aseismic ridges.

The plate model, in contrast, implies the western part of the Walvis Ridge flexurally loaded the oceanic lithosphere. One possible explanation for the differences in isostasy between the eastern and western parts of the Walvis Ridge is that it is related to an eastward shift relative to the Mid-Atlantic Ridge of the "hot spot" forming the Walvis Ridge ~80 m.y.B.P. (Ladd, 1974). This "hot spot" has remained beneath the African plate throughout the Cenozoic and is presently located at Tristan da Cunha (Morgan, 1971) about 300 km east of the Mid-Atlantic Ridge (Figure 4). After this off-axis shift in the "hot spot," the volcanism forming the Walvis Ridge became more intermittent in time and space forming a seamount province rather than a continuous ridge. The lithosphere was able to support these smaller loads elastically by bending. In this sense, the western Walvis Ridge seamount and guyot province is analogous to the Hawaiian-Emperor seamount chain. However, the western Walvis Ridge was built on younger, thinner and consequently much weaker lithosphere than that underlying the Hawaiian-Emperor seamount chain.

The estimated age of the shift in this "hot spot" is, however, poorly constrained by available data. Magnetic anomaly 34 (~80 m.y.B.P.) has

been identified on both sides of the ridge crest. Cande and Rabinowitz (in press) have mapped a large amplitude magnetic anomaly on the eastern flank of the Rio Grande Rise, which they tentatively identified as anomaly 34. If this anomaly has been correctly identified, it does suggest the Rio Grande Rise formed prior to anomaly 34. An eastward shift in the "hot spot" at this time could therefore explain both the flexural loading at the western Walvis Ridge and the abrupt termination of the Rio Grande Rise.

The isostasy of the Walvis and Ninetyeast Ridges was thus largely determined by the thin, relatively weak lithosphere on which they formed. The differences in isostasy between aseismic ridges and mid-plate island chains, like the Hawaiian-Emperor seamount chain, can be explained by differences in the age of the crust on which they formed. As the lithosphere cools and thickens, its rigidity increases. Thus mid-plate island chains load a much more rigid plate than aseismic ridges, and this is reflected in gravity anomalies of much higher amplitude and longer wavelength than are typical of aseismic ridges.

Although basement ages, and consequently the age of loading, vary systematically along the length of the Ninetyeast Ridge, we have found no evidence that this is accompanied by significant changes in its state of isostasy. The difference in the isostasy between the younger and older parts of the Walvis Ridge has been attributed to differences in the mode of origin (on-spreading axis vs. off-spreading axis) rather than viscoelastic relaxation. These observations suggest that the isostatic parameters determined at these ridges were "frozen in" at the time of their formation at or near a spreading center and have not

significantly changed through time. Thus the oceanic lithosphere appears to be able to support the large stresses associated with aseismic ridges for at least several tens of millions of years.

CONCLUSIONS

From this analysis of gravity and bathymetry profiles across the Ninetyeast and Walvis Ridge we draw the following conclusions:

1. The Ninetyeast Ridge and the eastern Walvis Ridge are locally compensated by an overthickening of the oceanic crust. Maximum crustal thicknesses beneath these ridges are estimated to be 15-25 km. This type of crustal thickening is consistent with most available seismic refraction and gravity data from aseismic ridges.

2. The western Walvis Ridge is morphologically and structurally different from the eastern Walvis Ridge or the Ninetyeast Ridge. It consists of numerous seamounts and guyots which are regionally supported by a lithosphere with an effective elastic plate thickness of 5-8 km. This is significantly less than the plate thicknesses of 20-30 km typically determined for loads on old (>80 m.y.) oceanic crust (Walcott, 1970; Watts and Cochran, 1974), but within the range of values determined for topography presumably formed at mid-ocean ridge crests (McKenzie and Bowin, 1976; Cochran and Watts, in preparation). The amount of crustal thickening inferred is 7-10 km.

3. These results indicate the Ninetyeast Ridge and the Walvis Ridge were formed on hot, relatively weak lithosphere. This is consistent with their formation at or near an oceanic spreading center by a mantle plume or "hot spot" as suggested by Wilson (1963) and Morgan (1971). The

differences in morphology and isostasy between the eastern and western Walvis Ridge are attributed to an off-axis shift in the "hot spot" forming the Walvis Ridge ~80 m.y.B.P.

4. The isostasy of aseismic ridges reflects the mechanical properties of the lithosphere at the time they formed. The stresses associated with the initial loading appear to be maintained for tens of millions of years without appreciable change.

5. These results and similar studies of mid-ocean ridges (McKenzie and Bowin, 1976; Cochran and Watts, in preparation) and mid-plate island chains (Watts, in preparation) indicate that the rigidity of the lithosphere increases by about an order of magnitude from ridge crests, where aseismic ridges form, to the 80-90 m.y. old lithosphere on which the Hawaiian Ridge has been built. The differences in isostasy between aseismic ridges and mid-plate island chains, like the Hawaiian chain, can thus be largely explained by differences in the age of the lithosphere at the time of loading.

ACKNOWLEDGMENTS

This work was supported by National Science Foundation grant NSF OCE 77-07941 at Lamont-Doherty Geological Observatory. R. S. D. also received financial assistance from the Woods Hole Oceanographic Institution Education Office and Office of Naval Research grant N00014-74-C-0262 NR083-004. The data used in this study was obtained mainly on cruises supported by the Office of Naval Research and the National Science Foundation. This manuscript benefitted from critical reviews by C. Bowin, C. R. Denham and H. Schouten.

REFERENCES

Bentley, L. R., Sutton, G. H., Shor, G. G., Jr., and Henry, M., Crustal structure of the Carnegie Ridge, Panama Basin and Cocos Ridge, in preparation.

Bolli, H. M., Ryan, W. B. F., et al., Basins and margins of the eastern South Atlantic, Geotimes, 20, 22-24, 1975.

Bott, M. H. P., Browitt, C. W. A., and Stacey, A. P., The deep structure of the Iceland-Faeroe Ridge, Mar. Geophys. Res., 1, 328-351, 1971.

Bowin, C., Origin of the Ninety East Ridge from studies near the Equator, J. Geophys. Res., 78, 6029-6043, 1973.

Cande, S. C., and Rabinowitz, P. D., Magnetic anomalies of the continental margin of Brazil, Lamont-Doherty Geological Observatory, Palisades, N. Y., in press.

Cochran, J. R., and Watts, A. B., An analysis of isostasy in the world's oceans: Part 2--Mid-Ocean Ridge Crests, submitted to J. Geophys. Res.

Connary, S. A., Investigations of the Walvis Ridge and environs, Ph.D. Thesis, Columbia University, Palisades, N. Y., 228 p., 1972.

Cutler, S. T., Geophysical investigation of the Nazca Ridge, M.Sc. Thesis, University of Hawaii, Honolulu, HA, 1977.

Davies, T. A., Luyendyk, B. P., et al., Initial Reports of the Deep Sea Drilling Project, 26, Washington, D. C. (U. S. Govt. Printing Office), 982 p., 1974.

Detrick, R. S., Sclater, J. G., and Thiede, J., The subsidence of aseismic ridges, Earth Planet Sci. Lett., 34, 185-196, 1977.

Dingle, R. V., and Simpson, E. S. W., The Walvis Ridge: A review, in Geodynamics Progress and Prospects, (ed.) C. Drake, A. G. U., Washington, D. C., 160-176, 1976.

Dorman, L. M., and Lewis, B. T. R., Experimental Isostasy 1: Theory of the determination of the Earth's isostatic response to a concentrated load, J. Geophys. Res., 75, 3357-3365, 1970.

Ewing, M., Le Pichon, X., and Ewing, J., Crustal structure of the Mid-Ocean ridges; Part 4, Sediment distribution in the South Atlantic Ocean and the Cenozoic history of the Mid-Atlantic Ridge, J. Geophys. Res., 71, 1611-1636, 1966.

Francheteau, J., and Le Pichon, X., Marginal fracture zones as structural framework of continental margins in South Atlantic Ocean, Am. Assoc. Pet. Geol. Bull., 56, 991-1007, 1972.

Francis, T. J. G., and Shor, G. G., Jr., Seismic refraction measurements from the northwest Indian Ocean, J. Geophys. Res., 71, 427-449, 1966.

Francis, T. J. G., and Raitt, R. W., Seismic refraction measurements in the southern Indian Ocean, J. Geophys. Res., 72, 3015-3041, 1967.

Goslin, J., and Sibuet, J. C., Geophysical study of the easternmost Walvis Ridge, South Atlantic: Deep structure, Geol. Soc. Am. Bull., 86, 1713-1724, 1975.

Gunn, R., A quantitative evaluation of the influence of the lithosphere on anomalies of gravity, J. Franklin Inst., 236, 373-396, 1943.

Hekinian, R., Petrology of the Ninety East Ridge (Indian Ocean) compared to other Aseismic Ridges, Contr. Mineral and Petrol., 43, 125-147, 1972.

Kogan, M. G., Gravity anomalies and origin of the Walvis Ridge, submitted to J. Geophys. Res.

Ladd, J. W., South Atlantic sea-floor spreading and Caribbean tectonics, Ph.D. Thesis, Columbia University, Palisades, N. Y., 1974.

Laughton, A. S., Matthews, D. H., and Fisher, R. L., The structure of the Indian Ocean, in The Sea, 4, ed. A. E. Maxwell, Wiley-Interscience, New York, 543-586, 1970.

Lewis, B. T. R., and Dorman, L. M., Experimental Isostasy 2: An isostatic model for the USA derived from gravity and topographic data, J. Geophys. Res., 75, 3367-3886, 1970.

McKenzie, D. P., and Bowin, C., The relationship between bathymetry and gravity in the Atlantic Ocean, J. Geophys. Res., 81, 1903-1915, 1976.

Morgan, W. J., Convection plumes in the lower mantle, Nature, 230, 42-43, 1971.

Munk, W. H., and Cartwright, D. A., Tidal spectroscopy and prediction, Phil. Trans. Roy. Soc. Lond., Series A, 259, 533-581, 1966.

Palmason, G., Crustal structure of Iceland from explosion seismology, Science Inst., Univ. of Iceland, Reykjavik, 239 p., 1970.

Perch-Nielson, K., Supko, P. R., et al., Leg 29 examines facies changes in South Atlantic, Geotimes, 20, 26-28, 1975.

Peterson, J. J., Fox, P. J., and Schreiber, E., Newfoundland ophiolites and the geology of the oceanic layer, Nature, 247, 194-196, 1974.

Pierce, J. W., The origin of the Ninetyeast Ridge and the northward motion of India, based on DSDP paleolatitudes, Ph.D. Thesis, Woods Hole Oceanographic Institution/Massachusetts Institute of Technology Joint Program in Oceanography, Woods Hole, MA, 283 p., 1977.

Pimm, A. C., McGowran and Gartner, S., Early sinking history of the Ninetyeast Ridge, Northeastern Indian Ocean, Geol. Soc., Am. Bull., 85, 1219-1224, 1974.

Rabinowitz, P. D., and La Brecque, J., The Mesozoic South Atlantic and evolution of its continental margins, submitted to Bull. Am. Assoc. Pet. Geol.

Sclater, J. G., and Fisher, R. L., Evolution of the east central Indian Ocean, with emphasis on the tectonic setting of the Ninetyeast Ridge, Geol. Soc. Am. Bull., 85, 683-702, 1974.

Sclater, J. G., Luyendyk, B. P., and Meinke, L., Magnetic lineations in the southern part of the central Indian Basin, Geol. Soc. Am. Bull., 87, 371-378, 1976.

Shor, G. G., Jr., and Pollard, D. D., Seismic investigations of Seychelles and Saya de Malha Banks, Northwest Indian Ocean, Science, 142, 48-49, 1963.

Thiede, J., Subsidence of aseismic ridges: Evidence from sediments on Rio Grande Rise (Southwest Atlantic Ocean), Am. Assoc. Pet. Geol. Bull., 61, 929-940, 1977.

Uchupi, E., and Hays, H. C., Bathymetric atlas of the Atlantic, Caribbean and Gulf of Mexico (Revised), Woods Hole Oceanographic Inst., Woods Hole, MA, 1978.

Vincent, E., Gibson, J. M., and Bran, L., Paleocene and early Eocene microfacies, benthonic foraminifera, and paleobathymetry of Deep Sea Drilling Project Sites 236 and 237, western Indian Ocean, in Fisher, R. L., Bunce, E. T., et al., Initial Reports of the Deep Sea Drilling Project, 24, 1974.

Von der Borch, C. C., Sclater, J. G., et al., Initial Reports of the Deep Sea Drilling Project, 22, Washington, D. C. (U. S. Govt. Printing Office), 890 p., 1974.

Walcott, R. I., Flexure of the lithosphere at Hawaii, Tectonophysics, 9, 435-446, 1970.

Walcott, R. I., Lithospheric flexure, analysis of gravity anomalies and the propagation of seamount chains in The International Woollard Symposium, AGU Mono. 19, Washington, D. C., 431-438, 1976.

Watts, A. B., An analysis of isostasy in the world's oceans: Part 1--Hawaiian-Emperor seamount chain, submitted to J. Geophys. Res.

Watts, A. B., and Cochran, J. R., Gravity anomalies and flexure of the lithosphere along the Hawaiian-Emperor seamount chain, Geophys. J. R. astr. Soc., 38, 119-141, 1974.

Wilson, J. T., Evidence from islands on the spreading of ocean floors, Nature, 197, 536-538, 1963.

CHAPTER 3

THE SUBSIDENCE OF ASEISMIC RIDGES

THE SUBSIDENCE OF ASEISMIC RIDGES*

Robert S. Detrick
Massachusetts Institute of Technology
Cambridge, Massachusetts 02139
Woods Hole Oceanographic Institution
Woods Hole, Massachusetts 02543

John G. Sclater
Massachusetts Institute of Technology
Cambridge, Massachusetts 02139

Jörn Thiede
Oregon State University
Corvallis, Oregon 97331

*Published in Earth and Planetary Science Letters, 34, (1977), p. 185-196.

ABSTRACT

All available Deep Sea Drilling Project results from aseismic ridges have been compiled. These results indicate that at least five major aseismic ridges--the Ninetyeast Ridge, the Rio Grande Rise, the Walvis Ridge, the Chagos-Laccadive Ridge and the southeast Mascarene Plateau--have formed close to sea level and have since subsided at rates comparable to that of normal oceanic crust. Two other aseismic ridges, the Iceland-Faeroe Ridge and Broken Ridge, may have undergone a similar but more complicated subsidence history. This subsidence is attributed entirely to the cooling and contraction of the lithospheric plate on which these ridges are built. Some geological and geophysical implications of this model are discussed including its applicability to the subsidence of oceanic island chains.

INTRODUCTION

Topographic and magnetic profiles from the Pacific, Atlantic and Indian Oceans and the inferred basement ages of Deep Sea Drilling Project (DSDP) holes have clearly established a general relationship between depth and age for normal oceanic crust. Depths increase from 2500±300 m at a spreading center to 5800±300 m in oceanic crust of early Cretaceous to late Jurassic age. These observations have been successfully explained by simple models involving the cooling and contraction of the oceanic lithosphere as it ages and moves away from a spreading center (Sclater et al., 1971). While this depth versus age relationship is generally applicable to most of the sea floor, there are prominent ridge and plateau like features scattered throughout the oceans that are anomalously shallow and noticeably distinct from the surrounding sea floor. These structural "highs," which have been variously termed plateaus, rises, oceanic ridges or aseismic ridges, interrupt the lineated magnetic anomaly pattern of normal oceanic crust and do not appear to have been created by simple sea floor spreading processes. Unfortunately, little geological or geophysical data is available from many of these features and what data does exist seems to suggest more than one type of crustal structure or origin. In this paper we will discuss one group of anomalous sea floor features--aseismic ridges. We will use the definition of an aseismic ridge first suggested by Laughton et al. (1970): a linear volcanic ridge free of earthquake activity.

Aseismic ridges are found in all major ocean basins--among the most familiar are the Rio Grande Rise, Walvis Ridge and Iceland-Faeroe Ridge in the Atlantic Ocean, the Ninetyeast and Chagos-Laccadive Ridges in the

FIGURE 1

Location of major aseismic ridges and Deep Sea Drilling Project sites discussed in this paper: (A) Iceland-Faeroe Ridge, (B) Rio Grande Rise, (C) Walvis Ridge, (D) Ninetyeast Ridge, (E) Chagos-Laccadive Ridge, (F) Southeast Mascarene Plateau, (G) Mozambique Ridge, (H) Madagascar Ridge, (I) Broken Ridge, (J) Naturalistic Plateau, (K) Cocos Ridge, (L) Carnegie Ridge and (M) Coiba Ridge.

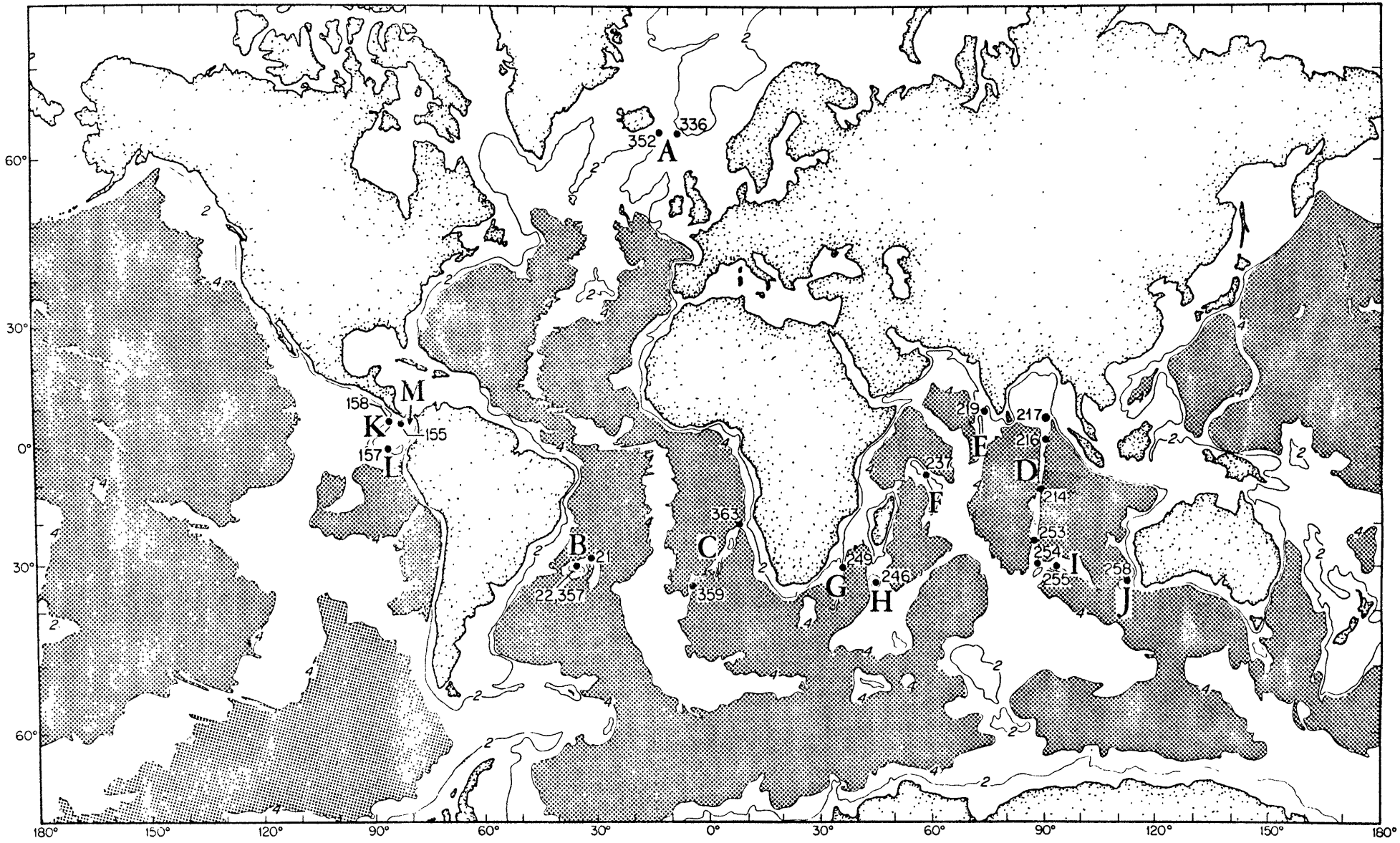
60°
30°
0°
30°
60°
180°
150°
120°
90°
60°
30°
0°
30°
60°
90°
120°
150°
180°
A
352
336
B
21
22,357
C
363
359
D
214
253
254
255
E
219
217
216
F
237
G
249
H
246
I
258
J
K
158
157
L
M
155

Indian Ocean, and the Cocos and Carnegie Ridges in the eastern Pacific (Figure 1). Because many of these shallow, structural highs have apparently had an important effect on sedimentary and paleocirculation patterns in the oceans and because of our rather meager knowledge of their origin or tectonic history, a number of Deep Sea Drilling Project (DSDP) sites have been located on these features. One important result of this drilling has been the recovery of shallow water sediments from aseismic ridges that today are several hundred and in many cases several thousands of meters below sea level. The sedimentary record from these sites indicates that shallow water, even subaerial conditions, existed early in the history of these ridges. Younger sediments indicate a progressively deeper water and more open marine depositional environment. In this paper we review the geological evidence for this subsidence, present a simple model which can account for these observations and discuss some of the model's geological and geophysical implications.

DEEP SEA DRILLING DATA

We have compiled available Deep Sea Drilling Project results for all major aseismic ridges (Table 1). In addition, we have tabulated drilling results from a number of other features which might be classed as aseismic ridges, but about which relatively little is known. In each case we have estimated the age of the site (generally from the paleontological age of the basal sediments) and the age of the adjacent oceanic crust based on magnetic anomaly identifications. We have used the biostratigraphic time scale of Berggren and van Couvering (1974) for the Tertiary and the preliminary scale of Thierstein (in press) for the Cretaceous/Jurassic. Basement depths have been corrected for isostatic loading by the overlying

TABLE I: APPARENT AND EXPECTED SUBSIDENCE AT DSDP DRILLING SITES ON ASEISMIC RIDGES.

Site	Position Latitude/ Longitude	Age (m.y.b.p.) Site/Adjacent Ocean Crust	Depth(m) Water/ Basement	Sediment Thickness (m)	Isostatically Corr.Basement Depth(m)	Expected Depth (m)	Comments
NINETYEAST RIDGE							
214	11°20'S 88°43'E	53.5-60 55	1665 2155	490	1984	2400	Emergent in Paleocene with onset of oceanic facies in early Eocene
216	1°28'N 90°13'E	65-67 68	2247 2704	457	2544	2600	Shallow in late Cretaceous gradually changing to open marine conditions by the earliest Paleocene
217	8°56'N 90°32'E	> 71-82 > 72	3020 +	> 664	> 3452	2700	Shallow water conditions in the Campanian with onset of oceanic facies in Campanian or early Maastrichtian
253	24°53'S 87°22'E	43-49 47?	1962 2521	559	2325	2200	Shallow water conditions in the middle Eocene with oceanic facies by the late Eocene
254	30°58'S 87°54'W	22.5-37.5 28?	1253 1554	~301	1449	1700	Shallow water sediments of Oligocene age; oceanic facies deposited in early Miocene
RIO GRANDE RISE							
21	28°35'S 30°35'W	> 71 ?	2102 +	> 130	> 2189	2700	Very shallow depths in Campanian or pre-Campanian times with deeper water facies present in late Campanian or early Maastrichtian
22	30°00'S 35°15'W	> 43-49 > 72?	2106 +	> 242	> 2263	2200	No obvious shallow water fauna
357	30°00'S 35°33'W	> 82-86 > 72?	2109 +	> 797	> 2627	2900	Shallow water conditions existed in the Santonian

TABLE I continued:

Site	Position Latitude/ Longitude	Age (m.y.b.p.) Site/Adjacent Ocean Crust	Depth(m) Water/ Basement	Sediment Thickness (m)	Isostatically Corr.Basement Depth(m)	Expected Depth (m)	Comments
WALVIS RIDGE							
359	34°59'S 4°30'W	38-43 57	1658 1765	107	1728	2000	Emergent in the late Eocene
363	19°39'S 9°03'E	>102-107 108	2248 †	> 715	> 2713	3100	Shallow water conditions prevailed in the Aptian; all younger sediments indicate bathyal conditions.
ICELAND-FAEROE RIDGE							
336	63°21'N 7°47'W	43-49 50	811 1311	500	1136	2200	Shallow water middle Eocene sediments
352	63°39'N 12°28'W	> 27.5-30 ?	990 †	>104	> 1058	1700	No published information on subsidence history at this site
BROKEN RIDGE							
255	31°08'S 93°44'E	> 82-86 > 41	1144 †	> 109	> 1215	2900	Complicated history with periods of uplift and subsidence - uplift between Cretaceous and Eocene, began sinking again in late Eocer
CARNEGIE RIDGE							
157	1°46'S 85°54'E	5-10 7-17	2591 3022	431	2871	1000	No obvious shallow water fauna - subsidence history unknown
CHAGOS-LACCADIVE RIDGE							
219	9°02'N 72°53'E	53.5-60 59-63	1764 †	> 411	> 2031	2400	Shallow water late Paleocene lms, ss and siltstones. By early Eocene open marine conditions prevailed

TABLE I continued:

Site	Position Latitude/ Longitude	Age (m.y.b.p.) Site/Adjacent Ocean Crust	Depth(m) Water/ Basement	Sediment Thickness (m)	Isostatically Corr.Basement Depth(m)	Expected Depth (m)	Comments
COCOS RIDGE							
158	6°37'N 85°14'W	10-16 10-19	1953 2275	322	2162	1300	No obvious shallow water fauna - subsidence history unknown
COIBA RIDGE							
155	6°07'N 81°03'W	10-16 23-25	2752 3271	519	3089	1300	No obvious shallow water fauna
MADAGASCAR RIDGE							
246	33°37'S 45°10'E	49-53.5 ?	1030 †	> 194	> 1156	2300	Complicated history with periods of uplifts and subsidence-shallow in the early Eocene, subsidence begins in Miocene, Quaternary uplift
MASCARENE PLATEAU							
237	7°05'S 58°08'E	60-65 ?	1623 †	> 694	> 2074	2500	Shallow water conditions in the early Paleocene
MOZAMBIQUE RIDGE							
249	29°57'S 36°05'E	> 120 ?	2088 2496	408	2353	3200	Subsidence history unknown
NATURALISTE PLATEAU							
258	33°48 'S 112°28 'E	> 98 ?	2793	525	> 3134	3000	Complicated history with periods of uplift and subsidence - gradual shoaling throughout the Cretaceous

† Volcanic basement not reached.

sediments using a method outlined by Sclater and others (in press). Where basement was not reached, the depth and age of the basal sediments have been used. We have also computed an expected depth, assuming each site was formed at sea level and has since subsided along a curve similar to that of normal oceanic crust.

The subsidence histories of several of the aseismic ridges compiled in Table 1 are either unknown or are complicated by subsequent uplift, and care must be taken in comparing data from these ridges with those that have had a simpler subsidence history. For example, sediments from DSDP sites on the Coiba (155), Carnegie (157) and Cocos (158) Ridges show no evidence of shallow water fauna even though volcanic basement was reached in each case. Apparently, these ridges never reached sea level when they were formed, and consequently they are now unusually deep (2162-3089 m) for their age (late to middle Miocene). The subsidence history of the Mozambique Ridge (249) is similarly unclear. While Madagascar Ridge (246), Broken Ridge (255) and the Naturaliste Plateau (258) have all been shallow at one time, they have had complicated subsidence histories with one or more periods of subsequent uplift. This uplift has left sites on Broken Ridge and Madagascar Ridge unusually shallow for their age.

We will consider only those aseismic ridges that are known to have formed near sea level and that have not experienced subsequent uplift (Figure 2). These aseismic ridges include the Ninetyeast Ridge, Rio Grande Rise, Walvis Ridge, Chagos-Laccadive Ridge, the southeast Mascarene Plateau and the Iceland-Faeroe Ridge. The rate of subsidence of these ridges is comparable to that of normal oceanic crust, although the actual amount of subsidence varies from site to site and is generally somewhat less than would be expected from our predicted subsidence curve.

FIGURE 2

Isostatically adjusted basement depth plotted against age for those aseismic ridges in Table 1 that are known to have been formed at or near sea level and that have not experienced subsequent uplift. Predicted subsidence curve (solid line) determined by assuming these ridges formed at sea level and then subsided along the empirical depth vs. age curve of Sclater, et al. (1971). Dashed line is this same curve displaced upward by 300 m. Numbers refer to DSDP site numbers. Horizontal bars indicate estimates of possible age error; question mark is used where basement was not reached. Key: ▲ Ninetyeast Ridge; X Rio Grande Rise; ● Walvis Ridge; ■ Iceland Faeroe Ridge; ○ Chagos-Laccadive Ridge; ◆ Southeast Mascarene Plateau.

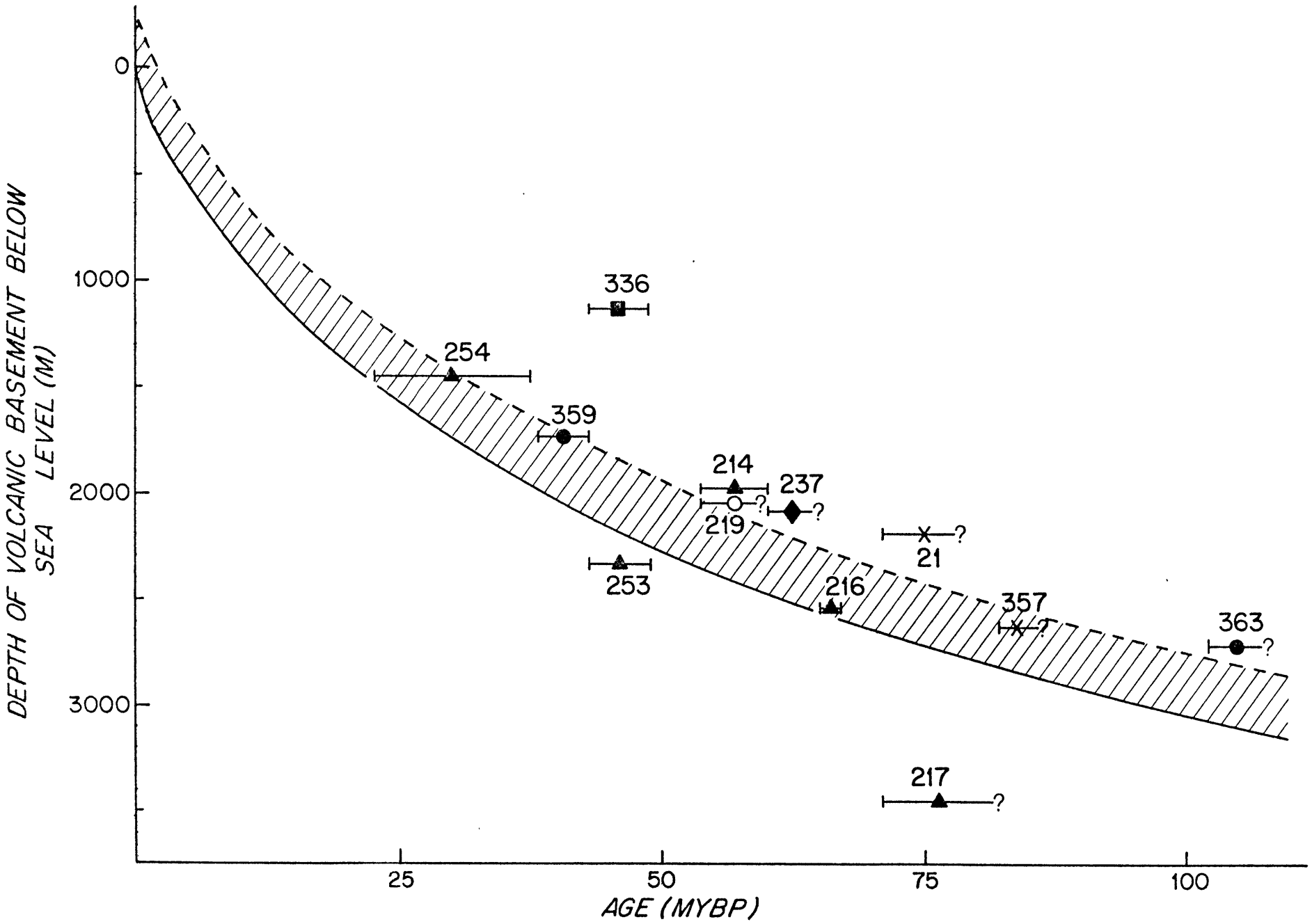
DEPTH OF VOLCANIC BASEMENT BELOW SEA LEVEL (M)
0
1000
2000
3000
25
50
75
100
AGE (MYBP)
336
254
359
214
237
219
21
253
216
357
363
217

Ninetyeast Ridge with five DSDP holes (217, 216, 214, 253 and 254) has been drilled more than any other aseismic ridge (von der Borch et al., 1974; Davies et al., 1974). Of these sites only hole 217 failed to reach volcanic basement. At each site a basal sequence of shallow water sediments was found, grading upward into deeper water pelagic calcareous oozes. The agreement between the predicted depth and the isostatically corrected basement depth is generally quite good at all sites except 217. This hole was drilled on the eastern flank of the ridge, which may partially explain why its corrected depth is much deeper than predicted. Site 216, which has subsided ~2500 m since the late Cretaceous, is within 60 m of its predicted depth, and site 253 with over 2300 m of subsidence since the middle Eocene is less than 150 m from its expected depth. Sites 254 and 214 both are 300-400 m shallower than expected, but clearly fall along the general subsidence trend for these aseismic ridges.

Three DSDP sites (21, 22 and 357) are located on the Rio Grande Rise (Maxwell et al., 1970; Perch-Nielson et al., 1975). Shallow water sediments were encountered at site 21 on the northeastern edge of the Rio Grande Rise and at site 357. Unfortunately volcanic basement was not reached at either of these sites; thus both age and basement depth values plotted are minimum estimates. Nevertheless both sites fall along the general subsidence trend of other aseismic ridges. Thiede (1977) has recently examined the subsidence history of the Rio Grande Rise, and he estimates a pre-Santonian basement age of ~97 m.y. for site 357 and an uncorrected basement depth of ~3800 m. A correction for the loading effect of ~1700 m of sediment would raise basement to a depth of ~3200 m. This age and corrected depth for site 357 would place it in somewhat better agreement with our predicted subsidence curve.

The Walvis Ridge has been drilled twice (359 and 363). Site 359 is situated on the flank of a seamount that is part of the southwestern segment of the Walvis Ridge. This hole bottomed in an alkali-rich, silica-rich ash-flow tuff, indicating that subaerial conditions probably prevailed at this site in the late Eocene (Bolli et al., 1975). The total subsidence since then has been at least 1700 m, close to the ~2000 m depth expected for a site of this age. At site 363 (Bolli et al., 1975), located on the eastern Walvis Ridge, basement was not reached but the hole bottomed in shallow water sediments of probable Aptian age (102-107 m.y.). These shallow water sediments including calcarenites with rounded limestone sand grains, calcareous algal remains and small amounts of phosphorite are probably displaced, but indicate a nearby source of shallow water sediments. Shallow water fossils of Aptian-Albian age have also been dredged from the eastern Walvis Ridge (Pastouret and Goslin, 1974).

The Chagos-Laccadive Ridge has been drilled only once (219) near its northern end. While basement was not reached, the hole bottomed in shallow water limestones, sandstones, and siltstones of late Paleocene age probably deposited in water depths of less than 100 m (Whitmarsh et al., 1974). The total subsidence since that time has thus been at least 2000 m, close to that expected from the subsidence rate of normal oceanic crust. This long 2200 km north-south trending ridge thus appears to have a subsidence history similar to that of the Ninetyeast Ridge, the Walvis Ridge and the Rio Grande Rise.

The southeast Mascarene Plateau (Saya de Malha Bank) is an enigmatic feature which might be classed as an aseismic ridge. The Seychelles Bank to the northwest is composed of pre-Cambrian, 600 m.y. old granites cut

by early Tertiary mafic dikes (Fisher et al., 1967). The nature of the basement of Saya de Malha Bank is not known though seismic refraction evidence (Shor and Pollard, 1963) suggests a basaltic composition. Site 237, drilled on a saddle between Seychelles and Saya de Malha Bank, did not reach basement but did bottom in early Paleocene sediments (Fisher et al., 1974), which indicate a nearby source of shallow water sediments. Vincent et al., (1974) have examined faunal assemblages at this site and report an abrupt change in sedimentary environment from upper bathyal (200-600 m) depths 57-62 m.p.b.p. to lower bathyal (600-2500 m) depths with characteristic deep water microfossil assemblages in the late Paleocene. This apparent subsidence was accompanied by a marked decrease in sedimentation rate. Assuming this site was near sea level in the early Paleocene (60-65 m.y.b.p.) the total subsidence has probably been greater than 2000 m--very similar to the observed subsidence for similarly aged sites on the Ninetyeast and Chagos-Laccadive Ridges.

Sediments from site 336 on the Iceland-Faeroe Ridge indicate a long history of submergence for this ridge; however, the corrected basement depth of this site is unusually shallow and does not appear to fall along the subsidence trend of the other aseismic ridges. This site and site 217 on the Ninetyeast Ridge show the largest difference between the actual and expected depth of any of the twelve sites we have discussed. With the simple model developed in the next section we will explore several factors which could be responsible for this discrepancy.

A SIMPLE MODEL

From the Deep Sea Drilling Project data discussed in the previous section, it appears that at least five major aseismic ridges--the Ninety-east Ridge, the Rio Grande Rise, the Walvis Ridge, the Chagos-Laccadive Ridge and the southeast Mascarene Plateau--all have formed at or close to sea level and have since subsided at rates comparable to that of normal oceanic crust. The basement ages on at least two of these ridges (Ninetyeast and Walvis Ridges) vary along their length and are similar to the age of normal oceanic crust adjacent to the ridge (Table 1).

These observations can be explained by the simple model presented in Figure 3. Aseismic ridges are formed at or very close to a spreading center by excessive volcanism which builds the ridge up to or even above sea level. This volcanism may be related to a mantle hot spot or plume as suggested by Wilson (1973) or Morgan (1971, 1972). It also may be related in some way to transform faulting (McKenzie and Sclater, 1971) since all or portions of these ridges appear to be aligned along fracture zones. By analogy with the large shield volcanoes along the Hawaiian chain, it is assumed that the major constructional phase of volcanism will be relatively short, probably no longer than 0.5-1.5 m.y. (Jackson et al., 1972) and that any isostatic adjustment due to loading of the underlying crust by the mass of the ridge will be essentially contemporaneous with the volcanism and will not occur long after volcanism has ceased. As spreading continues, the aseismic ridges will be carried away from the spreading center along with the lithospheric plate on which it is built. As this plate cools and contracts, the aseismic ridge will subside with it, and the rate of subsidence will be the same as that of normal oceanic crust.

FIGURE 3

Simple model which can account for the observed subsidence of many aseismic ridges. Measured subsidence is obtained by taking the present isostatically corrected depth of volcanic basement beneath sea level. The predicted subsidence is indicated by the solid line, actual subsidence by dashed line. The measured subsidence will generally be less than the actual and predicted subsidence if the ridge is initially built above sea level (see text for discussion).

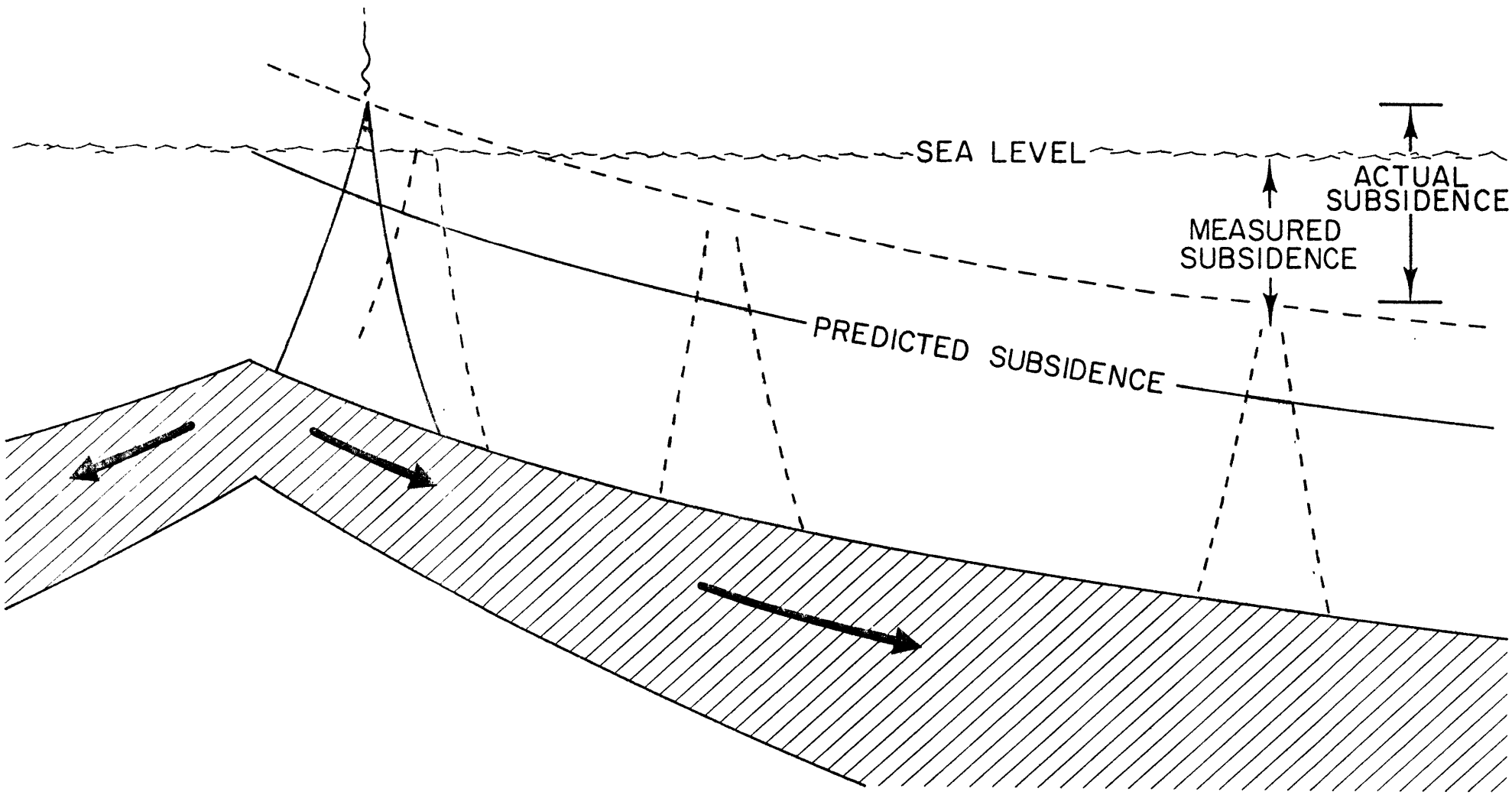
SEA LEVEL
ACTUAL SUBSIDENCE
MEASURED SUBSIDENCE
PREDICTED SUBSIDENCE

DISCUSSION

In this model we explain the observed subsidence of aseismic ridges as a purely thermal effect associated with the cooling and contraction of the lithosphere on which the ridge is built. The fact that many aseismic ridges appear to follow a simple $t^{\frac{1}{2}}$ subsidence law means that paleobathymetric backtracking techniques can be applied to the sediments on these ridges. Since aseismic ridges have apparently had a major effect on the sedimentation history and paleocirculation patterns of certain ocean basins, this model should provide a valuable framework in which the role of aseismic ridges can be properly evaluated.

The amount of subsidence of any point on an aseismic ridge is estimated by taking the present isostatically corrected depth of volcanic basement below sea level. Consequently, a point will fall on our "predicted" subsidence curve only if the aseismic ridge is built exactly to sea level at the spreading center (i.e., on 0 m.y. old crust; see Figure 3). Naturally, we expect some parts of the ridge will be built above sea level while other parts of the ridge may not quite reach sea level. This should result in a scatter of points above and below the predicted subsidence curve. However, most of the sites plotted in Figure 2 appear to fall above the predicted subsidence curve. At least three factors would cause the actual subsidence to differ from that predicted by our simple model: (1) the age of the crust the aseismic ridge is initially built on, (2) its original height relative to sea level, and (3) the amount of the ridge removed by subaerial erosion.

In our model we have assumed that aseismic ridges are formed at spreading centers. If in some cases they are built on older crust adjacent to a spreading center, then the actual amount of subsidence will be

less than that predicted by our model. This is, of course, because the underlying lithosphere will have already cooled and contracted by an amount proportional to the square root of its age. This effect can be very significant because of the initial steepness of the age-depth curve. The fact that the difference between the measured and predicted subsidence is generally no more than 300-400 m is consistent with our assumption that these features have formed on very young crust.

It is clear from DSDP results that parts of several aseismic ridges have at one time been above sea level. Subaerial conditions have been inferred at sites 214 and 253 on the Ninetyeast Ridge (von der Borch et al., 1974; Davies et al., 1974; Pimm et al., 1974) and site 359 on the Walvis Ridge (Perch-Nielson et al., 1975). Thiede (1977) believes that part of the Rio Grande Rise was also emergent during the late Cretaceous. If a point on an aseismic ridge is initially built above sea level, then the marine sediments subsequently deposited at this site will only record the later part of the subsidence history of the ridge. Since the amount of the subsidence which occurred prior to the time the ridge sank below sea level cannot be determined, we will underestimate the actual amount of subsidence by taking the present depth of the ridge below sea level. This will be partially offset by the effect of subaerial erosion, which may remove part of the ridge; however, the net effect, particularly if the site remains above sea level for a considerable time, will be that the measured subsidence will be less than that predicted by a simple $t^{\frac{1}{2}}$ subsidence law. It is apparent from Figure 3 that the present depth of any point on the ridge will depend only on the age of the underlying crust when the ridge finally sinks below sea level. Since most aseismic ridges fall close to

our predicted subsidence curve, these ridges probably have sunk below sea level within a few million years of their formation.

There are, however, aseismic ridges which have apparently remained above sea level for a considerable time after they were formed. DSDP site 336 on the Iceland-Faeroe Ridge is anomalously shallow for its age, falling ~1100 m above our expected subsidence curve. Normal ocean crust subsides about 1200 m in the first 15 m.y. after it is formed. If the Iceland-Faeroe Ridge remained emergent for this length of time after it was formed, then we could account for the unusually shallow depth of this ridge (Figure 4). There is some evidence from site 336 on the Iceland-Faeroe Ridge that this may have been the case. The oldest sediments overlying volcanic basement at this site are Middle Eocene (43-49 m.y.) in age (Talwani et al., 1975); however, the ridge may not have sunk below sea level until after the westward shift in the spreading center north of Iceland around anomaly 7 time, ~30 m.y.b.p. (M. Talwani, personal communication, 1976).

The isostatically corrected basement depth of site 255 on Broken Ridge is also much shallower (~1200 m) than would be expected from the age of the basal sediments (82-86 m.y.) at this site. While Broken Ridge has had a complicated tectonic history with periods of both uplift and subsidence, the model presented by Luyendyk and Davies (1974) to account for the latest period of subsidence is basically the same as suggested above for the Iceland-Faeroe Ridge. Broken Ridge is probably at least 80 m.y. old; however, between the Late Cretaceous and the Late Eocene, it was uplifted above sea level. This event probably coincided with the initiation of spreading on the Pacific-Antarctic Ridge ~55 m.y.b.p., which split Broken Ridge from the Kerguelen Plateau. The present depth of site 255

FIGURE 4

Expected subsidence curve for an aseismic ridge which does not sink below sea level until 15 m.y. after it is formed (dashed line). Normal subsidence curve indicated by solid line. Site 336 on Iceland-Faeroe Ridge also shown.

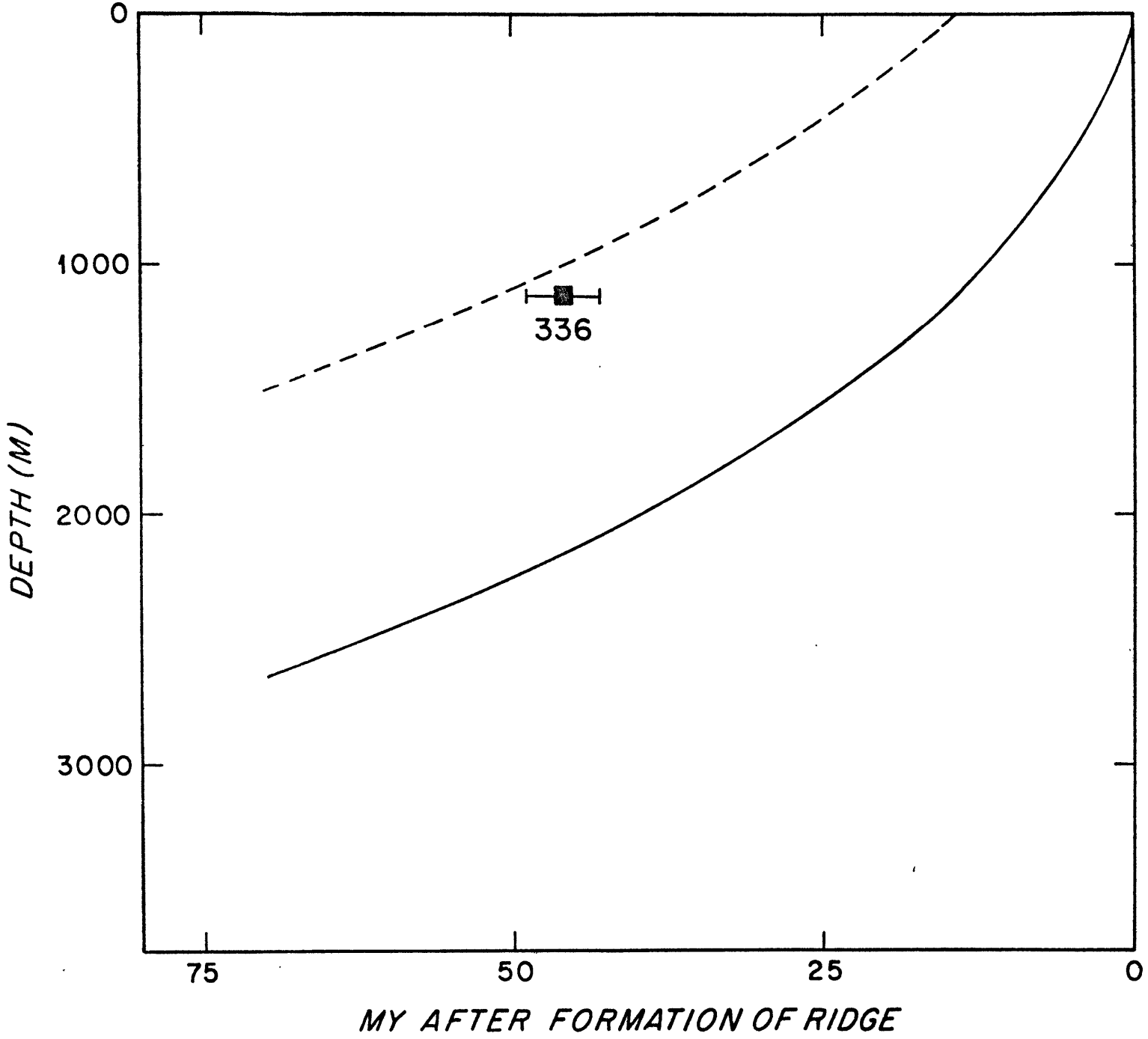
0
1000
2000
3000
DEPTH (M)
336
75
50
25
0
MY AFTER FORMATION OF RIDGE

on Broken Ridge can be explained if this site were emergent until ~38 m.y.b.p., after which it subsided at the same rate as the adjacent oceanic crust (see Figure 16 in Luyendyk and Davies, 1974). This is consistent with the age (upper Eocene) and lithology (beach gravels) of the oldest post-Cretaceous sediments found at site 255.

COMPARISON WITH OCEANIC PLATEAUS AND ISLAND CHAINS

There are two other major types of sea floor features which stand anomalously shallow compared to normal oceanic crust. They are the oceanic plateaus or rises such as the Manihiki Plateau or Magellan Rise and oceanic island chains such as the Hawaiian-Emperor Chain. There is some evidence that several western Pacific plateaus have formed near triple junctions (Winterer et al., 1974). Hence a model such as that proposed for aseismic ridges might also be applicable to these features. However, an examination of DSDP results from western Pacific plateaus shows that only in one case (site 317A--Manihiki Plateau; Winterer et al., 1974) is there any conclusive evidence for shallow water conditions early in the history of a plateau. At other sites either volcanic basement was not reached or only deep water pelagic sediments were recovered. From the available data it is therefore not possible to determine whether these features have a subsidence history similar to aseismic ridges.

The subsidence of western Pacific atolls and guyots has been well documented (Menard and Ladd, 1963). This subsidence continues long after volcanism has ceased and thus cannot easily be attributed to isostatic adjustments. Watts and Cochran (1974) have shown that it is also unlikely to be caused by any long-term inelastic behavior of the lithosphere beneath individual seamounts. While the simple model presented in Figure 3

has been developed for aseismic ridges which are believed to form at or very close to spreading centers, it should be equally applicable to features, such as the Hawaiian-Emperor seamount chain, which have formed on much older crust. Of course if a seamount or island is built on older crust away from a spreading center, the total expected subsidence will be much less than in the case of an aseismic ridge; however, the same conceptual model should apply.

Geological evidence from drilling on several western Pacific atolls (Ladd and Schlanger, 1960; Ladd et al., 1967) indicates that these features have subsided much more than would be expected from the thermal contraction of the adjacent crust. For example, Eniwetok in Marshall-Gilbert chain has subsided at a rate of about 20 m/my for the past 60 m.y. (Ladd et al., 1967) even though this island is located on oceanic crust of Jurassic age. This problem has been discussed by Menard (1973) and Watts and Cochran (1974). They suggest that the large amount of subsidence experienced by these western Pacific atolls and guyots is caused by the motion of the islands off broad regional topographic anomalies such as that associated with the southeastern portion of the Hawaiian ridge. If this explanation is correct, then we would expect the initial phase of subsidence to be quite rapid as the island moves off a topographic bulge. Following this the subsidence should be the same as the surrounding sea floor. This model has not, however, been adequately tested.

CONCLUSIONS

1. At least five major aseismic ridges--the Ninetyeast Ridge, the Rio Grande Rise, the Walvis Ridge, the Chagos-Laccadive Ridge and the southeast Mascarene Plateau--have formed at or close to sea level and have

since subsided at rates comparable to that of normal oceanic crust. The Iceland-Faeroe Ridge has probably undergone a similar subsidence history, but because parts of this ridge have remained above sea level for an unusually long time (~15 m.y.), its present depth is significantly less than other aseismic ridges of a similar age. Broken Ridge was uplifted above sea level in the Eocene; however, since it sank below sea level ~38 m.y. ago, it has subsided at rates comparable to that of similarly aged oceanic crust.

2. The subsidence of aseismic ridges is attributed entirely to the cooling and contraction of the lithospheric plate on which these ridges are built. In this model aseismic ridges are assumed to be built up close to sea level by excessive volcanism at or very near a spreading center. As spreading continues the aseismic ridge is carried away from the spreading center along with the plate on which it is built, sinking as this plate cools and contracts.

3. This simple subsidence model, which has been developed for aseismic ridges, should be equally applicable to features, such as the Hawaiian-Emperor seamount chain, which have formed on much older crust. However, drilling on several western Pacific atolls indicates these islands have subsided much more than would be expected from the thermal contraction of the adjacent crust.

ACKNOWLEDGMENTS

We benefited from discussions with B. Parsons and P. Molnar on the implications of this model. This work was sponsored by the National Science Foundation grant 74-02636 OCE and the Woods Hole Oceanographic Institution. Woods Hole Oceanographic Institution contribution 3886.

REFERENCES

Berggren, W. A., and J. A. van Couvering, The Late Neogene: Biostratigraphy, geochronology and paleoclimatology of the last 15 m.y. in marine and continental sequences, Paleogeogr., Paleoclimatol., Paleocol., 16, 1974.

Bolli, H. M., Ryan, W. B. F., et al., Basins and margins of the eastern South Atlantic, Geotimes, 20, 22, 1975.

Davies, T. A., et al., Initial Reports of the Deep Sea Drilling Project, 26, Washington, D. C. (U. S. Govt. Printing Office), 1974.

Fisher, R. L., G. Johnson and B. C. Heezen, Mascarene Plateau, Western Indian Ocean, Geol. Soc. Am. Bull., 78, 1247, 1967.

Fisher, R. L., et al., Initial Reports of the Deep Sea Drilling Project, 24, Washington, D. C. (U. S. Govt. Printing Office), 1974.

Jackson, E. D., E. A. Silver and G. B. Dalrymple, Hawaiian-Emperor chain and its relation to Cenozoic circumpacific tectonics, Geol. Soc. of Amer. Bull., 83, 601, 1972.

Ladd, H. S.,and S. O. Schlanger, Drilling operations on Eniwetok Atoll, U. S. Geol. Surv. Prof. Pap., 260-4, 1960.

Ladd, H. S., J. I. Tracey, Jr., and M. G. Gross, Drilling on Midway Atoll, Hawaii, Science, 156, 1038, 1967.

Laughton, A. S., D. W. Matthews and R. L. Fisher, The structure of the Indian Ocean in The Sea, vol. 4, (A. E. Maxwell, ed.) Wiley-Interscience, 543, 1970.

Luyendyk, B. P., and T. A. Davies, Results of DSDP Leg 26 and the geological history of the southern Indian Ocean in Davies, T. A., Luyendyk, B. P., et al., Initial Reports of the Deep Sea Drilling Project, 26, 1974.

Maxwell, A. E., et al., Initial Reports of the Deep Sea Drilling Project, 3, Washington, D. C. (U. S. Govt. Printing Office), 1970.

McKenzie, D. P., and J. G. Sclater, The evolution of the Indian Ocean since the late Cretaceous, Geophys. J. R. astr. Soc., 25, 437, 1971.

Menard, H. W., Depth anomalies and the bobbing motion of drifting islands, J. Geophys. Res., 79, 5128, 1973.

Menard, H. W., and H. S. Ladd, Oceanic islands, seamounts, guyots and atolls, in The Sea, vol. 3, (A. E. Maxwell, ed.) 365, 1963.

Morgan, W. J., Convection plumes in the lower mantle, Nature, 230, 42, 1971.

Morgan, W. J., Plate motions and deep mantle convection, in Studies in Earth and Space Sciences, Geol. Soc. Amer. Memoir, 132, edited by R. Shagam et al., Geol. Soc. of Amer., Boulder, Colorado, 1973.

Pastouret, L., and J. Goslin, Middle Cretaceous sediments from the eastern part of the Walvis Ridge, Nature, 248, 495, 1974.

Perch-Nielson, K., Supko, P. R., et al., Leg 39 examines facies changes in South Atlantic, Geotimes, 20, 26, 1975.

Pimm, A. C., B. McGowran and S. Gartner, Early sinking history of the Ninetyeast Ridge, Northeastern Indian Ocean, Geol. Soc. Amer. Bull., 85, 1219, 1974.

Sclater, J. G., R. N. Anderson and M. L. Bell, The elevation of ridges and the evolution of the central eastern Pacific, J. Geophys. Res., 76, 7888, 1971.

Sclater, J. G., and R. L. Fisher, The evolution of the east central Indian Ocean, Geol. Soc. Amer. Bull., 85, 683, 1974.

Sclater, J. G., D. Abbott and J. Thiede, Paleobathymetry and sediments of the Indian Ocean, Geol. Soc. Amer. Memoir (in press).

Shor, G. G., Jr., and D. D. Pollard, Seismic investigations of Seychelles and Saya de Malha Banks, Northwest Indian Ocean, Science, 142, 48, 1963.

Simpson, E. S. W., et al., Initial Reports of the Deep Sea Drilling Project, 25, Washington, D. C. (U. S. Govt. Printing Office), 1974.

Talwani, M. Udintsen, G., et al., Leg 38, Geotimes, 20, 24, 1975.

Thiede, J., Subsidence of Aseismic Ridges: Evidence from sediments on Rio Grande Rise (Southwest Atlantic Ocean), Amer. Assoc. Petrol. Geol. Bull., 61, 929, 1977.

Thiede, J., K. Perch-Nielson, P. R. Supko, et al., Sediments on Rio Grande Rise (S. W. Atlantic Ocean): Subsidence of an aseismic ridge, IX Congr. Internat. Sediment., 8, 67, 1975.

Thierstein, H., Mesozoic biostratigraphy of marine sediments by calcareous nannoplankton, in W. R. Riedel and J. Saito, eds., Marine Plankton and Sediments: 3rd Planktonic Conf., Kiel, 1974, (in press).

van Andel, T. J., et al., Initial Reports of the Deep Sea Drilling Project, 16, Washington, D. C. (U. S. Govt. Printing Office), 1973.

Vincent, E., J. M. Gibson and L. Bran, Paleocene and early Eocene microfacies, benthonic foraminifera, and paleobathymetry of Deep Sea Drilling Project Sites 236 and 237, western Indian Ocean; in Fisher, R. L., Bunce, E. T., et al., Initial Reports of the Deep Sea Drilling Project, 24, 1974.

von der Borch, C., et al., Initial Reports of the Deep Sea Drilling Project, 22, Washington, D. C. (U. S. Govt. Printing Office), 1974.

Watts, A. B., and J. R. Cochran, Gravity anomalies and flexure of the lithosphere along the Hawaiian-Emperor seamount chain, Geophys. J. R. astr. Soc., 38, 119, 1974.

Whitmarsh, R. B., et al., Initial Reports of the Deep Sea Drilling Project, 23, Washington, D. C. (U. S. Govt. Printing Office), 1974.

Wilson, J. T., Mantle plumes and plate motions, Tectonophysics, 19, 149 1973.

Winterer, E. L., Ewing, J. I., et al., Initial Reports of the Deep Sea Drilling Project, 17, Washington, D. C. (U. S. Govt. Printing Office), 1973.

Winterer, E. L., P. F. Lonsdale, J. L. Matthews and B. R. Rosendahl, Structure and accoustic stratigraphy of the Manihiki Plateau, Deep Sea Res., 21, 793, 1974.

CHAPTER 4

ISLAND SUBSIDENCE, HOT SPOTS, AND LITHOSPHERIC THINNING

ISLAND SUBSIDENCE, HOT SPOTS, AND LITHOSPHERIC THINNING*

Robert S. Detrick
Massachusetts Institute of Technology
Cambridge, Massachusetts 02139
Woods Hole Oceanographic Institution
Woods Hole, Massachusetts 02543

S. Thomas Crough
Woods Hole Oceanographic Institution
Woods Hole, Massachusetts 02543

*Published in Journal of Geophysical Research, 83,(1978), p. 1236-1244.

ABSTRACT

Drilling results from several western Pacific atolls indicate the long-term subsidence of these islands is much more than would be expected from the cooling and thickening of the underlying lithosphere. This excess subsidence cannot be satisfactorily explained by isostatic adjustments to the weight of the volcano or the coral reef cap. It appears to be related to island formation atop unusually shallow areas of sea floor, like the Hawaiian swell, associated with midplate hot spots. The excess subsidence is caused by the gradual return of these shallow areas to normal depths. Several authors have suggested that the Hawaiian swell is supported by upward flow in the asthenosphere. However, this model offers no reasonable explanation for the shape of the swell or the observed rates of atoll subsidence. The regional gravity anomaly over the Hawaiian swell indicates an average depth of compensation within the lower half of the lithosphere, not within the asthenosphere, as would be expected if the swell were maintained by asthenospheric flow. While the compensating mass may extend to greater depths, most of the density changes appear to occur within the lithosphere. We propose that the Hawaiian swell is formed by lithospheric thinning over the Hawaiian hot spot. Since the asthenosphere is less dense than the lithosphere, replacement of the lower portion of the lithosphere by asthenospheric material causes isostatic uplift of the surface of the plate. After the lithosphere moves away from the hot spot, it cools and thickens, and the swell subsides. The subsidence histories of the Hawaiian swell and several Pacific atolls are in quantitative agreement with this mechanism. The main problem with this model is that it requires extremely fast rates of lithospheric heating.

INTRODUCTION TO THE PROBLEM

The simplest explanation for the widespread occurrence of atolls and guyots and the subsidence of aseismic ridges is that these features ride passively atop the underlying lithosphere and subside as this lithosphere cools and thickens. Detrick et al. (1977) have shown that the basement depths and ages at Deep Sea Drilling Project sites on several prominent aseismic ridges, including the Ninetyeast Ridge, the Walvis Ridge, and the Rio Grande Rise, fall on a subsidence curve parallel to the empirical age-depth curve of normal oceanic crust, suggesting this model is essentially correct for these features. This same model should be equally applicable to the subsidence of island chains, like the Hawaiian-Emperor chain, formed in the interior of lithospheric plates. After an initial relatively short period of rapid isostatic adjustments these islands should subside at the same rate as the surrounding sea floor. However, geological evidence from drilling on several western Pacific atolls indicates the long-term subsidence of these islands is much greater than this model would predict.

Four western Pacific atolls have been drilled: Funafuti in the Ellice Islands, Eniwetok and Bikini in the Marshall Islands, and Midway in the Hawaiian-Emperor chain (Figure 1). The thickness of the coral reef cap at each of these islands can be used to estimate the minimum amount of subsidence they have experienced since their formation. At Funafuti, several holes were drilled, the deepest penetrating 340 m of coraline limestone (Sollas and David, 1904). While volcanic basement was not reached, seismic evidence indicates the total thickness of the coral reef cap is at least 1 km (Menard, 1963). Nearly 1400 m

FIGURE 1

Bathymetric map of the western Pacific. Solid circles indicate the locations of drilled western Pacific atolls, and open circles the locations of the guyots listed in Table 1. Average depths along dashed lines are plotted in Figure 6.

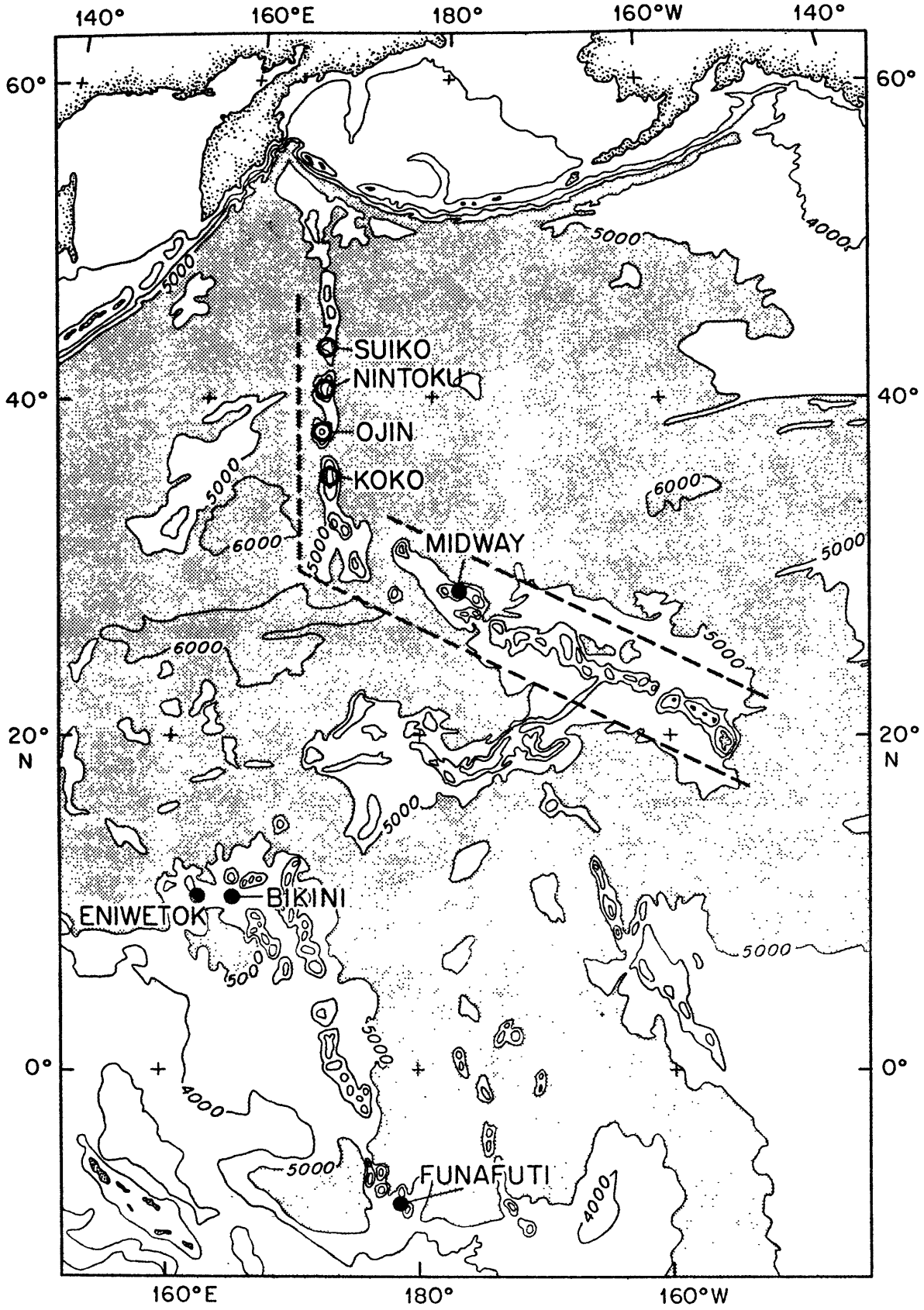
140°
160°E
180°
160°W
140°
60°
40°
20°
N
0°
SUIKO
NINTOKU
OJIN
KOKO
MIDWAY
BIKINI
ENIWETOK
FUNAFUTI
5000
6000
4000
500

of reef sediments were drilled at Eniwetok before reaching basalt (Ladd and Schlanger, 1960), while at nearby Bikini, 780 m of reef material were drilled, and seismic refraction data indicate about the same thickness for the coral reef cap as at Eniwetok (Raitt, 1954). Midway is the only atoll in the Hawaiian-Emperor chain that has been drilled, and here 384 m of reef material were found overlying basalt (Ladd et al., 1967). Stratigraphic horizons dated in the reef limestones at Midway, Eniwetok, and Bikini indicate an average subsidence rate of about 20 m/m.y. for the past 60 m.y. (Menard and Ladd, 1963), a remarkably fast subsidence rate when one considers that these islands are located on crust of Jurassic to early Cretaceous age.

The expected thermal subsidence of these islands can be calculated from an empirical age-depth curve for normal oceanic crust (Parsons and Sclater, 1977), since the age of the islands and the age of the surrounding crust are known. For example, Eniwetok is about 60 m.y. old (Kulp, 1963) and sits on Jurassic crust. It therefore formed on sea floor at least 90 m.y. old. Between the ages of 90 and 150 m.y. normal sea floor subsides about 500 m, which is only about one-third the observed subsidence at this island (Figure 2). Midway, which also formed on crust 80-90 m.y. old, has subsided about twice the expected amount.

The observed subsidence and the expected subsidence for these atolls and several guyots along the Hawaiian-Emperor chain are compiled in Table 1. The guyots have been included in order to provide some additional control on the subsidence of the Hawaiian-Emperor chain. Their subsidence has been estimated by determining the depth to slope break on bathymetric maps of Chase et al. (1970), except in the case of Koko seamount, where more detailed information has been published (Davies

FIGURE 2

Subsidence history of three western Pacific atolls that have been drilled (Ladd et al., 1967) and the present depth to slope break of several guyots along the Emperor seamount chain. Dashed line is predicted subsidence curve assuming these islands formed on 90-m.y.-old crust and have since subsided according to an empirical age-depth relation for the normal sea floor (Parsons and Sclater, 1977). Islands are identified by initial (Table 1).

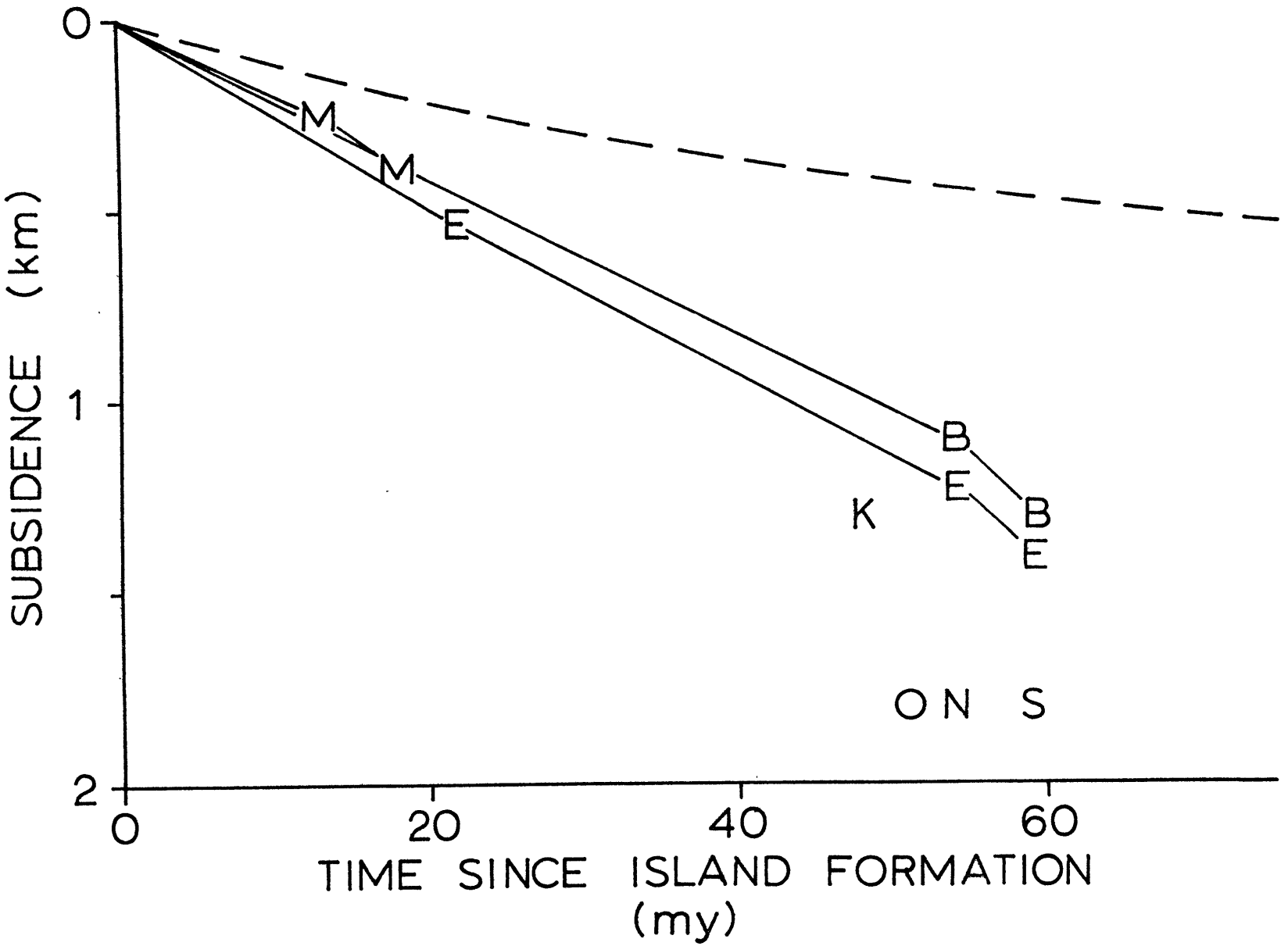
0
1
2
SUBSIDENCE (km)
M
M
E
B
E
K
B
E
O N S
0
20
40
60
TIME SINCE ISLAND FORMATION
(my)

TABLE 1. Subsidence Data for Some Western Pacific Atolls and Guyots

	Latitude	Longitude	t_s, m.y.	t_c, m.y.	Δ, m	Δh, m	Δh', m
			Atolls				
Funafuti	8.5°S	179.0°E	?		>340	--	--
Eniwetok	11.5°N	162.2°E	59 ± 2	>150	1405	500	1275
Bikini	11.6°N	165.3°E	37.5-53.5	>150	~1300	500	1275
Midway	28.3°N	182.7°E	18	~105	384	200	600
			Guyots				
Koko	35.2°N	171.8°E	~48	~110	~1300	600	1175
Ojin	38.0°N	170.5°E	~51	~106	~1800	700	1200
Nintoku	41.0°N	170.5°E	~54	~104	~1800	800	1225
Suiko	44.5°N	170.5°E	~59	<100	~1800	>1000	1274

Here t_s is age of seamount; t_c age of adjacent sea floor; Δ, thickness of coral reef cap (atolls) or depth to slope break (guyots); Δh, thermal subsidence of adjacent oceanic crust since island formed; and Δh', expected thermal subsidence if lithosphere thinned to same thickness as crust 30 m.y. old when island was formed. No calculations were made for Funafuti, since age is unknown. Thickness of reef cap at atolls is from Ladd et al. (1967), seamount ages are from Clague and Jarrard (1973).

et al., 1972). In all cases these islands have subsided at least 2-3 times the expected amount.

POSSIBLE MECHANISMS

There are several mechanisms that might explain the excess subsidence experienced by these atolls and guyots. They include isostatic adjustments to the weight of the volcano and the coral reef cap, viscoelastic flexure of the underlying lithosphere, and island formation atop anomalously shallow areas of sea floor.

Isostatic Adjustments

The major constructional phase of island volcanism is relatively short, usually not longer than 0.5-1.5 m.y. (Jackson et al., 1972). The underlying lithosphere responds to the mass of the volcano by bending, the actual deformation extending well beyond the load itself, resulting, in many cases, in a depression or moat immediately adjacent to the island and a rise or arch further seaward (Walcott, 1970a). These isostatic adjustments explain the extremely fast subsidence rates (>100 m/m.y.) determined from water well data on Hawaii (Stearns and Chamberlain, 1967) and may amount to several kilometers of total subsidence (Watts and Cochran, 1974). If the asthenosphere is sufficiently viscous, these isostatic adjustments could continue over a significant period of time, resulting in a much faster subsidence rate for the volcano than would be expected from a simple thermal model. There are, however, two serious objections to this explanation. First, the time scale of isostatic adjustments observed on the continents is of the order of 10^3-10^4 years (Walcott, 1970b). There is no reason to expect that the time scale for the oceans is any different; thus a volcano

should be completely compensated almost as soon as it is built. Second, free air gravity anomalies over the southeastern end of the Hawaiian chain (Watts, 1976) integrate to about zero (there is a small regional positive anomaly), indicating that even these very young volcanoes are almost perfectly compensated.

The loading effect of subsequent island formation further along the chain will be important if the island is located near enough to the new volcanoes to be in their developing moat. However, for rapidly propagating chains like the Hawaiian-Emperor chain these loading effects will only influence the subsidence history of the island for a short period of time (<3 m.y.). These rapid isostatic adjustments should then be followed by a long quiescent period in which the island rides passively atop the underlying lithosphere, sinking as this lithosphere cools and thickens. It is this later stage of island subsidence that is recorded by atoll drilling, and that is anomalously fast.

Sediment Loading

As the coral reef cap of an atoll grows, its weight will depress the underlying crust and effectively increase the observed subsidence rate. We have computed, using simple elastic beam theory (Walcott, 1970a), the additional flexure of the underlying lithosphere caused by the presence of the reef cap at Eniwetok. Using a flexural rigidity of 5×10^{29} dyn cm (Watts and Cochran, 1974) and assuming the moat around the island produced by this additional flexure is filled with sediment ($2.0\ g/cm^3$), these calculations indicate less than 100 m of the excess subsidence at Eniwetok is caused by the weight of the reef cap. This is clearly inadequate to explain the observed subsidence data at Eniwetok, and it is unlikely that sediment loading is responsible for a significant

portion of the excess subsidence experienced by any of the islands compiled in Table 1.

Viscoelastic Flexure

Walcott (1970b) has proposed that the lithosphere may respond to surface loads as a viscoelastic substance; that is, following an initial period of elastic strain it responds by viscous flow. The flexure of the lithosphere due to an applied load, such as a volcano, would thus increase with time, which might account for the excess subsidence of these atolls.

Unfortunately, this hypothesis is very difficult to test. The moat adjacent to the island should get deeper with time, but this deepening could be masked by sediments. The arch surrounding the island should get higher, but the change in elevation will probably be too small to measure. From two-dimensional beam theory the amplitude of the arch is known to be about one-twentieth the amplitude of the maximum deflection under the island (Walcott, 1970a). If the island subsides an additional 1 km, the arch should rise only about 50 m, which is too small to observe. While Watts and Cochran (1974) have concluded that there is no substantial viscoelastic relaxation along the Hawaiian-Emperor chain, the changes needed to explain excess atoll subsidence are so small we probably cannot rule out viscoelastic flexure as the subsidence mechanism. However, in the next section we describe an alternative mechanism which explains more of the available data.

Island Formation on Anomalously Shallow Sea Floor

The youngest portion of the Hawaiian-Emperor seamount chain is superimposed on a broad, elongate region of anomalously shallow depths (Figure 1).

This feature, known as the Hawaiian swell, is particularly well illustrated by the profile shown in Figure 3. The swell, which extends more than 2700 km WNW along the length of the Hawaiian-Emperor seamount chain, is about 1200 km wide and as much as 1600 m shallower than normal sea floor of the same age (Dietz and Menard, 1953; Watts, 1976). The amplitude of the swell gradually decreases toward the northwest, along the older portion of the chain, disappearing near the Hawaiian-Emperor bend.

The presence of this swell around Hawaii and its disappearance along the chain suggest a simple mechanism for explaining the excess subsidence of atolls and guyots (Figure 3b). If volcanoes form atop the swell on sea floor that is anomalously shallow for its age, then as the swell returns to near-normal depths, the islands will subside an extra amount equal to the original height of the swell (Watts and Cochran, 1974). The amplitude of the Hawaiian swell (about 1600 m) can qualitatively explain the excess subsidence of many of the older midplate volcanoes. While the Hawaiian swell is one of the most obvious features of this type, several other major oceanic volcanoes formed away from plate edges (Bermuda, Cape Verde Islands, Austral Islands) are also superimposed on broad, regional topographic swells. Since the Hawaiian swell has been well studied and since it probably has had an important effect on the subsidence history of islands along the Hawaiian-Emperor seamount chain, we will focus in the remainder of this paper on the processes which control the origin and disappearance of this feature.

FIGURE 3

(a) Bathymetric and free air gravity profiles across the Hawaiian ridge near Oahu showing Hawaiian swell, moat, and arch (from Watts, 1976); (b) Sketch drawn to scale of bathymetric profile in part (a) showing how subsidence of swell can account for the thickness of the coral reef cap.

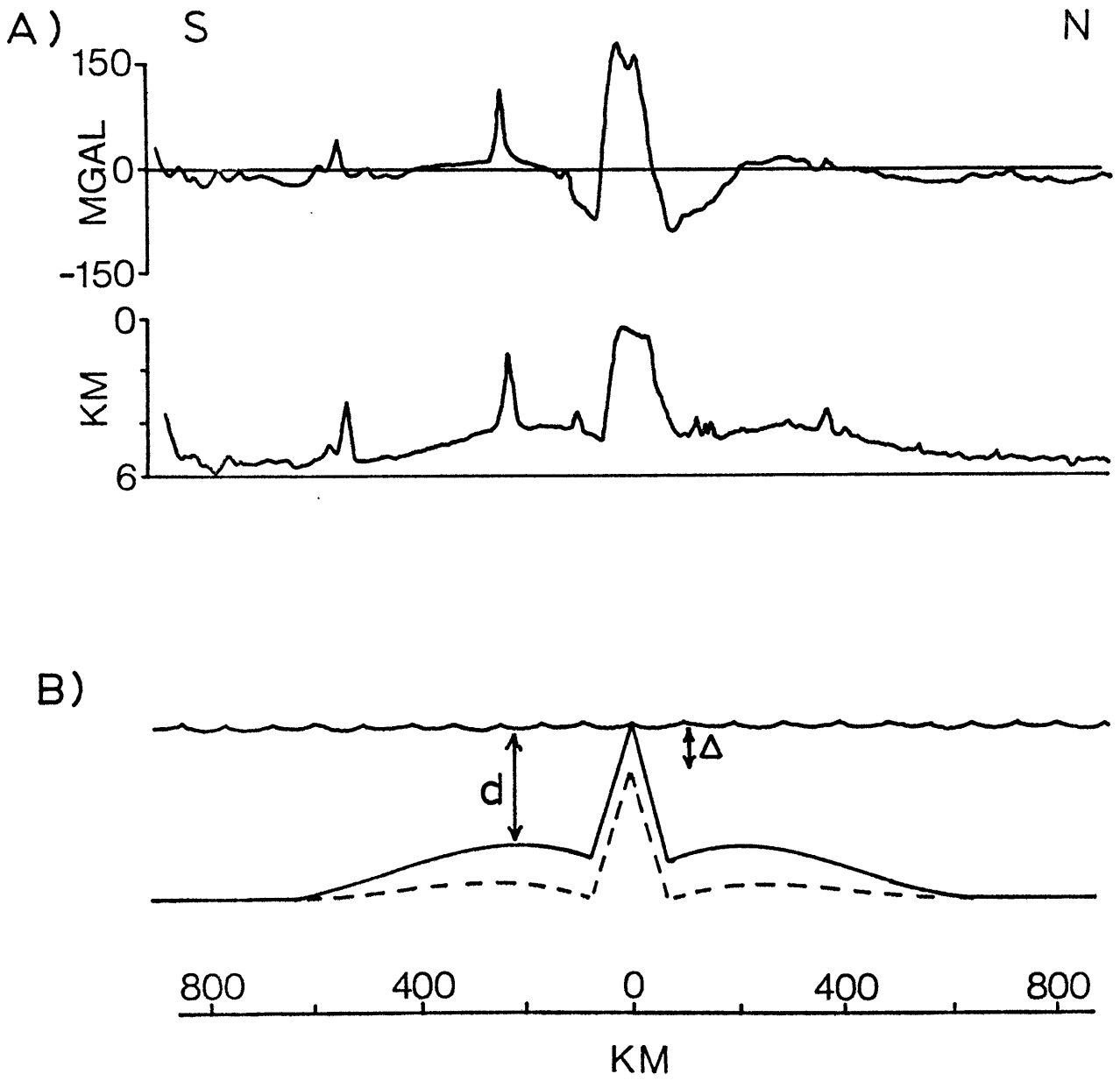
A)
S
N
150
0
-150
MGAL
0
6
KM
B)
d
Δ
800
400
0
400
800
KM

ORIGIN OF THE HAWAIIAN SWELL

Despite considerable crustal thickening beneath the Hawaiian ridge, Walcott (1970a) has shown that the Hawaiian swell is not formed in this manner. Seismic refraction results seaward of the islands indicate normal oceanic crustal thicknesses and velocities, even on the crest of the arch. However, the swell is also probably not caused by flexure of the lithosphere as suggested by Walcott (1970a). If the swell is a flexural feature, then it should maintain or increase its amplitude with age, but as we have noted, the swell is restricted to the youngest portion of the island chain.

Available gravity data from the Hawaiian area are also incompatible with a flexural origin for the swell. Watts (1976) has plotted $5^{o} \times 5^{o}$ averages of free air gravity versus bathymetry in the area around Hawaii and determined the slope to be ~21 mGal/km. As he mentions, this is a factor of 5 smaller than the slope of 96 mGal/km expected if the swell is flexural and uncompensated at depth (Watts and Talwani, 1974). We have examined the Hawaiian swell alone by digitizing profiles 4 and 5 in Watts (1976) and plotting gravity versus depth for the regions from the arch crest to the edge of the swell (neglecting points that occur on seamounts). For each track we have two data sets, one each for the areas NE and SW of the islands. For the four sets we get slopes of 13, 16, 19, and 27 mGal/km. The average slope is 19 mGal/km, not significantly different from the result Watts obtained using regional averages over an area which includes features other than the swell. Flexure undoubtedly occurs beneath the load of the Hawaiian ridge; however, the amplitude of the flexural arch is probably not much larger than a few hundred meters (model A of Walcott {1970a}) and clearly does not explain the origin of the Hawaiian swell.

Asthenospheric Origin

Dietz and Menard (1953) suggested that the Hawaiian swell was produced by uparching of the crust over a zone of divergent convection cells in the mantle (Figure 4a). Later calling these features "asthenospheric bumps," Menard (1973) suggested that the motion of a constant thickness lithosphere over these surface undulations on the asthenosphere could explain occasional interruptions in the general subsidence history of atolls. More recently, Watts (1976) has argued from gravity data that the Hawaiian swell is compensated by some pattern of flow beneath the lithosphere which maintains both the swell and its associated long-wavelength gravity anomaly.

However, there are several problems with this model. First, it offers no simple explanation for the shape of the Hawaiian swell. With most simple flow patterns, one would expect an approximately symmetric deformation of the lithosphere about the upward flow; yet the Hawaiian swell is clearly elongate, extending some 2700 km WNW along the island chain (this might of course be cited as evidence for a more complicated flow pattern, such as the cylindrical roll cells found experimentally by Richter and Parsons (1975); however, in this case it is not clear why volcanic activity does not occur along the entire length of the swell).

Second, Morgan (1971) noted that most volcanic centers that can be identified as "hot spots" are surrounded by regions of elevated topography. If these high areas are supported by upward flow in the asthenosphere, then hot spot related features formed at ridge crests, like aseismic ridges, should also experience a large excess subsidence. However, available data indicate aseismic ridges formed near ridge crests subside at the same rate as normal oceanic crust (Detrick et al., 1977).

FIGURE 4

(a) Asthenospheric bump model for the origin of the Hawaiian swell. A lithosphere of constant thickness is assumed to be supported over the swell by some pattern of convection in the upper mantle; (b) Schematic cross section of hot spot showing lithospheric thinning model for the origin of the Hawaiian swell. Thinning over the hot spot is assumed to be caused by increased asthenospheric heat flow Q' associated with the hot spot. (c) Schematic section along a hot spot trace showing the subsidence of the swell as underlying lithosphere cools and thickens. The sea floor along the hot spot trace will subside faster than would be expected from its crustal age but at the same rate as normal oceanic crust of a similar depth (lithospheric thickness).

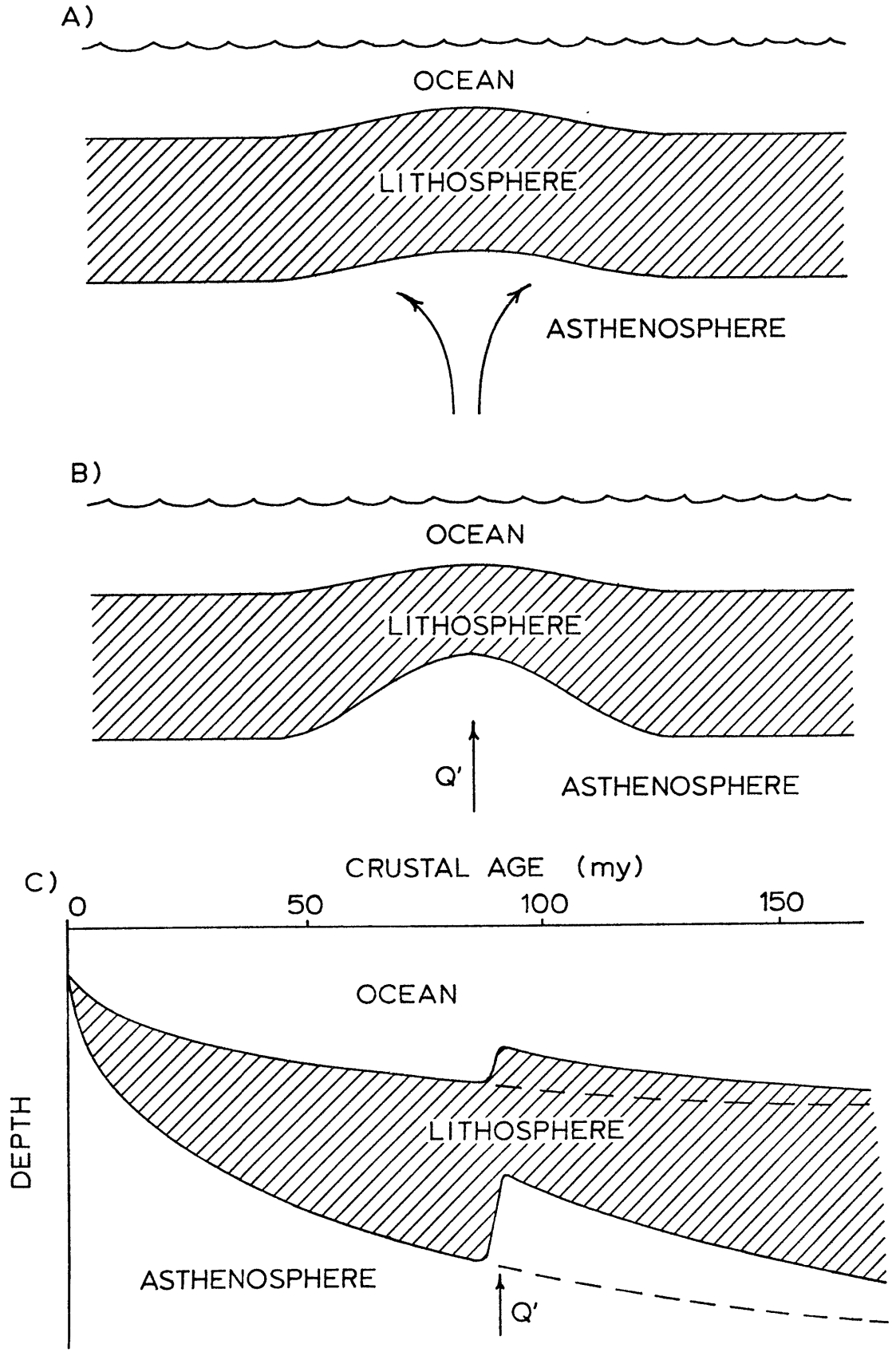
A)
OCEAN
LITHOSPHERE
ASTHENOSPHERE
B)
OCEAN
LITHOSPHERE
Q'
ASTHENOSPHERE
C)
CRUSTAL AGE (my)
0
50
100
150
OCEAN
DEPTH
LITHOSPHERE
ASTHENOSPHERE
Q'

Third, the gravity data over the Hawaiian swell indicate an average depth of compensation in the lower half of the lithosphere, not within the asthenosphere, as would be expected if the swell were maintained by some pattern of convection in the asthenosphere. Morgan (1971) and Watts (1976) have noted the presence of a regional positive free air gravity anomaly over the Hawaiian swell. Assuming that the swell is isostatically compensated by low-density material at depth, the size of the anomaly can be used to infer the average depth of the compensating mass (Sclater et al., 1975; Watts, 1976). For low-amplitude surface topography of the form $h(x,y) = h_o \sin(kx) \sin(\ell y)$ (where x and y are coordinates of the horizontal plane) the ratio between surface free air gravity Δg and topography is approximately

$$\Delta g/h = 2\pi G\rho\{ 1 - \exp(-k^2 + \ell^2 D)^{\frac{1}{2}}\} \qquad (1)$$

where G is the gravitation constant, ρ the density contrast, and D the depth to the compensating mass. This relation is not true for short wavelengths where lithospheric bending and the finite height of the gravity meter above the topography become important, but it is accurate for the wavelengths of features like the swells. This expression also does not take into account the sphericity of the earth; however, for features the wavelength of the swell (~1200 km) this correction is not important. Relation (1) is plotted in Figure 5 for various values of D using the half-wavelength $\lambda_{\frac{1}{2}}$ instead of k ($k = \pi/\lambda_{\frac{1}{2}}$) and assuming that $\rho = (3.3\text{-}1.0)$ g cm^{-3}. From Figure 3 it can be seen that the half wavelength of the Hawaiian swell is about 1200 km (±200 km). This is apparent from both the topography and the free air gravity anomaly. As we mentioned before, the gravity-topography ratio for the swell is about 20 m Gal/km (±5 mGal/km). These data indicate that the average depth of

the compensating mass beneath the swell is somewhere between 50 and 100 km (Figure 5). We stress that this is an average depth of compensation; from this analysis alone we cannot place any limits on how deep or how shallow the compensation may extend.

Thermal models of the lithosphere (Crough, 1975) and seismic evidence (Leeds et al., 1974) both indicate an expected thickness of about 90 km for lithosphere 90-100 m.y. old, the age of the crust around Hawaii. Here we are using a density definition of the lithosphere--a slab of cooler, denser asthenospheric material with a lower boundary determined by the depth to which the thermal boundary layer has penetrated. The gravity data thus indicate the Hawaiian swell is largely compensated at lithospheric depths. The compensation may extend to greater depths, but most of the changes must be within the lithosphere.

Watts (1976) has examined the same data and reached a different conclusion regarding the depth of compensation. We think this is because he determined the shape of the swell from a 5^{o} x 5^{o} average map of topography. This averaging makes the swell appear to be much wider than it is. If we used his width, $\lambda_{\frac{1}{2}}$ = 2200 km, in Figure 5, we would share his conclusion that the mass deficiency must be at or below the base of the lithosphere.

It can be argued that a sine function is not a good representation of the shape of the Hawaiian swell. However, it can be shown that relation (1) is an excellent approximation for a Gaussian-shaped swell ($h(x) = h_o \exp(-x^2/2\sigma^2)$), provided that the half wavelength used in (1) equals about 4σ (S. T. Crough, unpublished data, 1977). A Gaussian curve with σ = 300 km gives an excellent fit to the swell shape. Notice also that our estimates of depth are probably maximum estimates, since

FIGURE 5

Ratio of free air gravity anomaly and topography versus half wavelength $\lambda_{\frac{1}{2}}$ of surface topography. Solid lines are predictions for different depths D of compensation. First number gives depth in kilometers for the case where wavelength is the same in both horizontal directions. Number in parentheses gives depth when one horizontal wavelength is infinite. Data from the Hawaiian swell indicate that it is compensated within the lower half of the lithosphere (50-100 km).

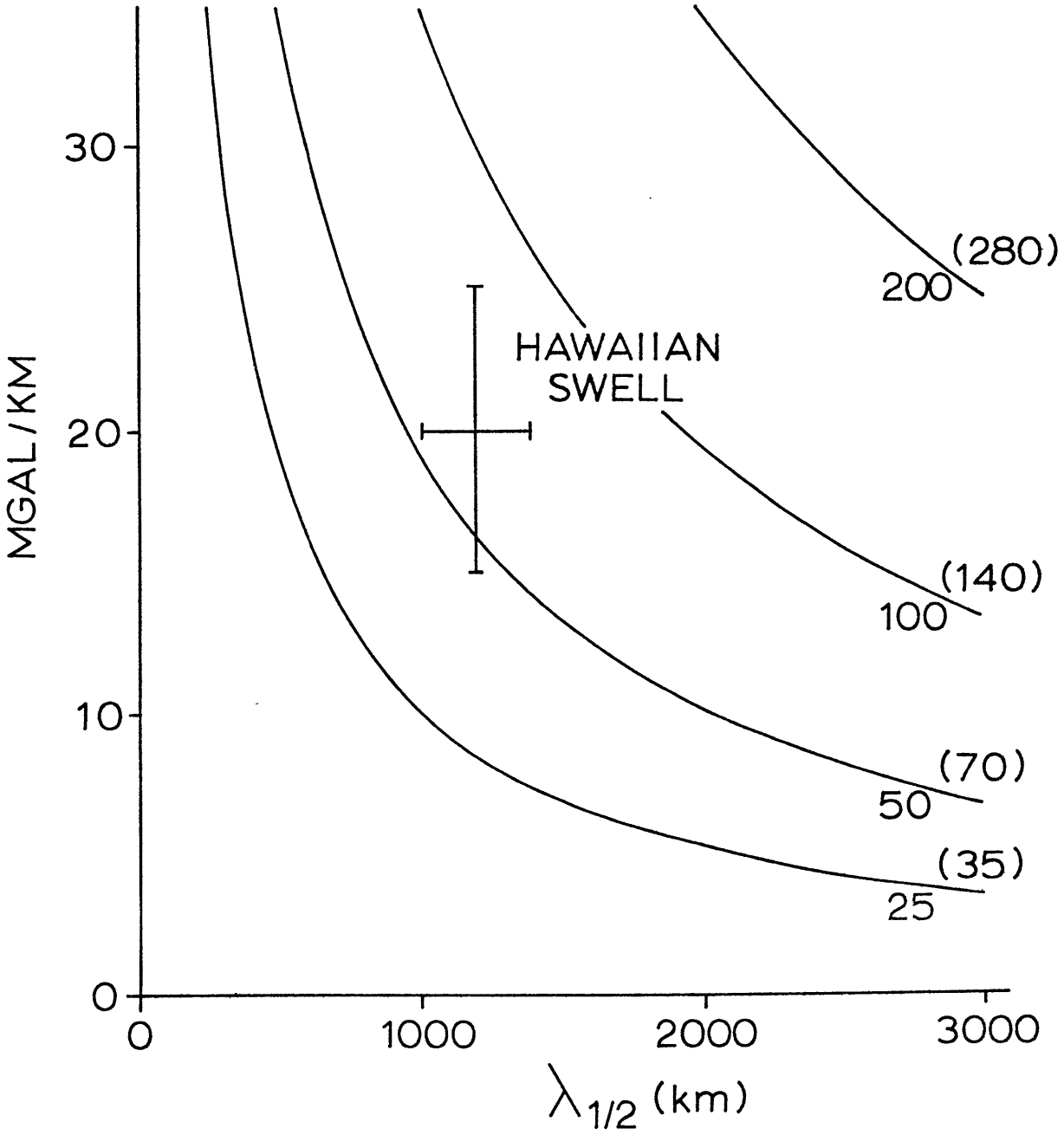
30
20
10
0
MGAL/KM
0
1000
2000
3000
$\lambda_{1/2}$ (km)
(280)
200
HAWAIIAN
SWELL
(140)
100
(70)
50
(35)
25

we have assumed that the swell is completely compensated. If as little as 50 m of the height of the swell is due to flexure, this would explain 5 mGal/km of the gravity-topography ratio. Explaining the remaining amount by compensation would force the compensation closer to the surface.

Finally, the bump concept is unsatisfactory because there is no evidence for it on the continents. The uplift of the western United States has been well studied, and geophysical data indicate that the uplift has been caused by lithospheric thinning (conversion of lithosphere to asthenosphere) rather than by dynamically supporting the lithosphere from below (Crough and Thompson, 1976b).

Lithospheric Thinning

We propose that the Hawaiian swell is caused by lithospheric thinning. We assume that the lithosphere-asthenosphere boundary is an isotherm near the solidus and that there is an increased asthenospheric heat flux Q', associated with the Hawaiian hot spot (Figures 4b and 4c). This higher heat flux thins the lithosphere by driving this isotherm upward. Since the asthenosphere is simply hotter, less dense lithospheric material, this results in isostatic uplift. The most obvious surface manifestation of this uplift will be a broad area of positive residual depth anomalies associated with the hot spot. As the lithosphere moves away from the hot spot, it gradually cools, thickens, and subsides, eventually approaching the normal thickness-crustal age relation.

This gradual thermal subsidence provides a simple explanation for why the Hawaiian swell is elongate in the direction of the volcanic chain. Lithospheric thinning also puts the compensating mass at the right depth to satisfy the gravity observations, since the dominant gravity signal

at these depths is expected to come from the lithosphere/asthenosphere boundary. The thinning model also explains why aseismic ridges which have formed near ridge crests have normal subsidence histories. The lithosphere at ridge crests is already exceptionally thin. A hot spot will not be able to thin it much further; so it should subside like normal sea floor of the same age.

In the thinning model it is useful to distinguish between the crustal age, which might be determined by identifying marine magnetic anomalies or the paleontological age of the oldest sediments in a particular area, and the thermal age, which depends on lithospheric thickness. Generally, the crustal age and the thermal age are the same, but over a hot spot the thermal "clock" in the crust may be reset to a younger age by lithospheric thinning. From that point on, the thermal age will differ from the crustal age. The lithosphere will still cool and subside as it ages but at a rate which depends on its thickness (thermal age), not on its crustal age. Thus hot spot generated midplate island chains formed atop an area of thinned lithosphere will subside at faster rates than normal sea floor of the same crustal age. This prediction provides us with a method for quantitatively testing the thinning model by examining the disappearance or subsidence of the swell along the Hawaiian-Emperor chain.

Testing the Model

We have visually estimated the average depth of the sea floor (excluding islands, guyots, and seamounts) in 1^{o} x 1^{o} squares of latitude and longitude in a broad band 1500 km wide along the Hawaiian-Emperor chain using the bathymetric maps of Chase et al. (1970). All depths were corrected for the velocity of sound in water using Matthews' (1939) tables.

Because the regional sediment cover is relatively thin and uniform along the chain (Ewing et al., 1968), we have not corrected for sediment loading. From this averaged depth map the shallowest depth within about 200 km of the volcanic chain was determined at intervals of about 100 km along the length of the chain. Wherever possible, we determined the depths on both sides of the chain, omitting values from the clearly anomalous Hess Rise and Emperor Trough. These values should be a good estimate of the depth to the top of the arch surrounding the islands, which is a reasonable estimate of the depth to the top of the swell (depth d in Figure 3).

In Figure 6 we have plotted these depths against age along the chain (ages are based on Figure 5 of Clague and Jarrard 1973). Though there is some scatter, the sudden development and gradual subsidence of the swell are clearly demonstrated. This subsidence is also apparent in actual bathymetric profiles parallel to the ridge (Figure 7 of Watts et al. {1976}). The shallowest point on the arch southeast of Oahu is at a depth of about 4300 m, which corresponds to an age of about 30 m.y. on the empirical depth-age curve of Parsons and Sclater (1977). Thus the lithospheric thinning concept predicts that the swell should subside like normal 30-m.y.-old crust. Indeed, the empirical subsidence curve for 30-m.y.-old crust provides a good fit to the data (Figure 6).

The sea floor between Bikini and Eniwetok is at 5100 m depth, about 500 m shallower than expected based on its age. Bikini and Eniwetok have subsided 1300-1400 m (Table 1). If the neighboring sea floor subsided with the islands, it was only 3700-3800 m keep when the islands formed. Depending on whether or not the 500 m depth anomaly present now also existed when the islands formed, this depth corresponds to an age of about 15-25 m.y. Yet, as we have mentioned, this area had a crustal age of

FIGURE 6

Depth of the crest of the Hawaiian swell plotted against age along the Hawaiian-Emperor chain (location approximately indicated by dashed lines in Figure 1). Hawaii is assumed to be 0 m.y. old. Age along the chain is taken from Clague and Jarrard (1973), negative ages corresponding to points southeast of Hawaii along the trend of the Hawaiian ridge. Shaded band indicates expected depth if normal age/depth relationship existed in this area. Solid line is empirical age-depth curve for normal oceanic crust between 30 and 100 m.y. old (Parsons and Sclater, 1977).

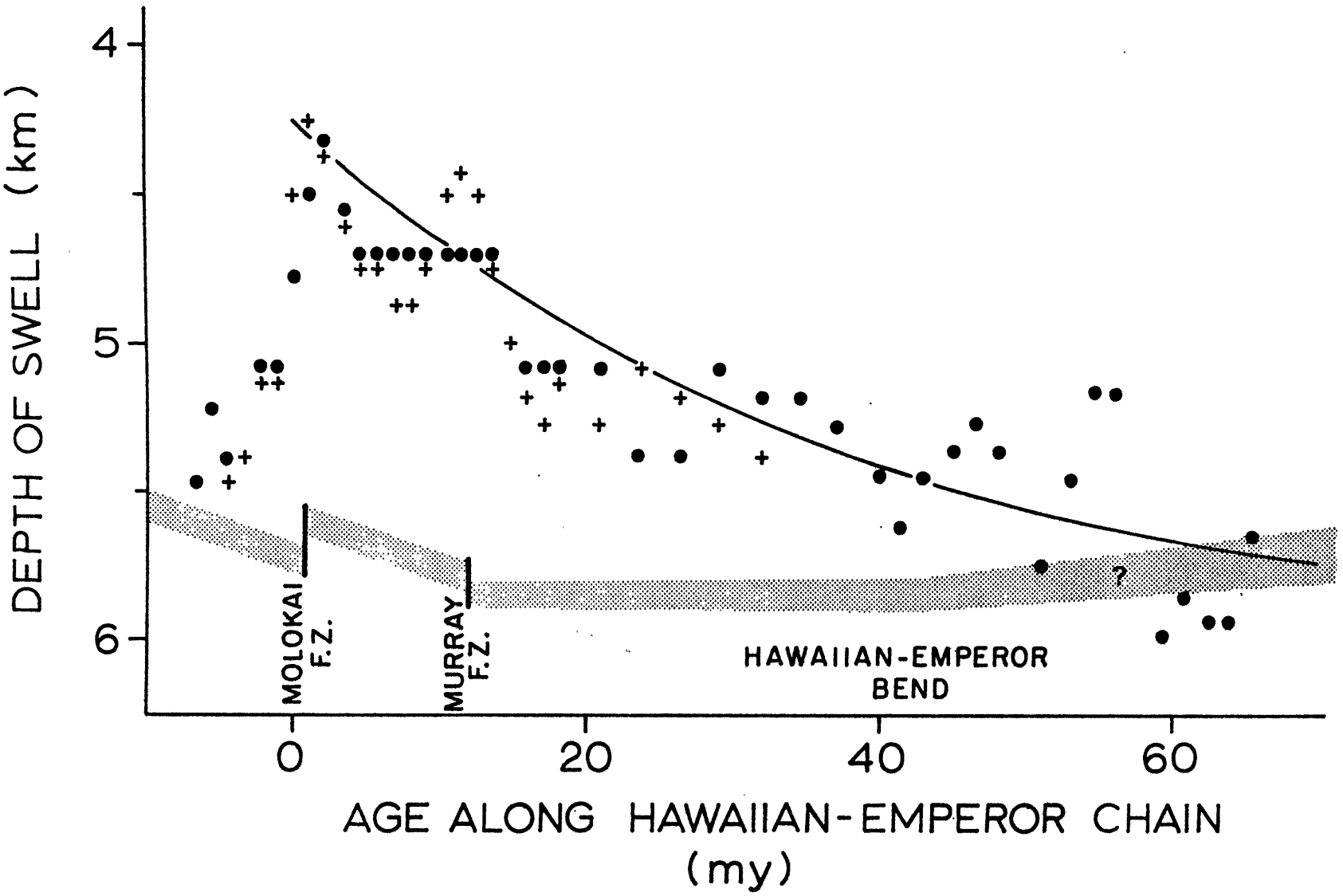
DEPTH OF SWELL (km)
4
5
6
MOLOKAI F.Z.
MURRAY F.Z.
HAWAIIAN-EMPEROR BEND
?
0
20
40
60
AGE ALONG HAWAIIAN-EMPEROR CHAIN (my)

about 90 m.y. during island construction. This evidence is consistent with the idea that Bikini and Eniwetok formed atop a swell. If the swell were formed by lithospheric thinning, then these islands should have subsided at the same rate as normal 15- to 25-m.y.-old lithosphere. Stratigraphic horizons dated within the reef limestones at Eniwetok and Bikini (Ladd et al., 1967) indicate the actual subsidence rate has been close to what would be expected if the islands formed on lithosphere with a thermal age of 25 m.y. (Figure 7).

We have also computed the expected subsidence $\Delta h'$, assuming lithospheric thinning for Midway and several guyots along the Emperor chain (Table 1). We have assumed that the lithosphere beneath each of these islands was originally thinned to the same value as that beneath Hawaii today. While the agreement is only fair, the significance of this result is difficult to judge, since the ages of most of these guyots are so poorly known.

DISCUSSION

The lithospheric thinning model thus provides a simple explanation for both the shape of the Hawaiian swell and the excess subsidence experienced by some western Pacific atolls. It also satisfies available gravity data, which indicate the Hawaiian swell is largely compensated at lithospheric depths. The compensation could extend deeper. We cannot preclude some density changes occurring in the asthenosphere; however, our results indicate that the density contrast with the surrounding asthenosphere must be small. Most of the density changes appear to occur in the lithosphere. The thinning model is also compatible with the measurement of normal heat flow on the swell near Hawaii (Sclater et al., 1976). If the lithospheric thickness over Hawaii were suddenly reduced

FIGURE 7

Predicted subsidence history of Eniwetok assuming that the lithosphere was initially thinned to the equivalent of normal 25-m.y.-old lithosphere. Solid line is prediction, and letters are dated horizons on Eniwetok.

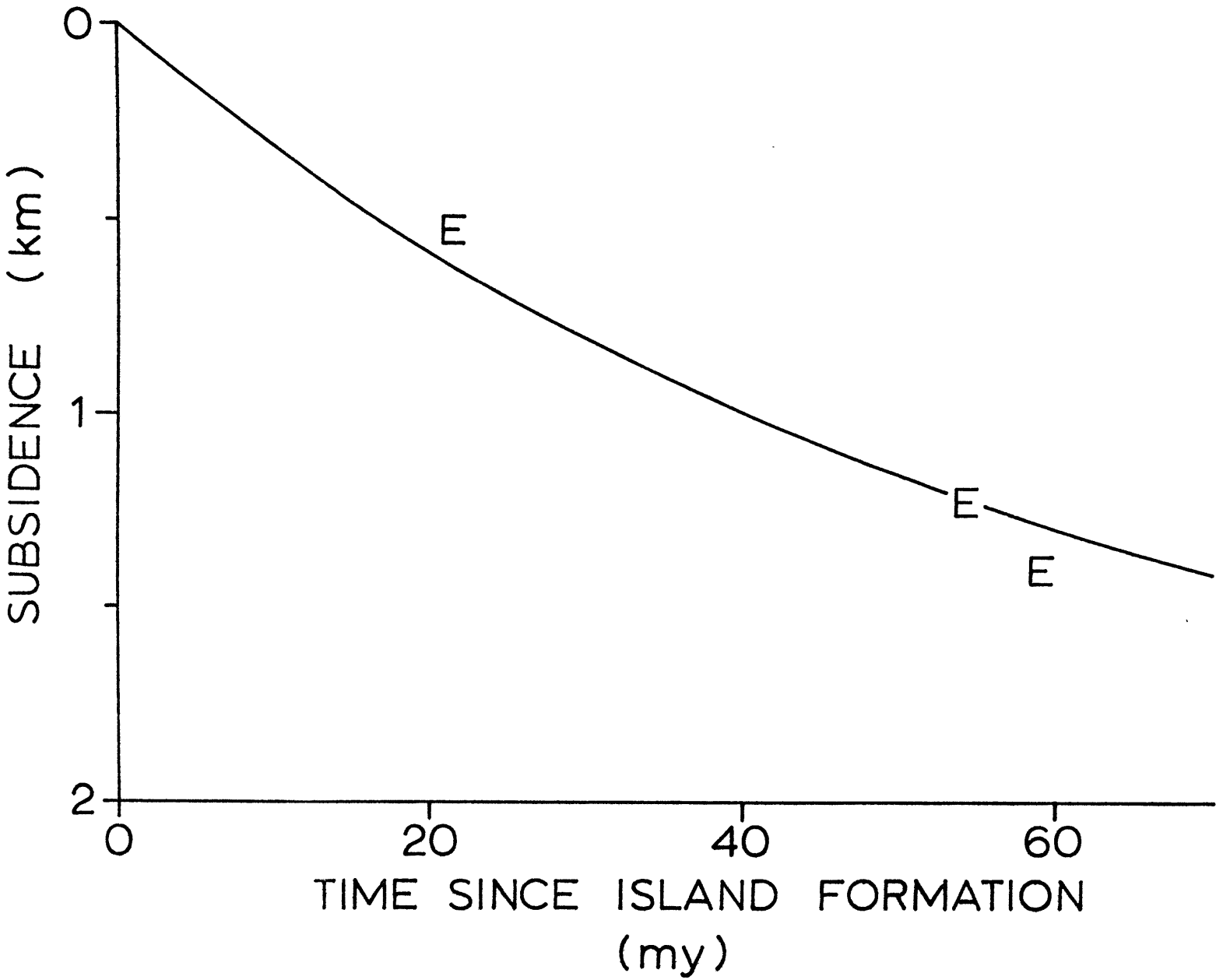
0
1
2
SUBSIDENCE (km)
E
E
E
0
20
40
60
TIME SINCE ISLAND FORMATION
(my)

by half, using reasonable values for thermal diffusivity, we would expect 20-40 m.y. to elapse before this thermal anomaly at depth could begin to affect surface heat flow measurements. By this time the lithosphere will already have cooled and thickened considerably, and thus while an anomaly should exist along the older portion of the island chain, it will be small and possibly unobservable in the normal scatter of heat flow values.

Our assumption that an anomalously high asthenospheric heat flow associated with hot spots causes the thinning may be wrong. Analytical studies assuming a constant thickness lithosphere (Birch, 1975) and numerical studies assuming a variable thickness (Crough and Thompson, 1976a) indicate that if hot spots have twice the normal heat flux, then it should take about 100 m.y. to conduct enough heat into the lithosphere to lift the Hawaiian swell to its maximum observed height. From Figure 6 it can be seen that the Hawaiian swell actually rises in about 3 m.y. With conductive heat transfer the only way to decrease this length of time is to increase the hot spot heat flux. However, the Hawaiian data would require a hot spot heat flux about 40 times normal, which seems unrealistic. At present, we offer no resolution of this problem, but we think that thermal conduction models are inadequate to explain the uplift rate of the swell. As alternative possibilities we suggest that (1) the thinning is not a thermal process but a mechanical one or (2) the thinning is thermal, but heat is transported convectively, perhaps by intrusion of magma into the lower lithosphere. The latter mechanism has been frequently proposed to explain rift valley uplifts and intracontinental hot spots (Burke and Whiteman, 1973).

Seismic studies probably offer the best future test of the lithospheric thinning model. Rayleigh wave phase and group velocities increase systematically as a function of crustal age (Leeds et al., 1974; Yoshii, 1975; Forsyth, 1975). If the lithosphere is thin beneath the Hawaiian chain, then surface wave velocities along the chain should be unusually low. If, on the other hand, the lithosphere has normal thickness, as the asthenospheric bump model predicts, then velocities will be normal.

IMPLICATIONS

While the lithospheric thinning model has been presented to explain atoll subsidence, the most important implications of this concept concern the nature of hot spots and the thermal and elastic response of the lithosphere to hot spot related mantle convection. Since the Hawaiian swell is compensated, lithospheric thinning must occur over an area comparable to its width. This requires the Hawaiian hot spot to be about 1200 km in diameter, which suggests that it is much more than a simple basalt conduit for surface volcanism. In fact, the data suggest that the Hawaiian swell is the main surface expression of the Hawaiian hot spot and that the volcanoes are not of fundamental tectonic significance. Volcanoes are not required by the lithospheric thinning model, and indeed, the Hawaiian swell still exists along the strike of the chain, even where there are few seamounts. The impressive width of the swell (1000-1400 km) supports the view of Wilson (1963) and Morgan (1971) that hot spots are the result of some deeper mantle process. It is difficult to imagine that any process confined solely to the lithosphere (like crack propagation) could produce the necessary width of thinning.

The origins of swells on midocean ridges (Iceland, Azores, Tristan/Gough) need to be re-examined to see if the anomalously elevated sea floor

associated with these hot spots is also caused by some change in the lithosphere. The bathymetric profiles of Sclater et al. (1975) across the Reykjanes Ridge and the aseismic ridge subsidence data cited earlier (Detrick et al., 1977) both indicate this sea floor subsides at normal rates, remaining shallower than normal sea floor of the same age long after it has left the ridge crest. This is not the expected pattern of movement off an asthenospheric bump.

There has recently been much geophysical interest in identifying those surface effects which may be related to convection patterns in the upper mantle (Menard, 1973; Anderson et al., 1973; Sclater et al., 1975; Watts, 1976). Long-wavelength free air gravity anomalies and systematic regional departures from the empirical age-depth relation have been used in these studies to infer patterns of mass flow in the upper mantle. In all these studies it is necessary to demonstrate that the observed correlations between long-wavelength gravity anomalies and residual depth anomalies do not have their origin within the lithosphere before the cause can be inferred to be convective processes occurring in the asthenosphere. The lithospheric thinning model is one mechanism for producing these long-wavelength topographic and gravity anomalies from sources within the lithosphere. In the case of the Hawaiian swell this model appears to be compatible with available bathymetric and gravity data. While the mechanism of this thinning is not understood, it is also probably related to mantle convective processes. However, in this case the swell has a lithospheric origin, and while it reflects the response of the lithosphere to upper mantle convection, it cannot be used directly to infer the extent or pattern of this convection.

CONCLUSIONS

From this study of the subsidence history of western Pacific atolls and surrounding features we draw the following conclusions:

1. Hot spot generated midplate island chains like the Hawaiian-Emperor chain or the Marshall-Gilbert chain have subsided much more than would be expected from the normal thermal subsidence of the surrounding sea floor.

2. This excess subsidence probably cannot be explained by isostatic adjustments to the weight of the coral reef cap or the weight of the volcano.

3. The excess subsidence is apparently related to island formation atop areas of anomalously shallow sea floor, such as the Hawaiian swell, associated with midplate hot spots. As this sea floor returns to its normal depth the islands subside an extra amount equal to the original height of the swell.

4. The wavelength and amplitude of the long-wavelength gravity anomaly associated with the Hawaiian swell indicate an average depth of compensation between 50 and 100 km. Thus a significant part of the compensation of the swell occurs within the lithosphere, not within the asthenosphere, as would be expected if the swell were supported from below by some pattern of mantle convection. The compensation may extend to greater depths, but most of the density changes appear to occur within the lithosphere.

5. Lithospheric thinning over the Hawaiian hot spot is proposed as a simple mechanism for the origin of the Hawaiian swell. Since the lithosphere is denser than the asthenosphere, this thinning results in a

broad regional isostatic uplift. As the lithosphere moves away from the hot spot, it cools and thickens, and the swell disappears. The subsidence of the Hawaiian swell and a number of western Pacific atolls is in quantitative agreement with this model. The model also satisfies the gravity data, which appear to require compensation in the lower half of the lithosphere.

6. We have no satisfactory mechanism to explain the initial thinning. It occurs too rapidly to be explained by conductive heat transfer alone unless an unrealistically high hot spot heat flux is assumed. Alternatively, the thinning may be mechanical rather than thermal or related to magma intrusion directly in the lower lithosphere.

Acknowledgments

This research has been supported by a contract with the Office of Naval Research and the Woods Hole Oceanographic Institution Education Office. S.T.C. was supported by a postdoctoral fellowship from the Education Office. Woods Hole Oceanographic Institution contribution 3962.

REFERENCES

Anderson, R. N., D. P. McKenzie, and J. G. Sclater, Gravity bathymetry and convection in the earth, Earth Planet. Sci. Lett., 18, 391-407, 1973.

Birch, F. S., Conductive heat flow anomalies over a hot spot in a moving medium, J. Geophys. Res., 80, 4825-4827, 1975.

Burke, K., and A. J. Whiteman, Uplift, rifting and the break-up of Africa, in Implications of Continental Drift to the Earth Sciences, vol. 2, edited by D. H. Tarling and S. K. Runcorn, p. 735, Academic, New York, 1973.

Chase, T. E., H. W. Menard, and J. Mammerickx, Bathymetry of the Northern Pacific, Institute of Marine Resources, La Jolla, Calif., 1970.

Clague, D. A., and R. D. Jarrard, Tertiary Pacific plate motion deduced from Hawaiian-Emperor chain, Geol. Soc. Amer. Bull., 84, 1135-1154, 1973.

Crough, S. T., Thermal model of oceanic lithosphere, Nature, 256, 388-390, 1975.

Crough, S. T., and G. A. Thompson, Numerical and approximate solutions for lithospheric thickening and thinning, Earth Planet. Sci. Lett., 31, 397-402, 1976a.

Crough, S. T., and G. A. Thompson, Thermal model of continental lithosphere, J. Geophys. Res., 81, 4857-4862, 1976b.

Davies, T. A., P. Wilde, and D. A. Clague, Koko seamount--A major guyot at the southern end of the Emperor seamounts, Mar. Geol., 13, 311-321, 1972.

Detrick, R. S., J. G. Sclater, and J. Thiede, The subsidence of aseismic ridges, Earth Planet. Sci. Lett., 34,185-196, 1977.

Dietz, R. S., and H. W. Menard, Hawaiian swell, deep, and arch and subsidence of the Hawaiian Islands, J. Geol., 61, 99-113, 1953.

Ewing, J., M. Ewing, T. Aitken, and W. J. Ludwig, North Pacific sediment layers measured by seismic profiling in The Crust and Upper Mantle of the Pacific Area, Geophys. Monog. Ser., vol. 12, edited by L. Knopoff, C. L. Drake, and P. J. Hart, pp. 147-173, AGU, Washington, D. C., 1968.

Forsyth, D. W., The early structural evolution and anisotropy of the oceanic upper mantle, Geophys. J. Roy. Astron. Soc., 43, 103-162, 1975.

Jackson, E. D., E. A. Silver, and G. B. Dalrymple, Hawaiian-Emperor chain and its relation to Cenozoic circumpacific tectonics, Geol. Soc. Amer. Bull., 83, 601-618, 1972.

Kulp, J. L., Potassium-argon dating of volcanic rocks, Bull. Volcanol., 26, 247-258, 1963.

Ladd, H. S., and S. O. Schlanger, Drilling operations on Eniwetok Atoll, U. S. Geol. Surv. Prof. Pap., 260-Y, 863-905, 1960.

Ladd, H. S., J. I. Tracey, and M. G. Gross, Drilling on Midway Atoll, Hawaii, Science, 166, 1038-1093, 1967.

Leeds, A. R., L. Knopoff, and E. G. Kausel, Variations in upper mantle structure under the Pacific Ocean, Science, 186, 141-143, 1974.

Matthews, D. J., Tables of the velocity of sound in pure water and sea water for use in echo sounding and sound-ranging, Rep. H. D. 282, Hydrogr. Dep., Admiralty Office, London, 1939.

Menard, H. W., Marine Geology of the Pacific, pp. 55-95, McGraw-Hill, New York, 1963.

Menard, H. W., Depth anomalies and the bobbing motion of drifting islands, J. Geophys. Res., 78, 5128-5137, 1973.

Menard, H. W., and H. S. Ladd, Oceanic islands, seamounts, guyots and atolls, in The Sea, vol. 3, edited by A. E. Maxwell, pp. 365-387, Interscience, New York, 1963.

Morgan, W. J., Convection plumes in the lower mantle, Nature, 230, 42-43, 1971.

Parsons, B., and J. G. Sclater, An analysis of the variation of ocean floor heat flow and bathymetry with age, J. Geophys. Res., 82, 803-827, 1977.

Raitt, R. W., Seismic refraction studies of Bikini and Kwajalein atolls, U. S. Geol. Surv. Prof. Pap., 260-K, 507-527, 1954.

Richter, F. M., and B. Parsons, On the interaction of two scales of convection in the mantle, J. Geophys. Res., 80, 2529-2541, 1975.

Sclater, J. G., L. A. Lawver, and B. Parsons, Comparison of long-wavelength residual elevation and free air gravity anomalies in the North Atlantic and possible implications for the thickness of the lithospheric plate, J. Geophys. Res., 80, 1031-1052, 1975.

Sclater, J. G., J. Crowe, and R. N. Anderson, On the reliability of oceanic heat flow averages, J. Geophys. Res., 81, 2997-3006, 1976.

Sollas, W. J., and T. W. E. David, The atoll of Funafuti, Rep. Roy. Soc. London, p. 428, London, 1904.

Stearns, H. T., and T. K. Chamberlain, Deep cores at Oahu, Hawaii, and their bearing on the geologic history of the central Pacific Basin, Pac. Sci., 21, 153-165, 1967.

Walcott, R. I., Flexure of the lithosphere at Hawaii, Tectonophysics, 9, 435-446, 1970a.

Walcott, R. I., Flexural rigidity, thickness, and viscosity of the lithosphere, J. Geophys. Res., 75, 3941-3954, 1970b.

Watts, A. B., Gravity and bathymetry in the central Pacific Ocean, J. Geophys. Res., 81, 1533-1553, 1976.

Watts, A. B., and J. R. Cochran, Gravity anomalies and flexure of the lithosphere along the Hawaiian-Emperor seamount chain, Geophys. J. Roy. Astron. Soc., 38, 119-141, 1974.

Watts, A. B., and M. Talwani, Gravity anomalies seaward of deep-sea trenches and their tectonic implications, Geophys. J. Roy. Astron. Soc., 36, 57-90, 1974.

Watts, A. B., M. Talwani, and J. R. Cochran, Gravity field of the northwest Pacific Ocean and its margin, in The Geophysics of the Pacific Ocean Basin and Its Margin, Geophys. Monogr. Ser., vol. 19, edited by G. H. Sutton, H. H. Manghnani, and R. Moberly, 431-438, AGU, Washington, D. C., 1976.

Wilson, J. T., A possible origin of the Hawaiian Islands, Can. J. Phys., 41, 863-870, 1963.

Yoshii, T., Regionality of group velocities of Reyleigh waves in the Pacific and thickening of the plate, Earth Planet. Sci. Lett., 25, 305-312, 1975.

APPENDIX A

APPLYING LINEAR TRANSFER FUNCTION TECHNIQUES TO MARINE GRAVITY DATA

THEORY AND METHOD

INTRODUCTION

Gravity anomalies can be treated as resulting from the convolution of an "Earth" filter with the topography. This filter defines the relationship between the gravity field and topographic variations and thus contains information on the isostatic response of the Earth to the topography. By comparing this filter, or its transform, the complex admittance, with models based on different hypotheses of compensation, the state of isostasy of the topography can be studied.

This is the basic approach involved in applying linear transfer function techniques to gravity data. The use of these techniques has been previously described by Dorman and Lewis (1970), Lewis and Dorman (1970), McKenzie and Bowin (1976), Walcott (1976), Watts (in press) and Cochran and Watts (in press). Similar techniques were used in Chapter 2 to investigate the crustal structure and isostasy of aseismic ridges. While the basic approach in each of these studies has been the same, several different methods have been used to calculate and interpret this transfer function. Therefore, while information on the theory and computational procedures involved in applying these techniques has been discussed in these earlier studies, this appendix has been written to serve as a convenient reference for individuals who might want to apply these techniques to other geological problems.

THEORY

The basic assumption in applying linear transfer function techniques to marine gravity data is that the observed gravity anomalies can be related to sea floor topography. The first step in applying these techniques

is, therefore, to obtain a filter which predicts the observed gravity from the bathymetry. This is a simple convolution operation, which can be represented schematically by the following block diagram:

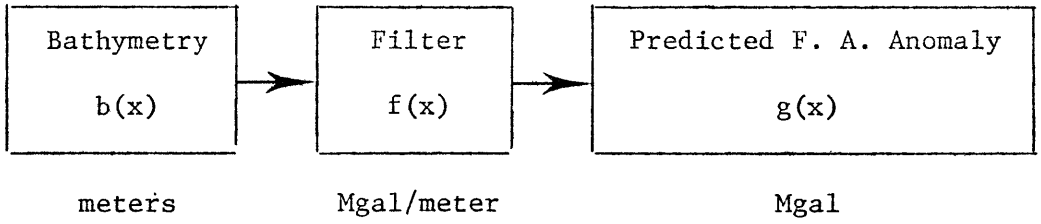

Various methods are available for calculating this filter. One approach is to minimize, in at least squares sense, the differences between the desired filter output (in this case the observed free-air gravity anomaly) and the actual output. This filter, known as a Wiener filter, can be easily computed from the autocorrelation coefficients of the bathymetry and gravity (Levinson, 1947; Treitel and Robinson, 1966). This was the procedure used by McKenzie and Bowin (1976) to compute filters for two long (~3000km) profiles across the Mid-Atlantic Ridge.

The computation of the Wiener filter is done in the space domain. In cross-spectral methods this filter is computed in the wavenumber (frequency) domain by a simple division of Fourier tranforms. As before we desire a filter which when convolved with the bathymetry yields a time series which resembles the observed free-air gravity anomaly. Since convolution in the space domain is equivalent to multiplication in the wavenumber domain, this can be expressed as:

$$B(k) \cdot Z(k) = G(k) \qquad (1)$$

where B(k), Z(k) and G(k) are the discrete Fourier transforms of b(x), f(x) and g(x) and k is wavenumber ($k = 2\pi/\lambda$). Thus the admittance, Z(k), is simply the Fourier transform of gravity divided by the Fourier transform of the bathymetry:

$$Z(k) = \frac{G(k)}{B(k)} \qquad (2)$$

This is the form of the transfer function used by Dorman and Lewis (1970) and Lewis and Dorman (1970). However, in the presence of noise a better estimate of Z(k) is given by McKenzie and Bowin (1976) as:

$$Z(k) = \frac{G(k) \cdot B(k)^*}{B(k) \cdot B(k)^*} \qquad (3)$$

where * indicates the complex conjugate. In this case the admittance is the complex cross spectrum of gravity and bathymetry divided by the power spectrum of the bathymetry. The desired filter is simply the inverse Fourier transform of the complex admittance.

METHOD

The computational steps involved in applying these cross-spectral techniques are relatively simple. The gravity and bathymetry data are first selected at equally spaced intervals along track by linear interpolation. Mean and trend are then removed and a cosine bell taper applied to the first and last 5% of each profile before the time series are Fourier transformed. These Fourier transforms can be rapidly and easily calculated on any digital computer using the Fast Fourier Transform algorithm of Cooley and Tukey (1965). The cross spectrum and power spectrum are then obtained by a simple multiplication of Fourier transforms.

At this point some type of spectral smoothing is necessary in order to reduce the noise in this estimate of the admittance. McKenzie and Bowin (1976) carried out ensemble averaging by subdividing their profiles into a number of shorter profiles of equal length. They then averaged the spectra for each sub-profile. The problem with this approach is that it requires very long profiles (~1000km) which may cross a number

of different geological features. In Chapter 2 a different approach was used since we wanted to study a single geological feature. In this approach, which was also used by Watts (in press) and Cochran and Watts (in press), spectral smoothing is accomplished by using a sufficiently large number of relatively short (~300-600 km) profiles, each of which represents an independent estimate of the cross spectrum and power spectrum of gravity and bathymetry. These spectra are summed, and the resulting averaged spectra are used to obtain a single admittance function for all the profiles:

$$Z(k) = \frac{\Sigma\, G_i(k) \cdot B_i(k)^*}{\Sigma\, B_i(k) \cdot B_i(k)^*} \qquad (4)$$

where $B_i(k)$ and $G_i(k)$ are the Fourier transforms of bathymetry and gravity of the i^{th} profile and n is the total number of profiles. An example of this smoothing process is illustrated in Figure 1. While the desired filter is actually the inverse Fourier transform of the admittance, this form of the transfer function is much more useful since the admittance amplitude can be directly related to the results of model calculations (McKenzie and Bowin, 1976).

In addition to determining the complex admittance, it also is useful to determine the coherence (McKenzie and Bowin, 1976). The coherence is a measure of that portion of the power spectrum of the observed gravity that can be directly attributed to the bathymetry. An estimate of the coherence is given (Munk and Cartwright, 1966) by:

$$\gamma^2(k) = \frac{(n(cc^*/E_G E_B) - 1)}{(n-1)} \qquad (5)$$

where $c = G(k) \cdot B(k)^*$, E_G and E_B are the power spectra of gravity and bathymetry respectively and n is the number of profiles.

FIGURE 1

Illustration of smoothing effect of averaging spectra from many profiles. Admittance estimates indicated by open circles, triangles, and solid circles were calculated from 2, 5, and 14 gravity/bathymetry profiles respectively. A minimum of 5-10 profiles are needed to obtain smooth spectral estimates.

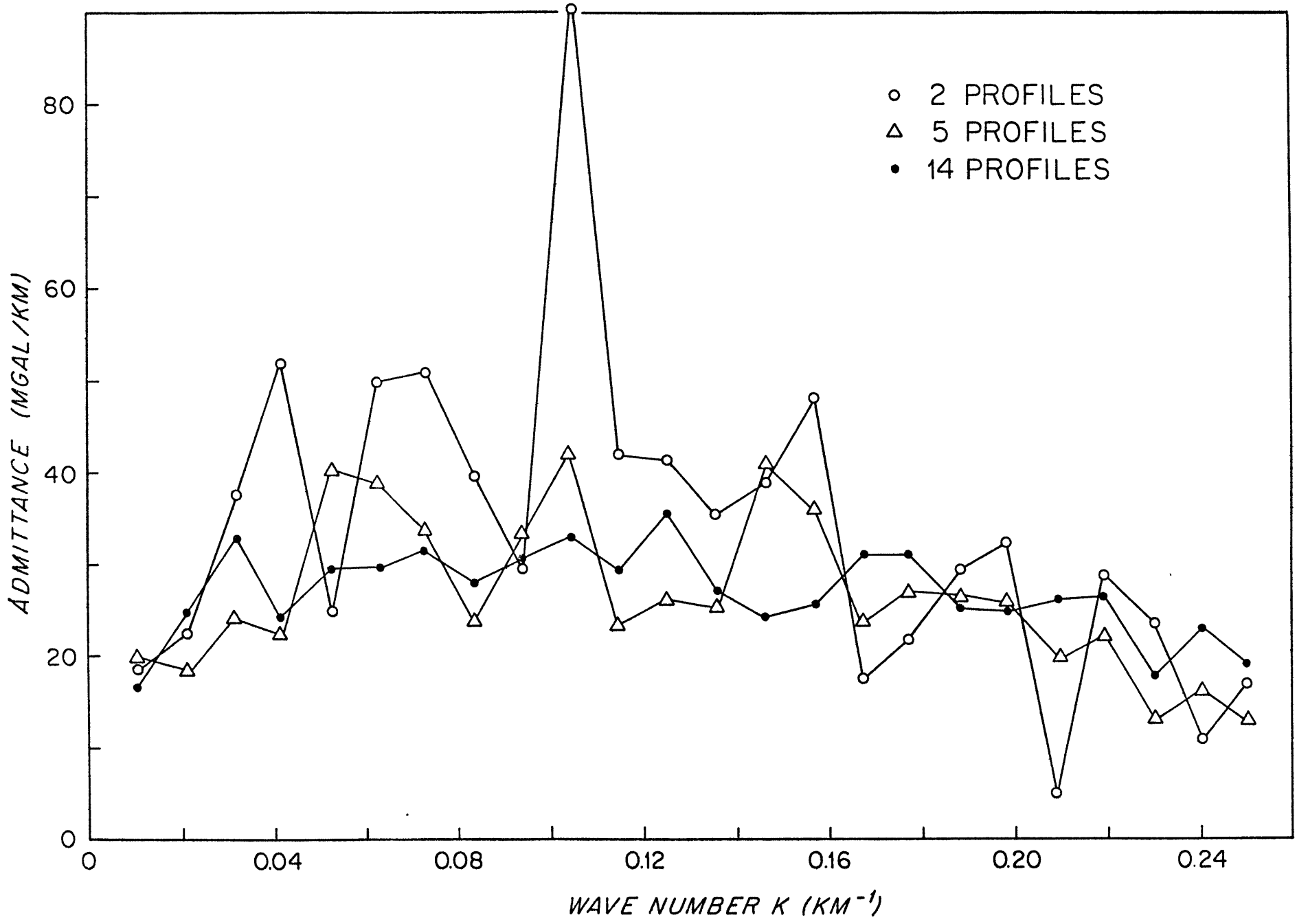
2 PROFILES
5 PROFILES
14 PROFILES
ADMITTANCE (MGAL/KM)
0
20
40
60
80
0
0.04
0.08
0.12
0.16
0.20
0.24
WAVE NUMBER K (KM⁻¹)

The coherence can be used to estimate errors in individual estimates of the admittance (Watts, in press). The noise parameter $\sigma(k)$ for an admittance estimate $Z(k)$ with coherence $\gamma^2(k)$ is (Munk and Cartwright, 1966):

$$\sigma(k) = \{(\gamma(k)^{-2}-1)/2p\}^{\frac{1}{2}} \qquad (6)$$

where p is the number of degrees of freedom, taken to be, n, the number of gravity and bathymetry profiles used to calculate the admittance. For $\sigma<0.25$ the standard error of an admittance estimate $Z(k)$ can be obtained by assuming a normal probability distribution of sample admittance/true admittance with standard error σ. For higher σ the probability distribution is not normal and is positively biased (Munk and Cartwright, 1966, Figure 16).

ADMITTANCE MODELS

By comparing the observed admittance with models based on different hypotheses of compensation, information can be obtained on the state of isostasy of geological features crossed by the gravity and bathymetry profiles used to calculate the admittance.

The simplest model to explain the observed admittance values is to assume that the free-air gravity anomalies are caused by uncompensated sea floor topography (Figure 2a). If the density contrast at the sea floor is represented by a layer with a flat lower boundary and an upper boundary defined by the function $b(x)$, then a well-known linear approximation to the complete gravity effect (Parker, 1972) is:

$$G(k) = 2\pi\Gamma(\rho_c-\rho_w)B(k)e^{-kd} \qquad (7)$$

where Γ is the gravitational constant, d is the mean water depth, ρ_c is the density of the crust, ρ_w is the density of sea water and $G(k)$ and

FIGURE 2

Theoretical admittance curves based on different isostatic models: A) uncompensated topography, B) Airy model of local compensation, C) elastic plate model of regional compensation and D) viscoelastic plate model.

ADMITTANCE MODELS

A) UNCOMPENSATED

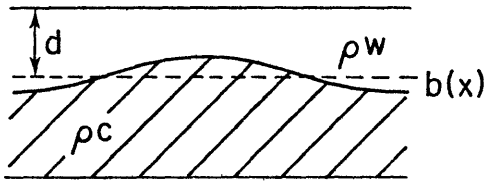

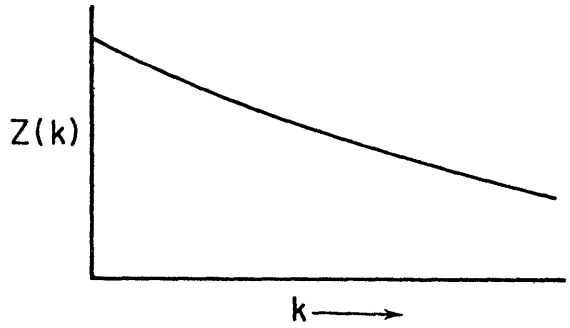

B) AIRY MODEL-LOCAL COMPENSATION

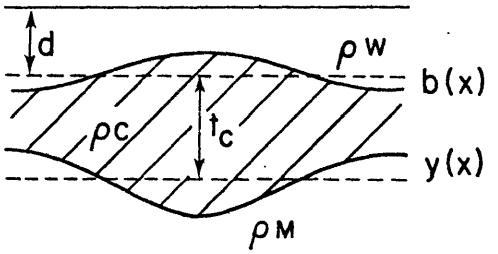

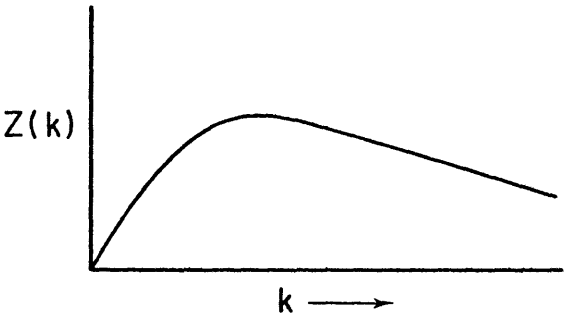

C) ELASTIC PLATE MODEL-REGIONAL COMPENSATION

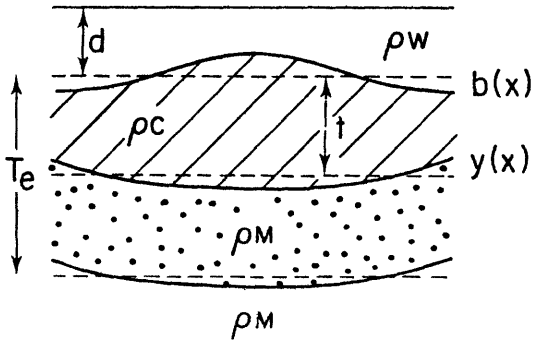

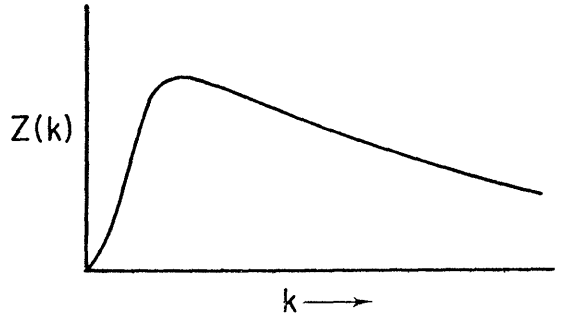

D) VISCOELASTIC PLASTIC MODEL-REGIONAL COMPENSATION

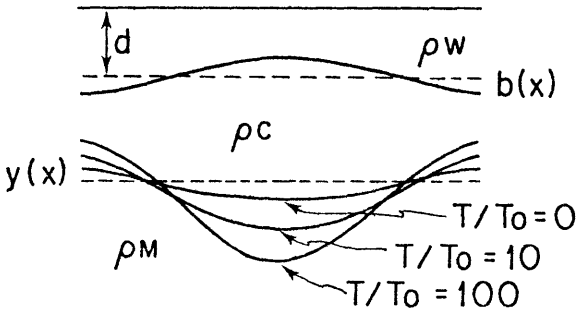

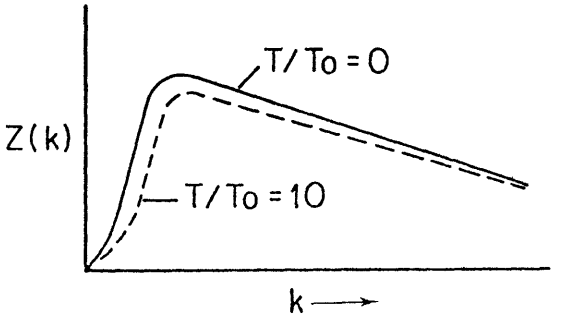

B(k) are Fourier transforms of gravity and bathymetry respectively. The admittance for uncompensated topography is therefore (McKenzie and Bowin, 1976):

$$Z(k) = \frac{G(k)}{B(k)} = 2\pi\Gamma(\rho_c - \rho_w)e^{-kd} \qquad (8)$$

This function is generally a good fit to the observed admittance values at relatively short wavelengths (λ<100km); however, as $k \to 0$ the observed behavior is quite different (see for example Figures 10 and 11 in Chapter 2). The most obvious explanation for the decrease in the admittance at long wavelengths is that it is the result of isostatic compensation, since this will produce long-wavelength topography without corresponding gravity anomalies.

This compensation can be represented by a second density anomaly corresponding to the crust-mantle boundary located at depth, t, below the sea floor. The gravity anomaly observed at the sea surface will be the sum of these two effects:

$$G(k) = 2\pi\Gamma\rho_t B(k)e^{-kd} - 2\pi\Gamma(\rho_m - \rho_c)Y(k)e^{-k(d+t)}$$

$$2\pi\Gamma\rho_t B(k)e^{-kd}\left\{\frac{1-(\rho_m - \rho_c)Y(k)e^{-kt}}{\rho_t B(k)}\right\} \qquad (9)$$

where $\rho_t = (\rho_c - \rho_w)$, ρ_m is the density of the mantle and Y(k) is the Fourier transform of the surface, y(x), representing the crust-mantle interface.

The function y(x) depends, in general, on the surface mass excess (or load), the rigidity of the lithosphere and the density contrast between crust and mantle. If the lithosphere is treated as a thin elastic sheet overlying a fluid layer, then the deflection of the crust-mantle interface, y(x), is given by the differential equation (e.g., Walcott, 1970):

$$D\nabla^4 y(x) + (\rho_m - \rho_c)gy(x) = p(x) \qquad (10)$$

where D is the flexural rigidity of the plate = $ET_e^3/12(1-\sigma^2)$ with E as Young's modulus, T_e as the plate thickness and σ as Poisson's ratio. The load $p(x) = g\rho_t b(x)$. Here we have assumed the material infilling the deflection has the same density as the load.

Airy Model

In the case of a lithosphere with no elastic strength, D = 0, leaving us with the well-known equation for local isostatic equilibrium by crustal thickening (Airy model), where

$$y(x) = \frac{\rho_t b(x)}{(\rho_m - \rho_c)} \qquad (11)$$

By taking the Fourier transform of equation (11) and substituting into equation (9), the admittance for a simple Airy isostatic model is obtained (McKenzie and Bowin, 1976):

$$Z(k) = \frac{G(k)}{B(k)} = 2\pi\Gamma\rho_t e^{-kd}\ (1-e^{-kt}) \qquad (12)$$

The admittance for this model (Figure 2b) decreases toward zero at wavelengths greater than ~200 km; at shorter wavelengths it asymptotically approaches the curve representing uncompensated topography. In Chapter 2 we show that this isostatic model is a good fit to observed admittance values for the Ninetyeast and eastern Walvis Ridges implying that these features are locally compensated by an overthickened crust.

Elastic Plate Model

In the more general case of a lithosphere with some rigidity, y(x) must be determined from solving equation (10). This equation can be solved any number of ways (Hertz, 1884; Gunn, 1943; Nadai, 1963); however, here we will use a Fourier approach. Taking the Fourier transform of

equation (10) we have:

$$Dk^4Y(k) + (\rho_m - \rho_c)gY(k) = P(k) \qquad (13)$$

Solving for Y(k), the deflection of the crust-mantle interface:

$$Y(k) = \frac{B(k)\rho_t/(\rho_m - \rho_c)}{(1 + Dk^4/g(\rho_m - \rho_c))} \qquad (14)$$

where P(k), the load, has been rewritten in terms of the sea floor topography $P(k) = \rho_t gB(k)$. Substituting for Y(k) in equation (9) we obtain the expression for the admittance for a plate model of regional compensation:

$$Z(k) = \frac{G(k)}{B(k)} = 2\pi\Gamma\rho_t e^{-kd}\{1-e^{-kt}(1+\frac{Dk^4}{g(\rho_m-\rho_c)})^{-1}\}$$

$$= 2\pi\Gamma\rho_t e^{-kd}\{1-e^{-kt}\phi(k)\} \qquad (15)$$

where $\phi(k)$ is the flexural response function as defined by Walcott (1976).

As $D \to \infty$, that is as the plate becomes perfectly rigid, $\phi(k) \to 0$ and $Z(k) \to 2\pi\Gamma\rho_t e^{-kd}$ indicating that the topography is completely uncompensated. As $D \to 0$, $\phi(k) \to 1$ and $Z(k) \to 2\pi\Gamma\rho_t e^{-kd}(1-e^{-kt})$, which is the condition that the topography is fully compensated (Airy model). In the oceans, the flexural rigidity is generally in the range 10^{28} - 10^{31} dyn-cm (Walcott, 1970; Watts and Cochran, 1974; McAdoo et al., in press). In Figure 2c the shape of the admittance curve for a typical plate model is shown. The main differences between the Airy and plate models occur at long wavelengths (λ>100 km) where the plate model admittance curves increase much more rapidly and peak at longer wavelengths than the corresponding Airy curves.

Equation (15) is, strictly speaking, only a thin plate approximation valid as long as the wavelength and amplitude of the deformation are small compared to the effective elastic plate thickness T_e. McKenzie and Bowin (1976) have outlined a procedure for deriving the more general

thick plate expression. In Chapter 2 we have used this thick plate expression, modified slightly to include another density contrast within the crust corresponding to the layer 2/layer 3 boundary. The resulting admittance (Watts, in press) is:

$$Z(k) = 2\pi\Gamma(\rho_2-\rho_w)e^{-kd}\{1-(e^{-kt_2}(\rho_3-\rho_2)+e^{-kt_c}(\rho_m-\rho_3)) /((\rho_m-\rho_2)+4(\rho_m-\rho_w)Mk'^2AB^{-1})\} \quad (16)$$

where t_2 and ρ_2 are the thickness and density of layer 2; ρ_3 is the density of layer 3, t_c is the mean crustal thickness; $M = E/3gh(\rho_m - 1.03)$ where the elastic plate thickness is 2h; $A = \{(\sinh 2k')/2k'\}^2-1$ and $B = \{(\sinh 4k')/4k'\}^2+1$ where $k' = kh$.*

The observed admittance values from the Hawaiian-Emperor seamount chain (Watts, in press), from normal mid-ocean ridge topography (McKenzie and Bowin, 1976; Cochran and Watts, in press) and from the western Walvis Ridge (Chapter 2) are best fitted by a plate model of compensation.

Viscoelastic Plate Model

Walcott (1970) has proposed that the lithosphere may respond to surface loads as a viscoelastic substance; that is, following an initial period of elastic deformation it responds by viscous flow. The admittance for this type of lithospheric behavior can be easily obtained.

---

*The expressions given for Z in equations A16 and A20 of McKenzie and Bowin (1976) are printed incorrectly. There should be a 2 in the denominator of the constants at the beginning of both these equations. The bracketed quantity in their expression for B_1 (equation A11) should be squared.

Walcott (1976) has given the flexural response function for a viscoelastic plate model:

$$\phi(k) = \{1 - \frac{Dk^4/g(\rho_m-\rho_c)}{1+Dk^4/g(\rho_m-\rho_c)} \cdot e^{\left(\frac{-T}{T_o(1+Dk^4/g(\rho_m-\rho_c))}\right)}\} \quad (17)$$

where T_o is the relaxation time constant and T is the time since loading. D, in this case, is the instantaneous (or initial) rigidity of the lithosphere. Substituting this expression for $\phi(k)$ into equation (15) we have the admittance for a viscoelastic plate model:

$$Z(k) = 2\pi\Gamma\rho_t e^{-kd} \cdot \{1-e^{-kt}(1 - \frac{Dk^4/g(\rho_m-\rho_c)}{1+Dk^4/g(\rho_m-\rho_c)} \cdot e^{\frac{-T}{(1+Dk^4/g(\rho_m-\rho_c))T_o}})\}$$

The effect of viscoelasticity is to increase gradually $\phi(k)$ with time, shifting the peak in the admittance curves to shorter wavelengths (Figure 3d). This reflects the decreasing rigidity of the lithosphere and its inability to support loads at longer wavelengths without bending. Whether or not oceanic lithosphere behaves viscoelastically depends on the relaxation time constant T_o. Estimates of T_o range from 10^5 - 10^7 yrs (Walcott, 1976; Watts, in press), and there is not, as yet, general agreement on the importance of viscoelastic behavior in the oceans. There is, however, increasing evidence that the range of elastic plate thicknesses determined in the oceans is due primarily to the thermal structure of the lithosphere at the time of loading rather than any viscoelastic behavior (Watts, in press).

SUMMARY

The linear transfer function techniques discussed here are a fast and relatively simple method of analyzing marine gravity data. One major advantage of these techniques is that they allow a quantitative estimate of the gravity/bathymetry relationship as a function of wavelength. This type of estimate is not possible with more conventional methods of gravity analysis. These cross-spectral techniques are also particularly well-suited to studying large numbers of gravity and bathymetry profiles across a single geological feature or from a single geological province.

These techniques represent a significant development over previous methods of studying the manner in which the lithosphere responds to surface loads, and they can provide new and more quantitative information on the long-term mechanical properties of the lithosphere. It is hoped that this appendix provides enough information on the theory and application of these techniques to be useful to anyone wishing to apply cross-spectral techniques to these or similar problems.

REFERENCES

Cochran, J. R., and A. B. Watts, An analysis of isostasy in the world's oceans: Part 2--Mid-ocean ridge crests, submitted to J. Geophys. Res.

Cooley, J. W., and J. W. Tukey, An algorithm for the machine calculation of complex Fourier series, Mathematics of Computation, 19, 297, 1965.

Dorman, L. M., and B. T. R. Lewis, Experimental isostasy 1. Theory of the determination of the Earth's isostatic response to a concentrated load, J. Geophys. Res., 75, 3357, 1970.

Gunn, R., A quantitative evaluation of the influence of the lithosphere on the anomalies of gravity, J. Franklin Inst., 236, 373, 1943.

Hertz, H., On the equilibrium of floating elastic plates, Wiedemann's Ann., 22, 449, 1884.

Levinson, N., The Weiner rms (root mean square) error criterion in filter design and prediction, J. Math. Phys., 25, 261, 1947.

Lewis, B. T. R., and L. M. Dorman, Experimental isostasy, 2. An isostatic model for the U. S. A. derived from gravity and topographic data, J. Geophys. Res., 75, 3367, 1970.

McAdoo, D. C., J. G. Caldwell and D. L. Turcotte, On the elastic-perfectly plastic bending of the lithosphere under generalized loading with application to the Kuril trench, Tectonophysics, in press.

McKenzie, D. P., and C. Bowin, The Relationship between bathymetry and gravity in the Atlantic Ocean, J. Geophys. Res., 81, 1903, 1976.

Munk, W. H., and D. E. Cartwright, Tidal spectroscopy and prediction, Phil. Trans. Roy. Soc. Lond., Series A, 259, 533, 1966.

Nadai, A., Theory of flow and fracture of solids, 2, McGraw-Hill, New York, 705 p, 1963.

Parker, R. L., The rapid calculation of potential anomalies, Geophys. J. R. astr. Soc., 31, 447, 1972.

Treitel, S., and E. A. Robinson, The design of high resolution digital filters, IEEE Trans. Geosci. Electron., 4, 25, 1966.

Walcott, R. I., Flexural rigidity, thickness and viscosity of the lithosphere, J. Geophys. Res., 75, 3941, 1970.

Watts, A. B., An analysis of isostasy in the world's oceans: Part 1--Hawaiian-Emperor seamount chain, submitted to J. Geophys. Res.

Watts, A. B., and J. R. Cochran, Gravity anomalies and flexure of the lithosphere along the Hawaiian-Emperor seamount chain, Geophys. J. R. astr. Soc., 38, 119, 1974.